uOttawa

L'Université canadienne
Canada's university

FACULTÉ DES ÉTUDES SUPÉRIEURES ET POSTOCTORALES

uOttawa

L'Université canadienne
Canada's university

FACULTY OF GRADUATE AND POSDOCTORAL STUDIES

Benoit-Michel Saumur
AUTEUR DE LA THÈSE / AUTHOR OF THESIS

M.Sc. (Earth Sciences)
GRADE / DEGREE

Department of Earth Sciences
FACULTÉ, ÉCOLE, DÉPARTEMENT / FACULTY, SCHOOL, DEPARTMENT

Serpentinites and Garnet Peridotites from an Oceanic Subduction Complex in Northern Dominican Republic

TITRE DE LA THÈSE / TITLE OF THESIS

Dr. Keiko Hattori
DIRECTEUR (DIRECTRICE) DE LA THÈSE / THESIS SUPERVISOR

CO-DIRECTEUR (CO-DIRECTRICE) DE LA THÈSE / THESIS CO-SUPERVISOR

EXAMINATEURS (EXAMINATRICES) DE LA THÈSE / THESIS EXAMINERS

Dr. Anthony Fowler

Dr. Brian Cousens

Gary W. Slater
Le Doyen de la Faculté des études supérieures et postdoctorales / Dean of the Faculty of Graduate and Postdoctoral Studies

# SERPENTINITES AND GARNET PERIDOTITES FROM AN OCEANIC SUBDUCTION COMPLEX IN NORTHERN DOMINICAN REPUBLIC

BY

**Benoit-Michel Saumur, B.Sc.H.**

A thesis submitted to the Faculty of Graduate & Postdoctoral Studies
in partial fulfillment of the requirements for the degree of M.Sc. in Earth Sciences

Ottawa-Carleton Geoscience Centre
University of Ottawa
Department of Earth Sciences
Ottawa, Canada

December 2007

*Your file Votre référence*
*ISBN: 978-0-494-49276-5*
*Our file Notre référence*
*ISBN: 978-0-494-49276-5*

# THESIS ABSTRACT

Subduction related rocks in northern Dominican Republic, Hispaniola, formed during the convergence of Proto-Caribbean oceanic lithosphere (part of North American plate) under the Caribbean plate between the Cretaceous and the mid-Eocene. Subduction was terminated by the oblique collision of the Bahamas Platform, which produced strike-slip faults, such as the Septentrional and Camù Faults. Serpentinites in two large inliers, the Puerto Plata Basement Complex (PPBC) and the Rio San Juan Complex (RSJC), were examined. Serpentinites are divided in three types based on their spatial distribution and their bulk rock and mineral chemistry. Serpentinites from the PPBC and the northern RSJC are slightly foliated and are composed of pseudomorphic lizardite and dusty magnetite. They have bulk rock compositions and Cr-spinel compositions similar to abyssal peridotites, and are interpreted to be hydrated abyssal peridotites. Serpentinites in central RSJC, which form mélanges containing blueschist and eclogite blocks, are composed of blady antigorite and chlorite that overprint pseudomorphic lizardite. Bulk rock compositions of these serpentinites suggest that they are abyssal peridotites hydrated on the sea floor. They were subducted and exhumed along the subduction plane together with blocks of blueschist and eclogite in a serpentinite-rich subduction channel. Finally, serpentinites near the major strike-slip fault zones are composed of pseudomorphic lizardite and magnetite, and have low Al and Ti compared to abyssal peridotite. They contain Cr-spinels with relatively high Cr# (Cr/[Cr+Al] atomic ratio) between 0.48-0.70. The data suggest that they are forearc mantle peridotites hydrated by slab-derived fluids at the base of the mantle wedge. Their presence along late strike-slip fault zones suggests that the fault zones directly tap the mantle wedge and that buoyant serpentinites protruded along the fault zones in response to transpressive collision. Furthermore, the presence of high pressure and ultra-high pressure rocks near the fault zones suggests that serpentinites may have played a role in the late stages of exhumation of these rocks, either by incorporating them during the protrusion or by lubricating the fault zone. In addition, the serpentinite along the fault zones could have facilitated aseismic creep.

Cr-spinels in serpentinites near the Septentrional Fault Zone are different from northern localities since they show gradational compositionally zoning; rims contain moderately high $Fe_2O_3$, FeO and $Cr_2O_3$, and slightly low MgO and $Al_2O_3$ compared to cores.

Furthermore, chlorite containing symplectic intergrowth of magnetite commonly surrounds chromite, forming partial to complete coronas. The ferritchromit and chlorite are interpreted as reaction products of spinel, magnetite and serpentine. Ferritchromit has been reported in rocks metamorphosed to amphibolite facies conditions, but ferritchromit from Dominican Republic contains less Fe and greater concentrations of Mg and Al than ferritchromit reported elsewhere. In addition, samples lack obvious evidence of thermal metamorphism: tremolite and cummingtonite are locally present in some samples, which suggests local heating, however all samples are dominated by lizardite, which is metastable at high temperatures. Therefore, poorly developed ferritchromit in Dominican Republic likely formed at low temperatures. Alternatively, ferritchromit formed during a short lived heating event during the intrusion of the Rio Boba Gabbroic Suite north of the Septentrional Fault Zone or during the ascent of the serpentinites through the hot interior of the mantle wedge.

Septentrional Fault Zone serpentinites are associated with garnet- and corundum-bearing wehrlites in the southern portions of the RSJC. Low concentrations in Ir-type platinum group elements and low Mg (Fo75-82) in olivine confirm that these rocks are cumulates. Clinopyroxene compositions are similar to those from other arc rocks, suggesting that clinopyroxene formed in a supra-subduction zone environment. Preliminary bulk rock data showing high concentrations of alkali and alkali-earth elements also suggest such an environment. Corundum occurs as inclusions in garnet, suggesting that it crystallized prior or during garnet formation during prograde metamorphism. Furthermore, textural evidence suggests that garnet, corundum, and clinopyroxene formed spinel and a liquid under ultrahigh pressure conditions. Preliminary results suggest that the garnet peridotites were recrystallized during prograde metamorphism.

# RESUME DE THESE

Des serpentinites et des péridotites à grenat sont exposées dans un complexe de subduction océanique le long de la côte nord de la République Dominicaine (île de Hispaniola). Le complexe a été formé par la subduction de la lithosphère Proto Caraïbe (plaque nord Américaine) sous la plaque Caraïbe entre le Crétacé et l'Éocène. La subduction a cessé lors de la collision oblique de la plate-forme des Bahamas, et depuis la morphologie originale du complexe de subduction a été modifiée par la déformation concentrée le long de deux failles de décrochement sénestres: les zones de failles Septentrionale (SFZ) et Camù (CFZ). Les roches du complexe de subduction sont exposées principalement dans deux fenêtres géologiques, soient les complexes de Puerto Plata (PPBC) et de Rio San Juan (RSJC), qui ont été cartographiés en détail par Pindell et Draper (1991) et Draper et Nagle (1991) respectivement. Les serpentinites exposées dans ces complexes peuvent être divisées en trois types selon leur distribution et leurs caractéristiques minéralogiques et géochimiques. Les serpentinites du PPBC et de la partie nord du RSJC sont quelque peu foliées et sont dominées par une matrice riche en lizardite et en magnétite définissant une texture pseudomorphique. Elles contiennent des compositions roche totale et des spinelles chromifères (chromites) avec des compositions semblables aux péridotites abyssales, et sont ainsi des serpentinites ophiolitiques océaniques déformées. Dans les portions centrales du RSJC, les serpentinites forment la grande partie du volume de mélanges tectoniques contenant des blocs de schistes bleus et d'éclogites formés par du métamorphisme de haute pression-basse température (HP-LT). Ces serpentinites sont composées d'une matrice riche en antigorite et en chlorite formant une texture non-pseudomorphique, suggérant que ce sont des serpentinites recristallisées. De plus, une chimie roche totale haute en Al suggère une origine océanique abyssale. Ces serpentinites océaniques ont été exhumées le long de l'interface de subduction dans un "chenal de subduction", entraînant avec elles des blocs de roches HP-LT. Finalement, les serpentinites localisées le long des failles SFZ et CFZ sont formées de lizardite et de magnétite pseudomorphiques, mais ont des compositions très pauvres en Al et Ti, ont des valeurs de Al/Si très basses, et ont des compositions de chromite relativement élevées en Cr. Ces observations suggèrent que ces serpentinites sont des péridotites du prisme mantellique "d'avant arc", et leur présence le long des failles de décrochement suggère les faillent traversent le manteau "d'avant arc" en profondeur et

que les serpentinites, étant relativement peu denses et ductiles en comparaison avec le manteau, ont profité de ces failles pour monter dans la croûte. La présence de serpentinites le long de zones de failles suggère que la celles-ci sont lubrifiées, suggérant que l'exhumation de blocs exotiques le long des zones de failles pourrait être facilitée. De plus, le comportement séismique des zones de faille pourrait être affectée.

Les chromites des serpentinites de la SFZ sont différentes si on les compare à celles des autres localités. En effet, elles montrent une variation compositionnelle graduelle, due à une augmentation en $Fe_2O_3$, FeO et $Cr_2O_3$ et une diminution de MgO et $Al_2O_3$ vers l'extérieur par rapport à la composition du noyau. Ce type de rebord de chromite est connu sous le nom de "ferritchromit", cependant celle produite ici est peu évoluée, étant relativement riche en Mg et Al et pauvre en Fe lorsqu'on la compare avec celle décrite dans la littérature. On retrouve souvent de la chlorite à proximité de ces grains, et cette chlorite est souvent enchevêtrée de magnétite. La zonation de chromite est due à une altération causée par une réaction entre le spinelle chromifère primaire, la serpentine et la magnétite, produisant de la "ferritchromit" et de la chlorite. D'après la littérature, ce type d'altération se fait à des températures plus élevées que celles de serpentinization, plus précisément à des températures dans le faciès amphibolite. Cependant, ces serpentinites sont dominées par la lizardite, qui est stable jusqu'à des températures de 300°C (Evans, 2004). Vu que la "ferritchromit" est peu évoluée et que les chlorites n'encerclent pas les entièrement les chromites, il est possible que cette altération débute à basse température. Mais, puisque la lizardite est métastable à haute température (Dungan, 1977), il est aussi possible qu'un évènement d'amphibolitization de courte durée ait causé l'altération. Peu importe le scénario, les serpentinites de la SFZ ont été chauffées quelque peu, soit lors de l'emplacement du Gabbro Rio Boba ou lors de leur montée le long de la SFZ puisque le centre du prisme mantellique est relativement chaud par rapport à sa base près du slab.

Des wehrlites à grenat et à corindon sont trouvées près de la SFZ, dans la partie sud du RSJC. Les compositions roche totale pauvres en éléments compatibles, ainsi que de l'olivine riche en fer ($Fo_{75-82}$) confirment l'origine magmatique. Des compositions pauvres en Zr et les compositions des clinopyroxènes suggèrent une origine dans un environnement de supra-subduction. Abbott et al. (2005) mentionnent que les péridotites à grenat contenant du corindon sont trouvées uniquement dans des veines où l'olivine est localement absente, et sont interprétées comme étant des pegmatites générées à des conditions UHP. Au contraire, nous observons du corindon et de l'olivine dans les mêmes

lames minces, provenant d'échantillons d'évolution magmatique intermédiaire et ne provenant pas de veines. Le corindon forme des inclusions dans les grenats, et ont donc crystallisé avant ou pendant la crystallization des grenats. Le corindon a été formé à des pressions relativement basses, suivis des grenats lors d'un métamorphisme prograde. De plus, l'évidence texturale suggère que le grenat, le corindon et le clinopyroxène ont réagi, produisant des spinelles et un liquide magmatique à des conditions UHP atteintes par métamorphisme prograde.

# ACKNOWLEDGEMENTS

First of all, I would like to thank my thesis supervisor, Dr. Kéiko Hattori, for her constant support, encouragement and availability, and also for her contagious enthusiasm and dedication towards research. Furthermore, I wish to thank Dr. Stéphane Guillot for providing valuable insights throughout this project, and for making me feel like family whilst I was working with him in France. I am extremely grateful for the opportunity given to me by Dr. Hattori and Dr. Guillot to work on spectacular rocks and to visit spectacular places, and for the many laughs and good times we had working together.

This project was funded in part by Natural Science and Engineering Research Council of Canada to Kéiko Hattori and grants under the DYETI program of INSU-CNRS to Dr. Stéphane Guillot. I would like to acknowledge the financial support of the NSERC Graduate Scholarship (ES M), the Ontario Graduate Scholarship, the FQRNT Québec Graduate Scholarship, the University of Ottawa Excellence Scholarship, and Travel Grants from GSAED and FGPS of the University of Ottawa.

This thesis would not have been possible without the valued efforts of many people. Peter Jones provided many hours of help and guidance on the microprobe. Monika Wilk-Alemany provided valuable ICP-MS and laboratory assistance (and made sure I didn't do anything dumb). Ron Hartree provided XRF analyses and help with XRD, and George Mrazek provided thin sections. Dr. Serge Desgreniers took valuable time to discuss Raman spectrometry and allowed me to use his setup. Dr. Mahmood Salman and Dr. Nimal De Silva also provided analytical assistance. Finally, Dr. Olivier Vidal gave insightful thoughts during fieldwork in Dominican Republic. The assistance provided by these people is greatly appreciated.

I wish to thank Drs. Tony Fowler and Brian Cousens for serving on my examination committee (on such short notice). I would like to thank Dr. Fowler in particular. He supervised my B.Sc. project three years ago, and ever since has been nothing less than a mentor whom I could always consult for advice when need be.

Fellow graduate students provided laughs, good times and intellectual support over the past two years. I would especially like to thank my colleagues in office MRN 205, who made coming into the office so enjoyable (yet occasionally unproductive). I would especially like to thank the eternally positive Mark D. Smith for providing insightful advice, comments and guidance that will be helpful for years to come.

On a more personal note, I would like to sincerely thank my mother Lorraine, my father Michel, and my sister Milaine for their unconditional support no matter what I take on. My friends provided many hours of good times, which were welcome breaks from work. Special thanks my fellow members of the band Fashion Bug (Julien, Rudy and Francis) for making summer 2006 so memorable.

Last but not least, I would like to thank Emily for her eternal love and constant support, and I look forward to the adventures that we will share in the very near future.

# TABLE OF CONTENTS

# LIST OF FIGURES

## CHAPTER 1



## CHAPTER 2

**CHAPTER 3**

# LIST OF TABLES

# LIST OF APPENDICES

*- Appendices are found on CD attached to this thesis*

# INTRODUCTION

## SECTION A: THESIS OBJECTIVES

This thesis addresses the origin and distribution of serpentinites exposed in an oceanic subduction complex in northern Dominican Republic, Hispaniola. Serpentinites have long been considered an interesting yet enigmatic and poorly studied rock type because of the apparent lack of geological applications. However, several studies have highlighted the relevance of serpentinite studies in various fields of the Earth Sciences and, in particular, their importance in the geodynamics of subduction zones.

The forearc mantle is known to be extensively serpentinized by fluids released from subducted slabs and sediments (e.g., Hyndman and Peacock, 2003; Brocher et al., 2003), and subduction induced corner flow can bring this forearc serpentinite to great mantle depths. Furthermore, oceanic mantle may be hydrated on the sea floor and later be subducted to great depths with oceanic lithosphere. Because serpentinites are stable up to depths of ~130 km (Wunder and Schreyer, 1997), and can contain up to 13 wt% $H_2O$, they have the potential of carrying significant amounts of water into deep portions of the mantle. The dehydration of serpentinites may produce deep seismic activity in subduction zones (Dobson et al., 2002), and fluids released during serpentinite dehydration are thought to trigger partial melting in the forearc mantle, generating arc magmas at volcanic fronts (Hattori and Guillot, 2003).

Serpentinites are commonly associated with HP-LT (high pressure - low temperature) metamorphic rocks in subduction complexes around the world (e.g., Tsujimori et al., 2006). Notable examples are in the western Alps (Schwartz et al., 2001; Federico et al., 2007), the Ladakh area in the Himalayas (Guillot et al., 2000, 2001), and in the northern Cascades, Washington (Brown et al., 1982). Furthermore, in the Mariana forearc, serpentinites form diapirs containing lawsonite-bearing blueschist (e.g., Maekawa et al., 1993). Such relationships have lead to the elaboration of several models involving the participation of serpentinite in the exhumation of HP-LT rocks (e.g., Guillot et al., 2001; Schwartz et al., 2001; Gerya et al., 2002). Serpentinite, compared to dry mantle peridotite and eclogite, is far less dense, and is therefore relatively buoyant at depth.

This, along with its ductility at higher pressures, may cause the flow of serpentinite towards the surface along the interface between the subducting plate and the forearc mantle (i.e., Serpentinite Subduction Channel, Gerya et al., 2002), and HP rocks may be incorporated during exhumation. These properties of serpentinites are also consistent with their presence along major deformation zones (i.e., San Andreas Fault, Page et al., 1998), where the ductility of serpentinite reduces friction along the fault plane and is thought to be a potential cause of aseismic creep (Irwin and Barnes, 1975).

Therefore, the main objective of this thesis is to determine the origins of serpentinites from northern Dominican Republic. Exposures of the subduction complex have been mapped in considerable detail (Draper and Nagle, 1991; Pindell and Draper, 1991; Abbott et al., 2006), yet little work has been done on the serpentinites, including those from HP-LT (high pressure-low temperature) mélanges and those cropping out along major strike-slip fault zones. Mineralogy, mineral compositions and bulk rock chemistries of serpentinites from different localities are documented and interpreted in order to determine the origin of their protoliths and to constrain metamorphic and geodynamic processes at play during subduction and exhumation in the northern Caribbean.

This thesis also addresses zoning in Cr-spinel, a feature found only in serpentinites cropping out near the Septentrional Fault Zone. Such zoning is rarely reported in forearc serpentinite, and such compositional changes in Cr-spinel are important to understand since spinels are extensively used as petrological indicators. The origin of this feature is determined, and is brought in context with metamorphic processes occurring on these particular serpentinites.

In addition, a preliminary report on garnet peridotites that occur near the Septentrional Fault Zone in the southern part of the Rio San Juan complex is presented. Garnet peridotites, formed at ultra-high pressures (UHP), are common in continental collision zones, yet this is only one of two known occurrences of garnet peridotite in oceanic subduction complexes worldwide and therefore their occurrence is significant. These rocks were first described by Abbott et al. (2001), and Drs. Richard N. Abbott Jr. and Grenville Draper have since published several papers on their paragenesis (e.g. Abbott et al., 2005; 2006; 2007). Their work is mostly based on mineral occurrences, mineral chemistry and P-T conditions. Therefore, bulk rock compositions, along with further mineral analyses and petrography, were carried out during this study in an attempt to constrain the origin of these garnet peridotites.

## SECTION B: THESIS OUTLINE

This thesis is presented as three papers (chapters 1, 2 and 3), all of which were written to address independent themes of this study. This method of presentation involves undesirable redundancies, especially with respect to regional geology and analytical procedures.

Chapters 1 and 2 are papers in preparation for submission to referred journals. Chapter 1 focuses on the origins of serpentinites from northern Dominican Republic, whereas chapter 2 focuses on Cr-spinel zoning. Chapter 3 is a report focusing on the occurrence of garnet peridotite and is not written with intent of publication.

### *STATEMENT OF ORIGINAL CONTRIBUTION*

To my knowledge, this is the first work reporting detailed petrography, bulk rock chemistry and mineral analyses of serpentinites from northern Dominican Republic, and is also the first to determine their protoliths and discuss detailed geodynamic processes associated with their occurrence. As mentioned, garnet peridotites have been previously examined (Abbott et al., 2001; 2005; 2006; 2007), yet this is the first contribution documenting bulk rock chemistry.

This study involved a total of 1 month of fieldwork in Dominican Republic. Prior to my participation in the project, sampling and field study was carried out for a two-week period in February 2005 by Drs. Kéiko Hattori and Stéphane Guillot. I conducted a second round of fieldwork involving further sampling and field study during a two-week period in February 2006.

All geochemical data, mineral analyses, petrological observations, Raman Spectroscopy data, XRD data, along with all interpretations, are the fruits of my original work. All three chapters benefited from edits, comments and suggestions from Dr. Kéiko Hattori. Chapter 1 benefited from edits and comments from Dr. Stéphane Guillot.

# SECTION C: BACKGROUND INFORMATION

This section is meant to serve as a guide to the uninitiated in serpentinite studies, and also provides relevant background information related to material presented in the following chapters. General information on serpentinites and serpentine group minerals is presented, and the possible origins of serpentinite protoliths, along with geochemical concepts used to determine the origins are discussed. Furthermore, the application of Cr-spinel compositions for petrogenetic interpretation is described and finally, a short summary of the tectonic development of the Caribbean is given.

Detailed geology of the subduction complex is provided in chapter 1, section 1.2.

### *SERPENTINITES AND SERPENTINE GROUP MINERALS*

Serpentinites are hydrated ultramafic rocks mostly composed of serpentine minerals. There are three minerals in the serpentine group: lizardite, antigorite and chrysotile, all of which can be described by the general formula $Mg_3[Si_2O_5](OH)_4$. Detailed structural and crystallographic differences between the three serpentine minerals are well established and are discussed in many mineralogy textbooks (e.g., Deer, Howie and Zussman, 1992). Lizardite is by far the most common serpentine mineral (e.g., Deer, Howie and Zussman, 1992; O'Hanley, 1996), yet chrysotile is the most famous one since it forms elongated fibres and was mined for asbestos.

In general, reactions occurring during serpentinization involve the interaction of olivine or pyroxene with water (fluids), and produces serpentine minerals and possibly brucite or talc. The amount and the presence of brucite or talc depend in part on the reaction taking place and the relative proportions of olivine and pyroxene prior to reaction (e.g., Bach et al., 2004). Iron oxides such as magnetite are also produced during serpentinization, because only very little Fe, originally from original olivine and pyroxene, can be taken up by the serpentine structure (e.g., Deer, Howie and Zussman, 1992). Several reactions producing serpentine are well defined and can be found in various papers and textbooks (e.g., O'Hanley, 1996; Bucher and Frey, 2002; Schulte et al., 2006). Finally, serpentinization of peridotite causes an important decrease in density: typical serpentinite has a density of 2600 $kg/m^3$, which is quite low compared to dry peridotite (3300 $kg/m^3$) (Guillot et al., 2001).

The stability of serpentine group minerals during metamorphism has been determined by several workers (e.g., Evans, 1977; Dungan, 1977; Caruso and Chernosky, 1979; Ulmer and Trommsdorff, 1995; Wunder and Schreyer, 1997; Evans, 2004). Serpentine stability is highly dependant on temperature. Lizardite and chrysotile are stable up to temperatures of approximately 300°C and 400°C respectively (Evans, 2004), and are commonly formed during low temperature hydration of peridotite. Lizardite is known to be metastable at higher temperatures (Dungan, 1977). Antigorite is stable up to temperatures of 600°C (Evans, 2004). However, at higher pressures, the stability of antigorite is pressure dependent, and Wunder and Schreyer (1997) have shown that antigorite is stable up to pressures of 44 to 55 kbar, which corresponds to depths between 130 and 160 km. Lizardite is recrystallized to antigorite during prograde metamorphism (e.g. Cerny, 1968; Evans, 2004), and consequently, most metamorphosed serpentinites associated with blueschists and eclogites in tectonic mélanges are composed of antigorite (O'Hanley, 1996).

Determining the mineralogy of serpentine is often difficult with microscopy alone since all three serpentine species (especially lizardite and antigorite) can be similar texturally (O'Hanley, 1996). In this study, Raman Spectroscopy (for in situ analysis of grains; e.g., Groppo et al., 2006; Auzende, 1999) and X-ray diffraction (for bulk mineralogy) are used to precisely determine the mineralogy of serpentine in select samples. Further information on these techniques is available in appendix H (Raman) and appendix I (XRD).

### *Identifying the Origins of Serpentinites in Subduction Complexes*

Precisely determining the origins of the ultramafic protoliths of serpentinites is key in the understanding of geodynamic processes occurring in subduction zones. There are three possible origins (Hattori and Guillot, 2007):

- **Forearc peridotite** hydrated at the base of the mantle wedge by fluids released by the subducted slab and sediments
- **Abyssal peridotite** hydrated on or near the seafloor and later subducted;
- **Ultramafic cumulate rock** from either the forearc or the oceanic crust.

Origins can be determined by primary mineral chemistries and by bulk rock chemistries. In essence, ultramafic cumulates were crystallized from melts generated by the partial melting of a mantle source and therefore have bulk rock compositions

enriched in incompatible elements and depleted in compatible elements. In contrast, forearc and abyssal peridotites are residues (i.e. mantle restites) after partial melting, and consequently have bulk rock compositions relatively depleted in incompatible elements while concentrations in compatible elements remain similar. However, because peridotites are extensively altered by hydration, concentrations in relatively immobile elements such as Ni, Cr, Mg, Al, Si, Ti and Platinum Group elements are used to determine the origins (e.g., Guillot et al., 2001).

Primary silicates, such as olivine and pyroxene, follow the same logic. Because Mg is more compatible than Fe during the partial melting of mantle, Fe is enriched in the melt. Therefore, cumulates commonly contain olivine and pyroxene relatively poor in Mg compared to olivine and pyroxene in mantle residues. For example, olivine from mantle residues typically has compositions between $Fo_{88-93}$ (Arai, 1994). In contrast, olivine from arc cumulates, such as the Quetico Intrusion (Pettigrew and Hattori, 2006), has $Fo_{75-80}$. Unfortunately, the preservation of primary silicates depends on the degree of serpentinization...

Forearc and abyssal peridotites are both mantle residues, yet they can be distinguished from each other because forearc peridotites generally show a higher degree of depletion compared to abyssal peridotites. This is likely related to the liberation of hydrous fluids during the dehydration of forearc serpentinite into the overlying forearc mantle wedge (Ulmer and Trommsdorff, 1995; Hattori and Guillot, 2003). Input of water is known to significantly depress the solidus of silicate systems (e.g., Best and Christiansen, 2001), and as a consequence the forearc mantle is extensively melted. In contrast, partial melting at mid-oceanic ridges is in essence controlled by mantle decompression (e.g., Best and Christiansen, 2001). Therefore, compared to forearc mantle, oceanic mantle is not as extensively melted.

As mentioned, both forearc and abyssal peridotites are mantle residues and therefore would be depleted in incompatible elements. However, one would expect forearc peridotites to be depleted in immobile incompatible elements (i.e., Ti, Al, etc.) more so than abyssal peridotites. The higher degree of depletion of forearc peridotites compared to abyssal peridotite is best observed in a plot of weight ratios of Al/Si vs. Mg/Si (Hattori and Guillot, 2007; see figure 1.7 from chapter 1). During partial melting of an original primitive mantle source, clinopyroxene is preferentially removed in the early stages of melting, followed by a decrease in modal proportions of orthopyroxene (Mysen and Kushiro, 1977; Jaques and Green, 1980; Kubo, 2002). Consequently, mantle residues

initially show lower Al and then lower Si during increasing degrees of partial melting. Abyssal peridotites characteristically have intermediate Al/Si. However, forearc peridotites, because of high degrees of depletion, plot in an array parallel to the Mg/Si axis with very low Al/Si. Mg/Si and Al/Si weight ratios in serpentinites can be compared to those from abyssal and forearc peridotite, since Hattori and Guillot (2007) noted that serpentinization of peridotite does not significantly alter these ratios.

The compositions of primary Cr-spinel can also be used to determine the protoliths of serpentinites, and are discussed at length in the following section.

### *Cr-spinel as a Petrological Indicator in Mantle Residues*

Primary Cr-spinel (or "chromite") compositions (formula $XY_2O_4$, where X = Mg, $Fe^{2+}$ and Y = Cr, Al, $Fe^{3+}$) is a powerful petrological indicator mineral in a wide variety of rock types (e.g., Irvine, 1967; Dick and Bullen, 1984; Barnes and Roeder, 2001). Although it is a minor component of most ultramafic rocks (< 1% volume), it is exceptionally useful for completely serpentinized ultramafic rocks since it is often the only primary mineral preserved after the pervasive hydration of primary silicates.

Cr-spinel compositions are commonly expressed with the following atomic ratios:

- Cr# = Cr / [Cr + Al]
- XMg = Mg / [Mg + $Fe^{2+}$]
- $YFe^{3+}$ = $Fe^{3+}$ / [$Fe^{3+}$ + Cr + Al]

The Cr# of spinel is highly dependant on the degree of melt extraction (e.g., Dick and Bullen, 1984), in essence because Al is incompatible and Cr is highly compatible during melting of the mantle. Consequently, forearc mantle peridotites tend to contain Cr-spinels with very high Cr# compared to abyssal peridotites (e.g., Barnes and Roeder, 2001). For example, Mariana forearc peridotites typically have spinels with Cr# = 0.40 - 0.80 (Ishii et al., 1992) and forearc serpentinites cropping out in Ladakh (NW India, Himalayas) have Cr# between 0.60 and 0.84 (Guillot et al., 2001). In contrast, abyssal peridotites typically have Cr# between 0.15 and 0.55 (e.g., Dick and Bullen, 1984; Michael and Bonatti, 1989).

XMg of spinel decreases with partial melting because the relative activities of Cr and Al have a strong effect on the partitioning of Mg and $Fe^{2+}$ between olivine and spinel (e.g., Dick and Bullen, 1984; Evans and Frost, 1975). Furthermore, lowering equilibrium temperatures has the effect of decreasing Mg content of spinels by re-equilibration with

olivine (e.g., Ozawa, 1983; Okamura et al., 2006). This is often the case for forearc peridotites may be cooled because of their proximity to the cold subducted slab.

High $YFe^{3+}$ has been correlated with high $fO_2$ and oxidizing conditions at the time of equilibration (e.g., Ohara and Ishii, 1998), which can be due to a hydrous environment (Sato, 1978) such as in the forearc mantle wedge. Therefore, forearc peridotites may have high $YFe^{3+}$ (up to ~0.10) because of interaction with slab-derived fluids.

Cr-spinel compositions give valuable information on the origins of serpentinized mantle residues. However, one must consider that primary spinel compositions can be affected by serpentinization and metamorphism. Notably, it has been shown that $Fe^{2+}$ substitutes for Mg slightly during low temperature serpentinization, but more so at greenschist grades, and at higher grades (~ amphibolite), $Fe^{3+}$ substitutes for Al (e.g., Bliss and McLean, 1975; Barnes, 2000), which produces an alteration product called "ferritchromit". For an extensive discussion on the alteration of primary Cr-spinel, I refer you to chapter 2.

### *TECTONIC SETTING OF THE STUDY AREA*

There are currently two opposing models proposing completely different origins for the Caribbean Plate. The first suggests that the plate was formed *in situ* between the North American and South American Plates (Meschede and Frisch, 1998; James, 2006), the second proposes that the Caribbean Plate has an allochthonous origin, suggesting that it was formed originally in the Pacific Ocean and that it migrated between North and South America (e.g., Pindell et al., 1988; Giunta et al., 2006; Pindell et al., 2006). The large majority of the Caribbean geoscientific community appears to have adopted the allochthonous tectonic model (Iturralde-Vinent and Lidiak, 2006). Thus in this section, a short summary of the tectonic development of the Caribbean according to the allochthonous "Pacific Origin" model is presented using the references mentioned above.

The continuing controversy between these two tectonic models is obviously beyond the scope of this work. No personal bias in favour of the allochthonous model is intended in the presentation of this summary. Furthermore, I wish to emphasize on the fact that ALL of the conclusions presented in this thesis are consistent with both tectonic models.

1. **Proto-Caribbean Spreading (Late Triassic - Mid Cretaceous):** After the breakup of Pangea, divergence between North and South America was accommodated by spreading at the Proto-Caribbean Ridge, producing the Proto-Caribbean oceanic

lithosphere. Spreading rates were extremely slow (5-20 mm/yr; Meschede and Frisch, 1998; Pindell et al., 1988). Meanwhile, the Caribbean plate was forming west of its present location in the Pacific Ocean. During the Mid-Cretaceous, the Caribbean Plate was subducting under Proto-Caribbean Lithosphere, and associated arc magmatism formed the Greater Antilles arc (including Hispaniola) on the Caribbean Plate, in the east-central Pacific Ocean.

2. **Switch of Subduction Polarity (Late Cretacous):** The exact date of this is uncertain (100 Ma, Pindell et al., 1988; 80 Ma, Pindell et al., 2006), and the cause of this is currently in doubt as well, yet according to this model there was a switch in subduction zone polarity, with the Proto-Caribbean lithosphere subducting under the Caribbean Plate. Spreading at the Proto-Caribbean Ridge ceased around this time.
3. **Subduction of Proto-Caribbean Lithosphere (Late Cretaceous - Mid Eocene):** The Caribbean Plate migrated east relative to North and South America and "wedged" itself in the space formed earlier by Proto-Caribbean spreading. The Greater Antilles Arc was located at the leading edge of the Caribbean Plate. It is during this time that the rocks exposed in the subduction complex in northern Dominican Republic were subducted.
4. **Collision with the Bahamas Platform (Mid Eocene):** Diachronous oblique collision between the Greater Antilles arc and the Bahamas Platform (North American continental crust) ended subduction along the northern margin of the Caribbean Plate.
5. **Strike-slip motion (Mid Eocene - Modern):** Transpression along the northern Caribbean is accommodated by sinistral strike-slip motion concentrated along major fault zones such as the Septentrional, Camú and Oriente Fault Zones (Mann et al., 1984). The final stages of uplift of the subduction complex also occurred in response to post-Eocene transpression (e.g., Mann and Gordon, 1996).

### *Serpentinites in the Earth Sciences*

In addition to the study of subduction zone geodynamics, serpentinites and serpentinization are relevant in many fields of the Earth Sciences. For example, serpentinization increases the magnetic susceptibility of peridotite, and this can obviously affect marine magnetic anomalies (e.g., O'Hanley, 1996). In addition, serpentinization is

thought to be a potential cause for the abiotic reduction of $CO_2$ producing hydrocarbons in igneous rocks (McCollom and Seewald, 2001), and some workers have suggested that serpentinization may have implications on the origin of life on Earth and possibly Mars (Schulte et al., 2006). Only now are geoscientists realizing the various aspects and applications of serpentinite and serpentinization, and future studies will likely bring forward new and exciting insights and applications.

# CHAPTER 1

# Protrusion of forearc serpentinites along late strike-slip fault zones and exhumation of oceanic serpentinites in a subduction channel, northern Dominican Republic.

***Benoit-Michel Saumur[1], Kéiko H. Hattori[1] and Stéphane Guillot[2]***

1. *Department of Earth Sciences, University of Ottawa, 140 Louis Pasteur, Ottawa, Ontario, K1N 6N5, Canada*
2. *University of Grenoble, OSUG - CNRS, 1381 rue de la Piscine 38041 Grenoble cedex 9, France*

***Manuscript in preparation for submission to a refereed journal***

**ABSTRACT**

Serpentinites from northern Dominican Republic, Hispaniola, are found in a subduction complex formed by the subduction of Proto-Caribbean oceanic lithosphere (North American Plate) under the Caribbean Plate between the Cretaceous and the mid-Eocene. The oblique collision with the Bahamas Platform ended subduction and caused the uplift of the subduction complex and strike-slip deformation. Strike-slip deformation has been concentrated along two major fault zones: the Camù Fault Zone (CFZ) and the Septentrional Fault Zone (SFZ). This contribution focuses on serpentinites from serpentinite-mélanges containing high pressure-low temperature (HP-LT) rocks (central Rio San Juan Complex, RSJC), from lower greenschist grade deformed ophiolites (northern RSJC, Puerto Plata Basement Complex), and from localities near the SFZ and the CFZ. All serpentinites are depleted in incompatible elements, and preserved primary silicates are high in Mg, suggesting that they are mantle residues. Samples from voluminous HP-LT mélanges and low grade deformed ophiolites have bulk rock and primary Cr-spinel compositions suggesting that they were originally abyssal peridotites. This is consistent with the fact that the Proto-Caribbean lithosphere was formed at a slow-spreading ridge, which implies that the subducted slab was rich in abyssal peridotite. HP rocks in the mélanges were likely incorporated with underplated oceanic serpentinite in a subduction channel located along the subduction plane.

Serpentinites from the SFZ and the CFZ are rich in hourglass and flaky lizardite, and show a greater degree of depletion with very low bulk rock Al/Si ratios, high contents in Ir-group PGEs and high Cr# (=atomic ratio of Cr/[Cr+Al]) in spinels (0.48 - 0.67). They are interpreted to be forearc mantle peridotites hydrated at the base of the mantle wedge by fluids derived from the slab. The absence of antigorite suggests that they are from the shallow forearc (< 30 km depth). Serpentinites from the SFZ show evidence for a higher exposure to slab-derived fluids than samples from the CFZ. SFZ serpentinites are higher in fluid mobile Pb and spinels have higher $YFe^{3+}$ (= atomic ratio of $Fe^{3+}/[Cr+Al+Fe^{3+}]$) suggesting higher $fO_2$. Furthermore, lower XMg (= atomic ratio Mg /[Mg + $Fe^{2+}$]) in SFZ serpentinites suggests lower equilibration temperatures due to re-equilibration with olivine before pervasive serpentinization, and in turn implies a position closer to the slab compared to CFZ serpentinites. The occurrence of mantle wedge serpentinites along large scale strike-slip fault zones suggests that the protrusion of serpentinites occurred in response to collision. The fault zones crosscut the forearc at depth and tap a hydrated layer rich in serpentinite most likely located at the base of the

mantle wedge. SFZ serpentinites are closely associated with ultra-high-pressure (UHP) Grt-peridotites, any may have played a role in the late syn-collisional stages of exhumation of these UHP rocks. Serpentinites in subduction complexes are commonly associated with fault zones, and the presence of forearc serpentinite in these fault zones could be a potential explanation for aseismic behaviour.

## 1.1) INTRODUCTION

Recent studies have highlighted the importance of serpentinites in the geodynamics of subduction zones. Serpentinites can hold up to 13% $H_2O$, and may be stable at depths up to 130 km (Wunder and Schreyer, 1997), which makes them an important host of water in the mantle. The dehydration of serpentinites may be responsible for deep seismic activity (Dobson et al. 2002), and partial melting of the mantle causing arc magmatism (Hattori and Guillot, 2003). Serpentinites have low densities (2600 kg/m$^3$) compared to anhydrous peridotites (3300 kg/m$^3$) and eclogites (3500 kg/m$^3$), and are relatively ductile at depth (e.g. Guillot et al., 2001). Furthermore, they are commonly associated with high pressure-low temperature (HP-LT) metamorphic rocks in subduction complexes (e.g., Schwartz et al., 2001; Guillot et al., 2001; Federico et al., 2007) and active convergent margins (i.e. Mariana Forearc, Maekawa et al., 1993), suggesting that serpentinites assist in the exhumation of HP-LT rocks because of their relatively high buoyancy and ductility. Serpentinite-rich subduction channels are thought to play an important role in the exhumation of HP-LT rocks along the subduction plane (Gerya et al., 2002), and such models are supported by the presence of a thick serpentinite layer (~10 km) along the base of the forearc mantle in many subduction zones (e.g. Brocher et al., 2003; Kamimura et al., 2002). Moreover, serpentinites are exposed along major lithospheric strike-slip faults such as the San Andreas fault (Page et al., 1998), and have been proposed to be a potential cause of aseismic creep (Irwin and Barnes, 1975). Serpentinites exposed in subduction complexes have three possible ultramafic protoliths: (i) forearc mantle peridotites hydrated at the base of the mantle wedge by fluids released from slabs and sediments, (ii) abyssal peridotites hydrated on the sea floor and at mid-oceanic ridges, and (iii) hydrated ultramafic cumulates in oceanic lithosphere or in the forearc (e.g. Hattori and Guillot, 2007). Determining the origins of serpentinites is therefore key in the understanding of subduction and exhumation processes occurring in a given subduction zone.

This contribution focuses on the origin of serpentinite occurrences from the oceanic subduction complex exposed in northern Dominican Republic, Hispaniola. We document the distribution of serpentinite in the subduction complex and we determine their protoliths based on mineralogy, bulk rock composition and mineral chemistry. Finally we discuss their contribution to the exhumation of HP-LT rocks, their relationship with syn-collisional strike-slip fault zones, and general implications on subduction zone processes at play along the northern Caribbean Plate margin.

## 1.2) GEOLOGICAL SETTING

The Caribbean Plate was located west of its current position between the Early Jurassic and the Late Cretaceous, and divergence between North and South America was accommodated in part by rifting at the Proto-Caribbean Ridge (Meschede and Frisch, 1998; Pindell et al., 1988). Subduction of the Proto-Caribbean oceanic lithosphere (part of the North American Plate) under the east migrating Caribbean Plate occurred between the Late Cretaceous and the Mid-Eocene and ceased when the Bahamas Platform collided with the trench (Fig. 1.1; e.g. Mann et al., 1991). The oblique collision of the Bahamas Platform produced left-lateral strike-slip deformation zones in northern Hispaniola: the Septentrional and Camù Fault Zones (Mann et al., 1984; Fig. 1.1). Subduction-related rocks are in large part covered by Post-Eocene sedimentary rocks and are only exposed in five inliers in northern Dominican Republic (Fig. 1.1). The Pedro Garcia and Palma Picada inliers are essentially comprised of arc igneous rocks (Lewis et al., 1990), and the Samaná Peninsula Complex is composed of marble and blueschist-bearing calc-schists (Joyce, 1991).

Our study area (Fig. 1.2) includes the Puerto Plata Basement Complex and the Rio San Juan Complex. The Puerto Plata Basement Complex consists of variably brecciated and sheared serpentinite, tectonized harzburgite, gabbro and volcanic rocks, and is interpreted as a deformed ophiolitic complex (Pindell and Draper, 1991). Sheeted diabasic dykes are not observed, but brecciated serpentinites commonly contain altered gabbroic clasts. The Rio San Juan Complex was mapped in detail by Draper and Nagle (1991), and we refer to the unit names given by these workers throughout this paper. These workers recognized a general increase in metamorphic grade from north to south. The northern part of the Rio San Juan Complex is composed of brecciated and massive serpentinites of low metamorphic grade known as the Gaspar Hernandez Serpentinites, which are similar to serpentinites near Puerto Plata. The central part of the complex is comprised of

retrograded blueschists and eclogites. These high-pressure rocks are intruded by two serpentinite mélanges which contain meter scale blocks of blueschists, eclogites and metamorphosed felsic rocks aligned with a sub-vertical foliation: the Jagua Clara Mélange and Arroyo Sabana Mélange. The southern part of the complex consists of the Cuaba Amphibolites and the Rio Boba Gabbro, which intrudes into the Cuaba Amphibolites. These units were attached to the northern and central parts of the Rio San Juan Complex by strike-slip faulting during subduction (Draper and Nagle, 1991). The Cuaba Amphibolites originated from oceanic gabbros (Abbott et al., 2005) and part of the unit contains retrograded eclogites and lenses of garnet peridotite (Abbott et al., 2005; 2006).

Serpentinites in the southern part of the Rio San Juan area occur near the major deformation zones defined by the intersection of the Septentrional and Bajabonico Faults (Draper and Nagle, 1991). Serpentinites in the Lomá Quita Espuela area form massive, locally faulted, lenses between 100 to 500 meters in length within the Cuaba Amphibolites. Foliation in the Cuaba Amphibolites wraps around the lenses, suggesting that the serpentinites were emplaced during the ductile deformation of the Cuaba Amphibolites. Furthermore, large (up to 2 m) serpentinite boulders were found together with boulders of garnet peridotite and eclogite in the narrow (< 6 m) and shallow (<30 cm) stream of Rio Cuevas. The distribution of serpentinite boulders is restricted to a narrow zone in the stream, and serpentinites cannot be transported great distances because they are highly susceptible to physical weathering. Therefore, they were most likely derived from proximal sources, although outcrops of serpentinites were not identified near Rio Cuevas because of dense vegetation.

The Camù Fault Zone marks the northern boundary of the Rio San Juan Complex, where the fault widens into an array of splay faults, and the southern boundary of the Puerto Plata Basement Complex (Fig. 1.2). A horizontal strike-slip displacement of greater than 60 km is suggested along the Camù Fault, assuming the Puerto Plata and Rio San Juan Complexes were once continuous (Pindell and Draper, 1991; Draper and Nagle, 1991). A greater displacement (> 200 km) was suggested along the Septentrional Fault Zone since rocks similar to northern Hispaniola occur in Cuba (Mann et al., 1984; Draper and Nagle, 1991). The fault zones in Northern Hispaniola form a gentle restraining bend, which allowed the uplift of the assembled complexes during Plio-Pleistocene transpression (Mann et al., 1991; Mann and Gordon, 1996).

## 1.3) SAMPLING AND ANALYTICAL PROCEDURES

Serpentinite samples were collected along the CFZ (RD9A, RD18b, RD6-80, RD6-81), and in the "northern terranes" which are cut by the CFZ, in the Puerto Plata Basement Complex (RD31, RD4, RD6a) and the Gaspar Hernandez Serpentinites of the Northern Rio San Juan Complex (RD8b) (Fig. 1.2). Serpentinites from the northern terranes and the CFZ are texturally similar in the field, and thus no distinction is made in the literature. In the central Rio San Juan Complex, 2 samples were taken from the Arroyo Sabana Mélange (RD87, RD89) and 6 from the Jagua Clara Mélange (RD21a, RD91, RD94, RD6-50c, RD6-52a and RD6-54a) (Fig. 1.2). In the southern part of the Rio San Juan Complex, near the Septentrional Fault Zone, 5 serpentinite samples were collected from large (~100 m) outcrops (RD34a, RD34c, RD68, RD6-36a, RD6-36c) in Lomá Quita Espuela. Furthermore, 3 serpentinite boulders were sampled in the stream of Rio Cuevas (RD45, RD48, RD60)

Mineral compositions were determined using an automated 4 spectrometer CAMEBAX MBX electron probe (Carleton University) by the wavelength dispersive X-ray analysis method (WDX). Counting times were 15 seconds per element, except for Fe (20 s) and Ni (40 s). A 15 kV accelerating potential and a 20 nA beam current were applied. The calibration standards used were pure wollastonite (Si, Ca), synthetic spinel (Al), synthetic $Cr_2O_3$ (Cr), forsterite (Mg), synthetic $MnTiO_3$ (Mn, Ti), pure vanadium metal (V), albite (Na), fayalite (Fe in silicates) and synthetic $Fe_2O_2$ (Fe in oxides). $Fe_2O_3$ contents of spinel were determined assuming that stoichiometry is respected.

Major and minor element concentrations were determined at the University of Ottawa, using a Phillips PW 2400 X-ray fluorescence spectrometer after fusing bulk rock powder with a flux composed of 78.5% lithium tetraborate ($Li_2B_4O_7$) and 21.5% lithium metaborate ($LiBO_2$). S and Cu were determined using a VISTA-PRO ICP-AES after digesting samples in aqua regia (3 HCl : 1 $HNO_3$). Platinum group element (PGE) concentrations were determined by isotopic dilution techniques using a mixed spike of $^{101}Ru$, $^{105}Pd$, $^{190}Os$, $^{191}Ir$ and $^{194}Pt$. PGEs were pre-concentrated in a Ni-sulphide bead which was dissolved in 6N HCl, and the filtrate was dissolved in concentrated $HNO_3$. Mass ratios were determined using an Agilent HP 4500 inductively coupled plasma mass spectrometer (ICP-MS; University of Ottawa). Blanks were 0.002-0.007 ng Ir/g flux, 0.002-0.006 ng Os/g flux, 0.07-16 ng Pt/g flux and 0.03-0.9 ng Pd/g flux and 0.002-0.007 ng Ru/g flux. These values are negligible compared to amounts in samples and thus blank corrections were not

applied to the results. Rock references MRG-1 and JP-1 were used to evaluate the accuracy of the analyses.

Lead concentrations* were determined by ICP-MS (University of Ottawa) after digestion of samples with a HF-$HNO_3$ mixture.

The identification of in-situ individual serpentine grains was carried out at the University of Ottawa (Department of Physics) using micro-Raman spectroscopy techniques (Fig. 1.3) using a frequency doubled Nd: YAG laser at a wavelength of 532 nm. Analysed areas were approximately 10 microns in diameter. Our methodology is similar to those described by Groppo et al. (2006) and Auzende (1999). X-Ray powder diffraction using a Phillips X'PERT X-ray diffractometer (University of Ottawa) was used to determine the mineralogy of bulk samples (Fig. 1.4).

## 1.4) PETROLOGY OF SERPENTINITES

### *1.4.1) Serpentine mineralogy and Mineral assemblages*

Serpentinites from the SFZ, CFZ and the northern terranes are completely hydrated (~13 wt% LOI; Table 3) and are composed of pseudomorphic locally foliated fine grained flaky lizardite with hourglass texture, minor magnetite and trace diopside. No antigorite was detected in Raman spectra or X-Ray powder diffraction patterns (Fig. 1.3-1.4). Some samples from Lomá Quita Espuela (SFZ) contain fine grained talc, blady tremolite and rare cummingtonite. Tremolite and cummingtonite are stable in amphibolite facies conditions in ultramafic rocks (e.g., Evans, 1977), suggesting that localized amphibolitization occurred. Lizardite is known to be metastable at amphibolite grades (Dungan, 1977).

Samples from the mélanges from the central Rio San Juan Complex are also totally hydrated (11% LOI; Table 3), and are composed of blades of interpenetrating antigorite and variable amounts of fine grained magnetite (Fig. 1.3B). Sample RD94 shows remnants of a lizardite hourglass texture. In all other samples, antigorite blades are penetrative with non-pseudomorphic textures, and are therefore interpreted to replace earlier formed lizardite. Some samples also contain variable amounts of well-crystallized chlorite, talc and tremolite (Fig. 1.4), and together with antigorite suggest blueschist to

* Multiple runs to determine Pb were carried out. Unfortunately, reproducibility was variable, especially for samples with higher concentrations (see appendix B.4 for detailed results). Pb data is presented nonetheless since is used for qualitative comparisons only (see section 1.6.4). Future work will involve precise determination of Pb contents with a $Pb^{204}$ spike.

amphibolite facies conditions. (e.g., Evans, 1977). Veinlets of tremolite and chlorite occur in RD94, which are considered to be reaction products between mafic blocks and the serpentinite matrix in the mélange during blueschist metamorphism (Draper and Nagle, 1991).

### *1.4.2) Chromian spinel*

In serpentinites from the northern terranes and the CFZ, primary Cr-spinel grains are large (1- 3 mm), are subhedral to anhedral and are rimmed by magnetite. Cores of spinels from the CFZ have Cr# (= atomic ratio of Cr/[Cr+Al]) between 0.47 and 0.69 and XMg (= atomic ratio of $Mg/[Mg+Fe^{2+}]$) between 0.62 and 0.50, and generally fall within the field of forearc peridotite (Table 1.1; Fig. 1.5). Furthermore, they have very low $YFe^{3+}$ (= atomic ratio of $Fe^{3+}/[Fe^{3+}+Cr+Al]$) contents (< 0.04; Table 1; Fig. 1.5B). Samples from the northern terranes generally plot in the fields of abyssal peridotites. Samples RD4 and RD6a have low Cr# values (0.20 -0.40), whereas samples RD31 and RD8b have moderate Cr# (~ 0.53) and higher $YFe^{3+}$ (0.04 - 0.11), similar to abyssal plagioclase peridotite.

In serpentinites from the SFZ, anhedral to subhedral grains of Cr-spinel (0.5-2 mm) are commonly rimmed by magnetite or intertwined chlorite and magnetite. Spinels often show gradational zoning with greater amounts of Cr, $Fe^{2+}$ and $Fe^{3+}$ towards the rims*. Primary compositions are preserved in cores of spinels from samples RD34c, RD68, RD45, RD48 and RD6-36a: compositions of spinels within these samples are similar with low $TiO_2$ (< 0.21 wt%) and low $YFe^{3+}$ (0.03 - 0.10). Spinels from the SFZ have similar Cr# as CFZ spinels (0.48 - 0.67) but with relatively low XMg (0.50 - 0.40). Therefore SFZ and CFZ spinels have distinct trends in the XMg vs. Cr# diagram (Fig. 1.5A). Furthermore, the values of $YFe^{3+}$ in SFZ spinels are higher than in those from the Camù Fault Zone and are similar to those from harzburgites and dunites from the Mariana Forearc (Ishii et al., 1992).

In the Arroyo Sabana and Jagua Clara Mélanges, Cr-Spinel grains are, in most cases, altered to ferritchromite or aggregates of fine grained Cr-bearing magnetite. RD89 and RD94 contain Cr-spinels, but they are altered to have highly variable compositions within samples. Their compositions are therefore not listed in this paper.

---

* Note to reader: These are the subject of chapter 2

### *1.4.3) Olivine and Orthopyroxene*

Primary silicates are rarely preserved. Olivine is commonly replaced by pseudomorphic hourglass lizardite and fine-grained magnetite, and orthopyroxene is replaced by 1-2 mm pseudomorphic lizardite bastites. When preserved olivines and occasionally orthopyroxenes have mesh textures with lizardite, which confirms that these silicates are indeed primary. Olivines have high Mg content ($Fo_{89-90.8}$), and orthopyroxenes are high in the enstatite component ($En_{89.4-91.1}$) and are low in $Al_2O_3$ (< 2.23 wt%; Table 1.2). Such compositions are consistent with a primary origin for olivine and orthopyroxene.

## 1.5) BULK ROCK COMPOSITIONS

### *1.5.1) Major Elements*

All samples from northern Dominican Republic have refractory bulk rock compositions with low contents of immobile incompatible elements, such as Al, Ti and V (Table 1.3, Fig. 1.6). Most samples are high in immobile refractory elements, such as Ni (>2000 ppm) and Cr (>2200 ppm). Bulk rock Mg# (= atomic ratio of $Mg*100/[Mg+Fe_{total}]$) is high, ranging between 88.0 and 91.0, and CaO is low (<1 wt %) for most samples. Ca is known to be mobile because clinopyroxene is dissolved in saline fluids during serpentinization (Allen and Seyfried, 2003). However, low CaO, along with low $Al_2O_3$, high Mg# and high Cr suggests that most samples were initially dunites or harzburgites. RD6-52a and RD6-54a are exceptions: they have low bulk Mg# (86.7 - 87.2) and high Ca (~3.0 wt %) which suggests that they were originally lherzolites. The data suggest that all samples are residues from mantle partial melting.

Based on bulk rock compositions, serpentinites from the SFZ and CFZ are more refractory than samples from central RSJC and the northern terranes. They are on average higher in MgO (average of 37.5 wt %) compared to other samples (average 36.1 wt%) and lower in $Al_2O_3$ contents (< 0.75 wt %) compared to samples from the central RSJC mélanges and the northern terranes (between 1.0 and 3.0 wt %). This is best illustrated in a diagram of Al/Si vs. Mg/Si weight ratios (Hattori and Guillot, 2007; Fig. 1.7). Clinopyroxene is preferentially removed in the early stages of partial melting, followed by orthopyroxene (e.g., Kubo, 2002). Consequently, during increasing degrees of partial melting, residual mantle peridotites initially show lower Al, then lower Si compared to primitive mantle values, which results eventually in a vertical array along the Mg/Si axis.

Samples from near the SFZ and CFZ have such a vertical array at low Al/Si and plot in the forearc peridotite field, whereas samples from the central RSJC mélanges and the northern terranes are less depleted and plot in the field of abyssal peridotites (Fig. 1.7).

### *1.5.2) Platinum Group Elements*

Iridium-group PGEs (Ir, Os and Ru) remain in the mantle residue during partial melting as opposed to the relatively incompatible Pd-group PGEs (Pt, Pd and Rh) (e.g., Brenan et al., 2005). All samples, with the exception of RD94, have flat to Ir-group PGE enriched primitive-mantle normalized spectra (Fig. 1.8). The data confirm that they are all mantle residues. The slightly high contents of Pd-group PGEs in some samples may be due to their mobility in aqueous fluids (Hinchey and Hattori, 2005; Hattori and Cameron, 2004). Sample RD94 contains exceptionally high Pt and Pd, which may be related to late veinlets containing tremolite and chlorite.

Samples from the SFZ and the CFZ have Ir-group PGE concentrations higher than primitive mantle values (Fig. 1.8A). This is difficult to explain when invoking partial melting alone, yet it is consistent, along with low Cu, with the highly refractory nature of these serpentinites. Samples from the northern terranes plot very close to primitive mantle values with unfractionated PGE patterns, suggesting that they are mantle residues that underwent minor degrees of partial melting (Fig. 1.8B). Samples from the Arroyo Sabana and Jagua Clara Mélanges show the most fractionated PGE patterns with low contents of Pd-group PGEs (Fig. 1.8B). There does not appear to be a correlation between IPGE and S contents, suggesting that sulphides are not major carriers of PGEs.

## 1.6) DISCUSSION

### *1.6.1) The Origins of the serpentinites*

A cumulate origin for serpentinites in this study can be negated because all samples are depleted in incompatible elements and rich in refractory elements (Figs. 1.6-8, Table 1.3), and primary olivine and orthopyroxene are rich in Mg (Table 1.2). In contrast, these suggest that the serpentinites were initially mantle residues. Serpentinites from the central RSJC mélanges and the northern terranes have moderately depleted bulk rock compositions similar to abyssal peridotites, whereas serpentinites near the SFZ and the CFZ have highly refractory bulk rock compositions with very low $Al_2O_3$ and $TiO_2$, and plot in the field of Mariana forearc peridotites (Fig. 1.7). High values of Cr# for spinel also support a highly depleted source for serpentinites from the SFZ and the CFZ, as

Cr# increases in residues with increasing degrees of partial melting (e.g. Dick and Bullen, 1984).

In some samples, spinel compositions plot in the zone where abyssal and forearc peridotite compositional fields overlap (Fig. 1.5A). Such is the case for samples RD6-81 and RD18b from the Camù Fault Zone. However, these serpentinites are most likely forearc peridotites because such high Cr# are found only in abyssal peridotites formed at fast-spreading ridges (i.e., East Pacific Rise, Niu and Hékinan, 1997). The Proto-Caribbean lithosphere was produced at the Proto-Caribbean ridge, which had a very slow spreading rate between 0.5 and 2 cm/yr (Meschede and Frisch, 1998). Abyssal peridotites formed at such slow-spreading ridges commonly have Cr# lower than 0.40 (i.e., Atlantic Mid-Oceanic Ridge, Michael and Bonatti, 1989). A mantle wedge origin for samples RD6-81 and RD18b is further supported by very low Al/Si ratio (Fig. 1.7) and high Ir-group PGE contents (Fig. 1.8). Cr-spinel in samples RD8b and RD31 from the northern terranes also have high Cr# values and plot in the zone of overlap in figure 1.5A. Such spinels with high Cr# and $YFe^{3+}$ are encountered in abyssal plagioclase peridotites which form approximately 30% of all abyssal peridotites encountered on the sea floor (Dick and Bullen, 1984). Furthermore, bulk rock compositions (Fig. 1.6-7) and unfrationated PGE patterns (Fig. 1.8) are consistent with an abyssal peridotite protolith. No plagioclase is observed in these samples, but any plagioclase initially present was likely in very small amounts (< 2%, Dick and Bullen, 1984) and obliterated during hydration.

Serpentinites associated with late strike-slip fault zones originated from the mantle wedge. Their compositions are similar to serpentinites from the Zaza deformation zone in Cuba (Hattori and Guillot, 2007) and the Puerto Rico Trench (Bowin et al., 1966). They all have similar Mg/Si ratios (Fig. 1.7), and similar Cr# in spinels (~0.56 for Cuba; ~0.55 for the Puerto Rico Trench). These similarities are expected because they were formed in the same subduction system (Draper and Nagle, 1991). In addition, northern Caribbean serpentinites have relatively low Mg/Si ratios (Fig. 1.7) and spinels with moderate Cr# compared to peridotites from the Mariana Forearc (Cr# up to 0.82, Ishii et al., 1992, Fig. 1.5) and forearc serpentinites from Ladakh, Himalaya (Cr# up to 0.84, Guillot et al., 2001), suggesting that the northern Caribbean mantle wedge was relatively fertile.

### *1.6.2) Hydrated abyssal peridotite associated with high pressure rocks*

The Proto-Caribbean lithosphere, which formed at a slow-spreading ridge, likely contained high proportion of hydrated abyssal peridotites similar to Atlantic lithosphere (Cannat et al., 1995; Mével, 2003). The majority of serpentinites in the Puerto Plata Basement Complex and the Rio San Juan Complex (i.e. Gaspar Hernandez Serpentinites, the Arroyo Sabana Mélange and the Jagua Clara Mélange) originated from abyssal peridotites of the Proto-Caribbean lithosphere. The interpretation is in accord with abundant metabasites and metamorphosed gabbros in the Puerto Plata Basement Complex and the Rio San Juan Complex (Pindell and Draper, 1991; Draper and Nagle, 1991): the subduction complex is in large part dominated by oceanic rocks derived from the Proto-Caribbean Lithosphere.

In the Arroyo Sabana and Jagua Clara Mélanges, lizardite is overprinted by non-pseudomorphic antigorite, which is characteristic of progressive metamorphism of serpentinite and the onset of blueschist conditions (O'Hanley, 1996; Evans, 1977). Antigorite is the predominant serpentine species in HP-LT mélanges worldwide (e.g., O'Hanley, 1996) since it is the only serpentine mineral stable at temperatures higher than 400°C (e.g. Evans, 2004); its occurrence is therefore consistent with its association with HP blueschists and eclogites. Furthermore, amphibolitization in the central RSJC is not only recorded in serpentinites but also in eclogites from the mélanges (Schertl et al., 2006). The evidence suggests that serpentinites and HP rocks have similar thermal histories.

Schertl et al. (2006) suggested that the mélanges were formed in a serpentinite-rich subduction channel based on P-T paths of eclogites and blueschists included in the mélanges. Recent models have shown that the genesis of serpentinite mélanges is related to subduction channels located along the subduction plane formed in large part of hydrated forearc peridotite incorporated from the hanging wall of the subduction zone (e.g., Gerya et al., 2002). In contrast, our data suggest that the subduction channel in northern Dominican Republic is composed at least in part of hydrated abyssal peridotite. This is not unique to Dominican Republic, since oceanic serpentinites are associated with HP rocks in the western Alps (i.e., Monviso, Lagabrielle and Cannat, 1990). Furthermore, numerical models by Gorczyk et al. (2007) show that the subduction of oceanic lithosphere generated at slow spreading ridges produces a funnel-shaped serpentinite channel consisting of accreted (underplated) hydrated abyssal peridotite containing fragments of mafic oceanic crust. Our results for the central RSJC mélanges are

consistent with such models, and highlight that oceanic serpentinite can contribute to the exhumation of HP-LT rocks.

For the serpentinite occurrences in the northern terranes, our findings are in agreement with interpretations by Pindell and Draper (1991) and Draper and Nagle (1991), which suggest that serpentinites from the Puerto Plata Basement Complex and the Gaspar Hernandez Unit have an oceanic origin. They are dominated by low temperature lizardite and magnetite, and primary Cr-spinels are relatively fresh suggesting that they were buried at most to lower greenschist conditions.

### *1.6.3) Hydration of forearc peridotites at shallow levels*

Lizardite is the dominant serpentine species in mantle wedge serpentinites from the SFZ and the CFZ and no evidence of antigorite is present. This finding is surprising because SFZ serpentinites are spatially associated with HP-eclogites and UHP-Grt peridotites in the Cuaba Amphibolite and antigorite is usually the reported serpentinite species from mantle wedge serpentinites associated with HP rocks (e.g., O'Hanley 1996). Lizardite is stable at LT and up to temperatures of 300°C (O'Hanley 1996; Evans, 2004), whereas antigorite is stable at temperatures as low as 250°C (e.g. Evans, 2004) and is commonly preserved (is metastable) at LT conditions (such as in the central RSJC mélanges). We therefore interpret that serpentinites from the SFZ and the CFZ were never brought to HP conditions because, if initially present, antigorite would have persisted at LP-LT conditions.

Lizardite or chrysotile have been reported as the major constituent of several serpentinites in the Mariana forearc (Ohara and Ishii, 1998; D'Antonio and Kristensen, 2004) which were formed at depths of up to 25-30km (e.g. Fryer et al., 1999) and at temperatures below 300°C (Benton et al., 2001). Hydration at shallow depths, < 25 km, is also proposed for forearc serpentinites in the Ladakh subduction complex based on the presence of As(V) (Hattori et al., 2005). The evidence suggests that mantle wedge serpentinites near the Septentrional and Camù Fault Zones were hydrated at the base of the mantle wedge at low temperatures and at shallow depths. This interpretation is supported by a low geothermal gradient in the subduction zone based on the P-T estimates of metamorphic rocks from the Samaná Peninsula (e.g., Zack et al., 2004; Escuder-Viruete and Pérez-Estaún, 2006).

### *1.6.4) Different forearc sources for SFZ and CFZ serpentinites*

Cr-spinels from SFZ serpentinites have lower XMg than spinels from the CFZ for a given Cr# (Fig. 1.5A). Lower XMg values in Cr-spinel are associated with lower equilibrium temperatures with olivine at sub-solidus conditions (e.g. Evans and Frost, 1975) and also with cooling of the forearc mantle near the slab interface from input of slab derived fluids (Ohara and Ishii, 1998; Okamura et al., 2006). Assuming that the modal proportions of Cr-spinel are similar everywhere in the forearc mantle, we interpret the lower XMg of SFZ serpentinites to record cooling before pervasive serpentinization.

SFZ serpentinites are higher in $YFe^{3+}$ (Fig. 1.5B), which reflect higher $fO_2$ and therefore a higher exposure to slab-derived fluids. Furthermore, Pb is one of well-known fluid-mobile elements in subduction zones (e.g., Hofmann et al., 1986), it is highly soluble in aqueous fluids at low temperatures, < 150°C (Hanor, 1979), and is enriched in serpentinites at the base of mantle wedges at shallow depths (Hattori and Guillot, 2003). Serpentinites from the SFZ are much higher in Pb (0.68 - 2.9 ppm) than serpentinites from the CFZ (0.02 - 0.21 ppm).

These differences in composition can be explained by origins from different domains in the forearc mantle. The protoliths of SFZ serpentinites were probably in a position very close to the slab, which is consistent with lower temperatures of equilibration and an exposure to large amounts of slab-derived fluids. In contrast, the protoliths of CFZ serpentinites may have been in a position farther away from the subduction plane. The differences in composition could also be due to longer lasting fluid inputs on SFZ serpentinites. Serpentinization in the mantle wedge is known to be heterogeneous, since it depends in part on the amount of fracturing in the mantle wedge (e.g., Hyndman and Peacock, 2003) and on the lithology of the subducting slab (Rüpke et al., 2004).

### *1.6.5) Protrusion Of Forearc Serpentinites Along Strike-Slip Fault Zones*

The spatial association of mantle wedge serpentinites with the strike-slip faults zones suggests that the protrusion of these serpentinites occurred in response to the collision with the Bahamas Platform and that the fault zones directly tap the base of the forearc mantle wedge at depth. The proposed interpretation is supported by several lines of evidence. Mann et al. (1991) suggested that the Late Cretaceous subduction zone was NW-SE trending based on the structural study of schists and the overall distribution of arc and oceanic terranes in northern Hispaniola. The Septentrional and Camù Fault Zones,

trending between 090° and 110° (Mann et al., 1984), crosscut this primary geometry (Figs. 1.9-10; Mann et al., 1991). Strike-slip faulting juxtaposed the Pedro Garcia arc terrane with low grade oceanic rocks of the Puerto Plata Basement Complex (Fig. 1.10). More importantly, the fault zones cutting both accretionary and arc terranes implies that they likely tap the forearc mantle at depth (Fig. 1.9). Additional evidence supporting the protrusion of forearc mantle serpentinites is the foliation in the Cuaba Amphibolites wrapping around serpentinite lenses in Lomá Quita Espuela, which suggests that the protrusion of serpentinites occurred during ductile strike-slip deformation of the Amphibolites. In addition, the Camù Fault Zone cuts the once-continuous Puerto Plata Basement Complex and the Rio San Juan Complex, both of which are oceanic. The likeliest scenario for protrusion of mantle wedge material between two oceanic terranes is for the fault to directly tap the mantle wedge, allowing the protrusion of mantle wedge along its strike (Fig. 1.10). Finally, SFZ and CFZ serpentinites preserve evidence of exhumation from different mantle domains, which is consistent with the interpretation that the fault zones directly tap distinct areas in the shallow mantle wedge.

Occurrences of serpentinites and ultramafic rocks along strike-slip fault zones are known in other subduction and collision zones. For example, in New Zealand, Williams et al. (2006) reported a large ultramafic body that protruded along a major suture zone formed by strike-slip deformation. However, the best example of protrusion of serpentinites is in the Mariana forearc where serpentinites rise as diapirs along faults which cross-cut the forearc (e.g., Fryer et al., 1999). We envision a similar scenario for serpentinites along major faults in northern Dominican Republic, with the notable difference that the generation of strike-slip fault zones and serpentinite protrusions are generated in response to post-subduction transpression.

Blueschist clasts have been reported in fault-gouge zones in the Gaspar Hernandez serpentinites (Weyl, 1941; Draper and Nagle, 1991) and also in the Barabas Mélange Unit in the southern part of the Puerto Plata Basement Complex near the CFZ (Pindell and Draper, 1991). Furthermore, a close spatial association between SFZ serpentinites with HP and UHP rocks in a restricted zone in Rio Cuevas is noted. These relationships suggest that the protrusion of forearc serpentinites along the fault zones was contemporaneous with and may have contributed to the late stages of exhumation of HP and UHP metamorphic rocks during collision, either by lubricating the fault zones or by entraining exotic blocks during protrusion.

Despite the presence of serpentinite, there is considerable yet discontinuous seismic activity along the Septentrional, Camù and Puerto Rico Trench Fault Zones (Mann et al., 1984). However, along the San Andreas fault, numerous bodies of serpentinites occur (Page et al., 1998) and its northern termination in Oregon is near the Cascadia margin where serpentinized forearc is highlighted (Brocher et al., 2003). It is therefore possible that forearc serpentinite protruded along the San Andreas fault, which would reduce friction in the fault zone and could therefore be a potential cause for the well documented aseismic behaviour of the fault.

## 1.7) CONCLUSIONS

Two types of serpentinite are recognized in the subduction complex of northern Dominican Republic: hydrated abyssal peridotites and hydrated forearc mantle wedge peridotites. The former occurs in HP-LT serpentinite mélanges and low grade serpentinite terranes. Voluminous occurrence of serpentinites of abyssal peridotite origin suggests abundant peridotites in the subducted Proto-Caribbean slab, which is consistent with the formation of the subducted oceanic plate at a slow-spreading ridge. Mélanges containing clasts of HP rocks likely represent a subduction-channel developed during the subduction of Proto-Caribbean oceanic lithosphere, and these results highlight that oceanic serpentinite may play an important role in the exhumation of HP rocks.

Highly refractory hydrated forearc mantle wedge peridotites occur along major strike-slip fault zones that formed during collision of the Bahamas Platform. Forearc serpentintes were hydrated at the base of the mantle wedge at shallow levels, and their association with late strike-slip faults shows that ductile serpentinites from different mantle domains were brought to the surface from the base of the mantle wedge along the SFZ and CFZ. Such an occurrence of mantle wedge serpentinite, to our knowledge, has not yet been reported in other subduction complexes. Serpentinites are reported along major faults in other subduction zones and therefore protrusion of mantle wedge serpentinites may in fact be a common process for the exhumation of forearc material and be important in the late stages of exhumation of metamorphic rocks and the seismic behaviour of fault zones.

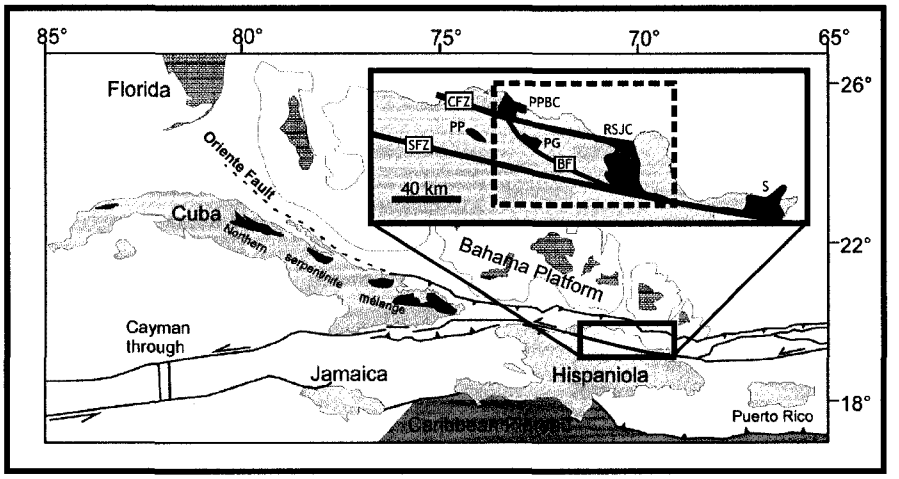


**Figure 1.1:** Map of the Greater Antilles and the northeastern Caribbean plate margin (modified from Dolan et al., 1998). The inset is a zoomed in view of northern Hispaniola and the inliers exposing pre-Mid-Eocene rocks from the subduction complex (modified from Draper and Nagle, 1991). The dashed box indicates the study area (see Fig.1.2). PPBC: Puerto Plata Basement Complex; RSJC: Rio San Juan Complex; S: Samaná Peninsula Complex; PG: Pedro Garcia; PP: Palma Picada; CFZ: Camù Fault Zone; BF: Bajabonico Fault Zone; SFZ: Septentrional Fault Zone (see text for description).

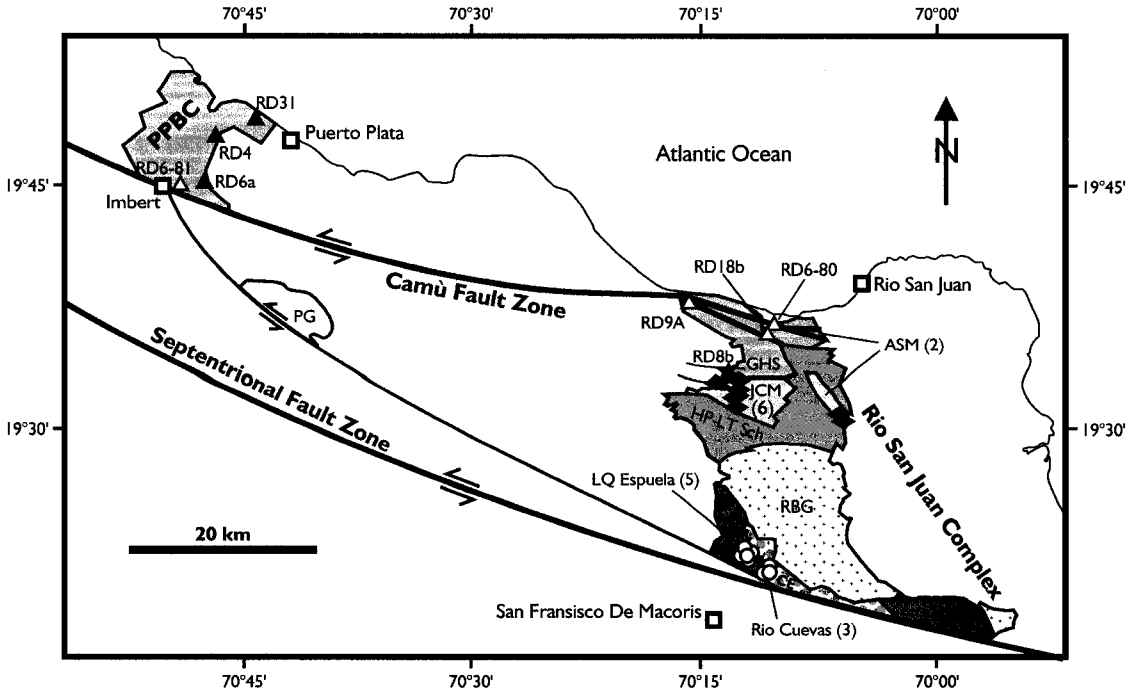


**Figure 1.2:** Simplified geology of inliers in the study area which expose Cretaceous to mid-Eocene rocks formed as a result of subduction: The Rio San Juan Complex, the Puerto Plata Basement Complex (PPBC) and the Puedro Garcia inlier (PG). In the area, most of the strike-slip motion has been concentrated along the Septentrional (SFZ) and Camù (CFZ) fault zones. The locations of studied serpentinite samples are shown: **(1)** white triangles represent samples found along the CFZ including near splay faults at the northern edge of the Rio San Juan Complex; **(2)** filled triangles represent samples taken in the Northern Terranes of low metamorphic grade that are cut by the CFZ (the PPBC and the Gaspar Hernandez Serpentinites (GHS)); **(3)** Dark losanges indicate serpentinites from the Arroyo Sabana Mélange (ASM) and the Jagua Clara Mélange (JCM); **(4)** white circles represent serpentinites sampled near the SFZ in both the Lomá Quita Espuela (5 samples) and Rio Cuevas (3 samples) areas. Symbology is consistent throughout this manuscript. For samples from JCM, Lomá Quita Espuela and Rio Cuevas, sample locations overlap at the scale of the map and therefore positions are slightly shifted on the map. Other units shown are the Rio Boba intrusive suite (RBG), the Cuaba Amphibolites (CA) and a particular zone in the Cuaba Amphibolites which contains eclogite and UHP-Garnet Peridotites (CE). The rest of the study area is covered by Late-Eocene, Neogene and Quaternary sedimentary rocks. The map is modified from Mann et al. (1991), de Zoeten et al. (1991); Lewis et al, (1990); Pindell and Draper, (1991); Draper and Nagle, (1991) and Abbott et al. (2006). See text for discussion.

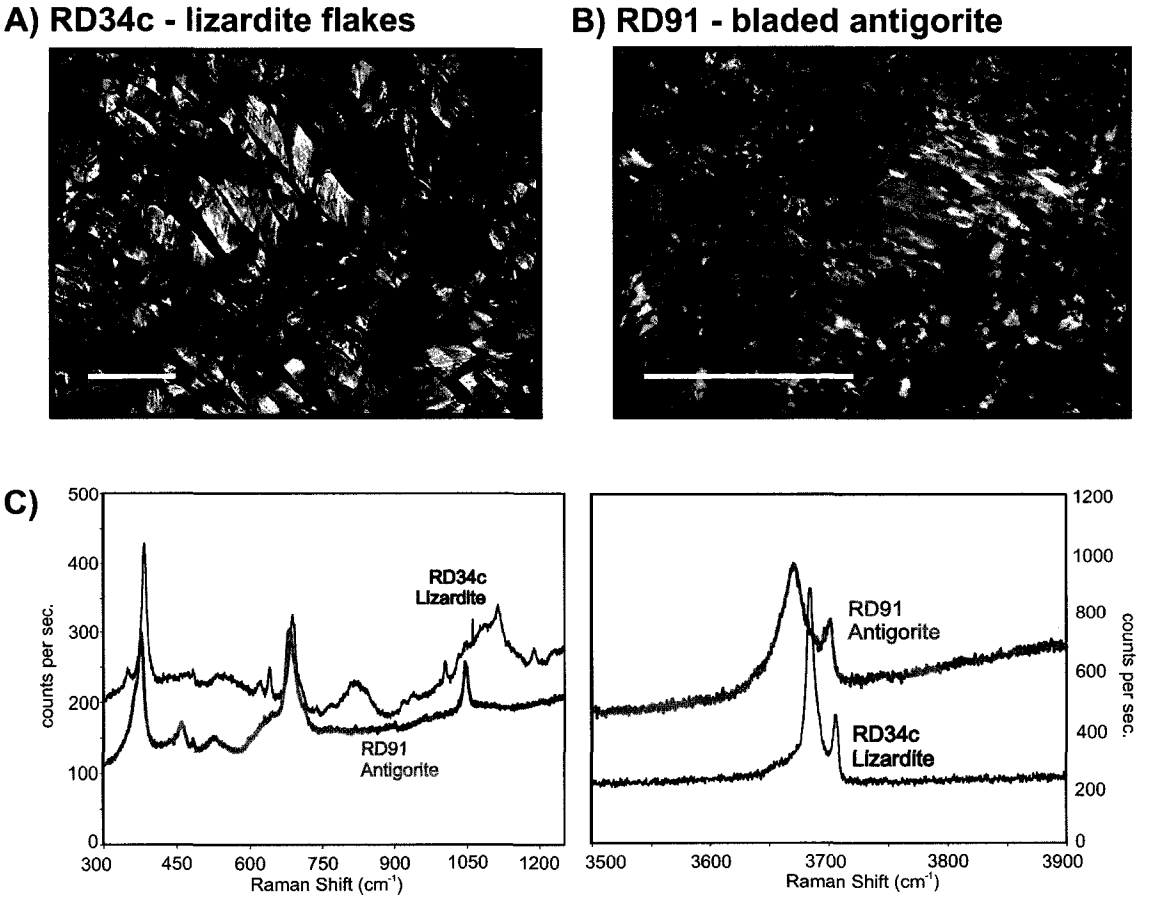


**Figure 1.3:** Photomicrographs of serpentinites under crossed polars; white lines = 0.3 mm. **A)** Sample RD34c: Foliated flaky lizardite **B)** Sample RD91: Large, well crystallized blady antigorite in antigorite-rich matrix. **C)** Selected Micro-Raman spectra from flaky lizardite (RD34c) and large blady antigorite (RD91), for raman shifts between 300 $cm^{-1}$ and 1200 $cm^{-1}$ (Si-O and Mg-O bonds) and between 3500 $cm^{-1}$ and 3900 $cm^{-1}$ (OH bonds). Spectra of RD34c between 300$cm^{-1}$ and 1200 $cm^{-1}$ is affected by some background radiation. Spectra were best from large serpentine grains such as the ones shown in figures 3A and 3B. The size of the analyzed areas was 10 microns, using a frequency-doubled Nd :YAG laser with a wavelength of 532 nm and a power of 50 mW on the sample. Reference data for Raman Spectra of serpentine minerals are from Auzende (1999), Rinaudo et al. (2003), Auzende et al. (2004) and Groppo et al. (2006).

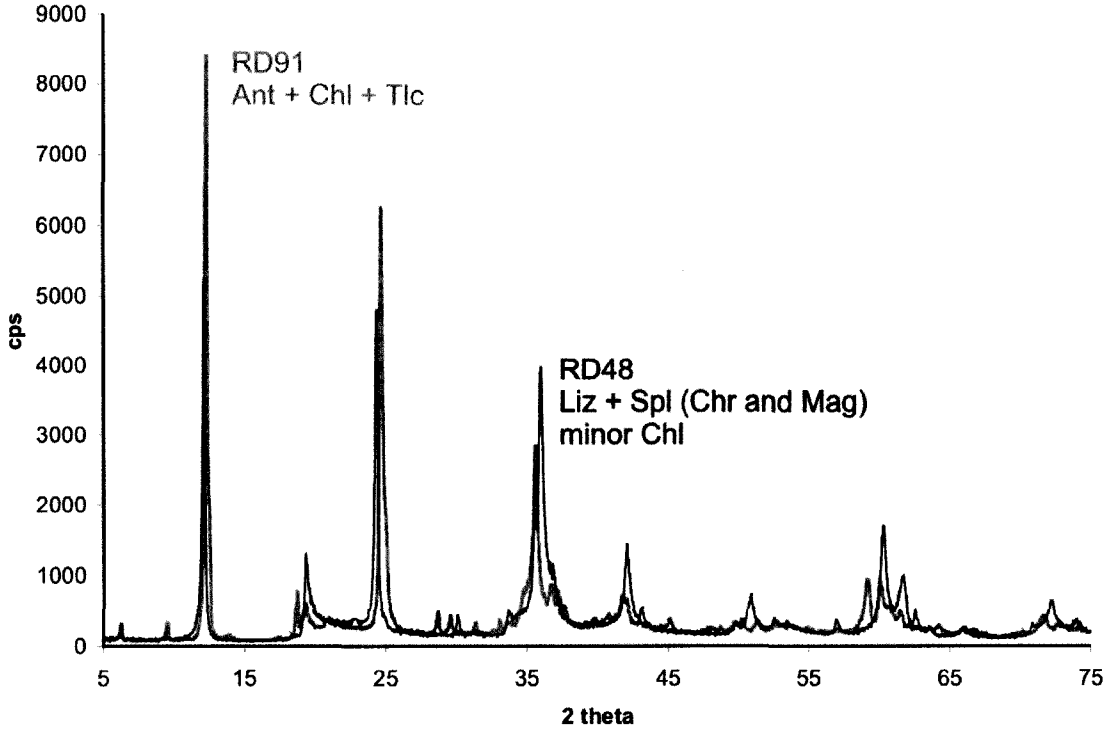


**Figure 1.4:** Selected bulk rock powder X-ray diffraction spectra. Lizardite is the only identified serpentine phase in samples from near fault zones and in the northern terranes (example RD48), whereas samples from the Arroyo Sabana and Jagua Clara mélanges in the central part of the Rio San Juan Complex are antigorite rich (example RD91).

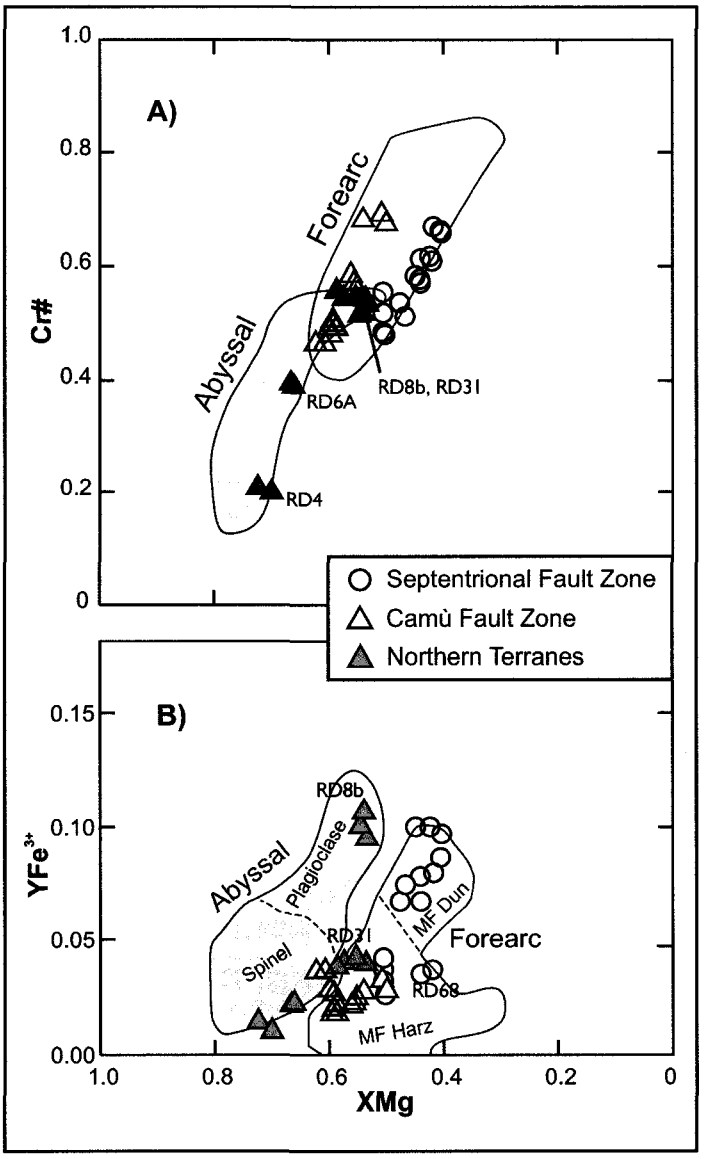


**Figure 1.5:** Plots of the composition of spinel cores from serpentinites of northern Dominican Republic. Each point represents the composition of the core of one grain, and only grains with primary compositions are plotted. The fields of abyssal peridotite include both abyssal spinel peridotite and abyssal plagioclase peridotite (Dick and Bullen, 1984). The forearc field is defined by Cr-spinel data from serpentinized peridotites exhumed in the Mariana forearc (Ishii et al, 1992). **A)** Plot of Cr# vs. XMg of Cr-spinels. The fields of abyssal spinel peridotite and abyssal plagioclase peridotite overlap, yet the high Cr#, low Mg# end of the "abyssal peridotite field" (RD31 and RD8b) is mostly abyssal plagioclase peridotite. Note the different trends for SFZ and CFZ serpentinites in the "Forearc" field. **B)** Plot of $YFe^{3+}$ vs. XMg of Cr-spinels (MF Harz: Mariana Forearc Harzburgite; MF Dun: Mariana Forearc Dunite; Ishii et al., 1992). Cr-spinels from serpentintes from the SFZ and CFZ have compositions similar to Cr-spinels of forearc peridotites. RD8b plots in the abyssal plagioclase peridotite field, whereas RD31 plots very close to this field.

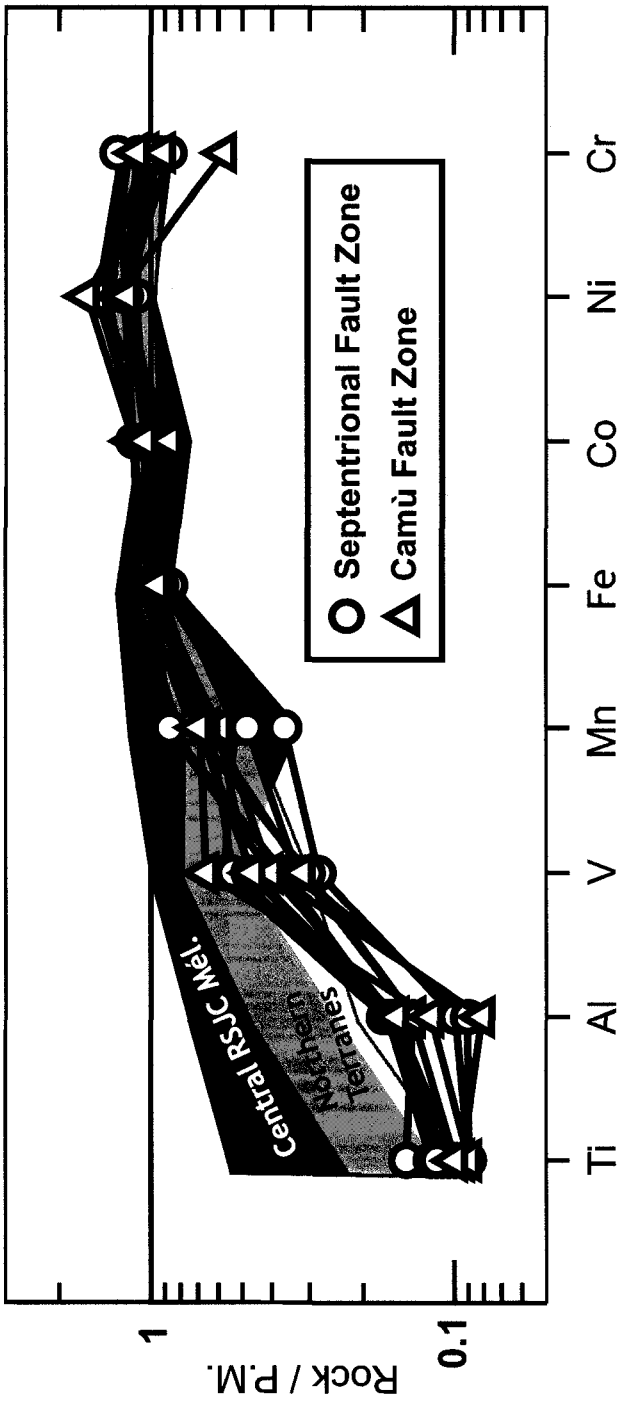


**Figure 1.6:** Primitive Mantle-normalized immobile elements of serpentinites from northern Dominican Republic. All samples are depleted in incompatible elements and enriched in compatible elements, suggesting that they are mantle residues. Moreover, samples from the SFZ and the CFZ are more depleted in Ti, Al and V compared to samples from the Arroyo Sabana and Jagua Clara Mélanges (central RSJC mélanges) and the northern terranes. Primitive mantle values are from McDonough and Sun (1995).

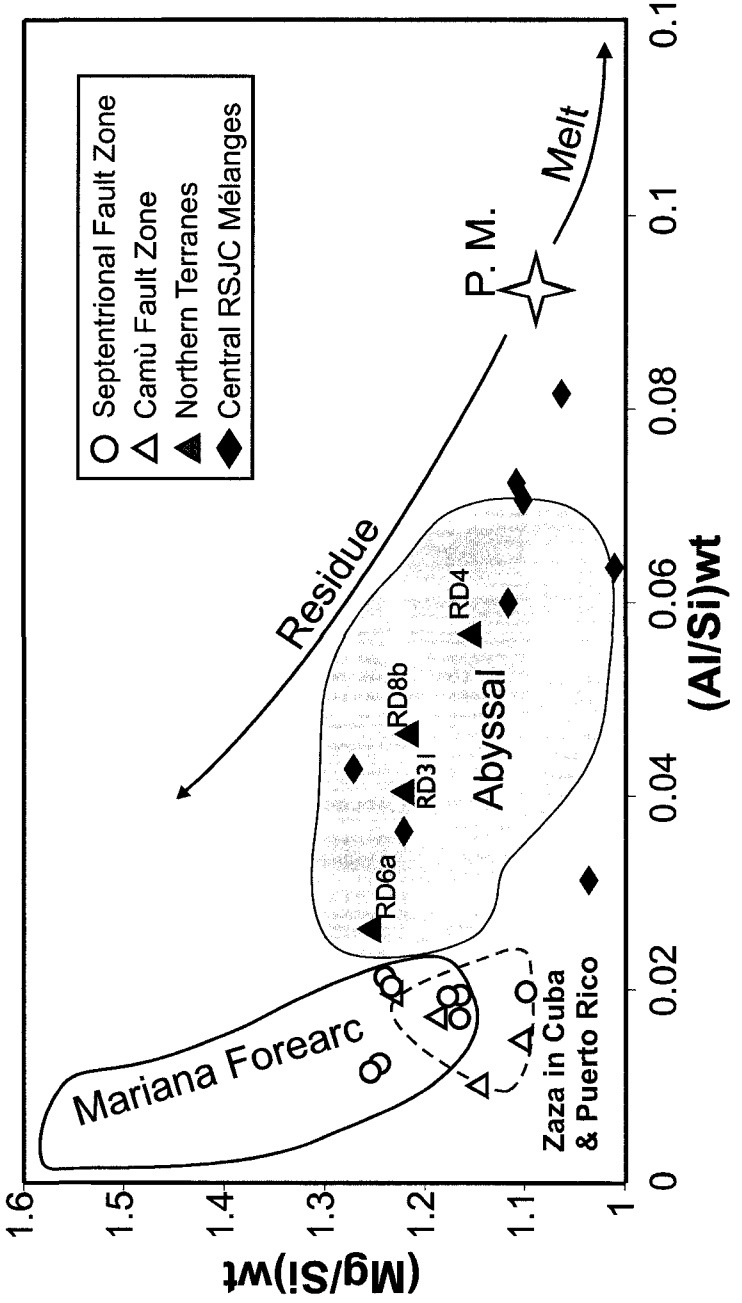


**Figure 1.7:** Weight ratios of Mg/Si vs. Al/Si of serpentinites from northern Dominican Republic (modified from Hattori and Guillot, 2007). The compositional variations expected during partial melting are shown with arrows (see text). Once again, all samples plot as mantle residues, but serpentinites from the SFZ and CFZ are more highly depleted. They plot in the fields of forearc peridotites and are similar in composition to Cuban mantle wedge serpentinites from the Zaza deformation zone (Hattori and Guillot, 2007) and Puerto Rican Trench serpentinites (Bowin et al., 1966). Samples from the HP-LT Mélanges and from the Northern LT Terranes (RD6a, RD31, RD4 and RD8b) have compositions similar to less depleted abyssal peridotite. Data from the Mariana Forearc was obtained from Ishii et al., (1992), Yamamoto et al., (1992) and Parkinson and Pearce (1998). The field of abyssal peridotite is defined by data compiled by Niu (2004), with outlier values discarded. Primitive mantle values (P.M.) were taken from McDonough and Sun (1995).

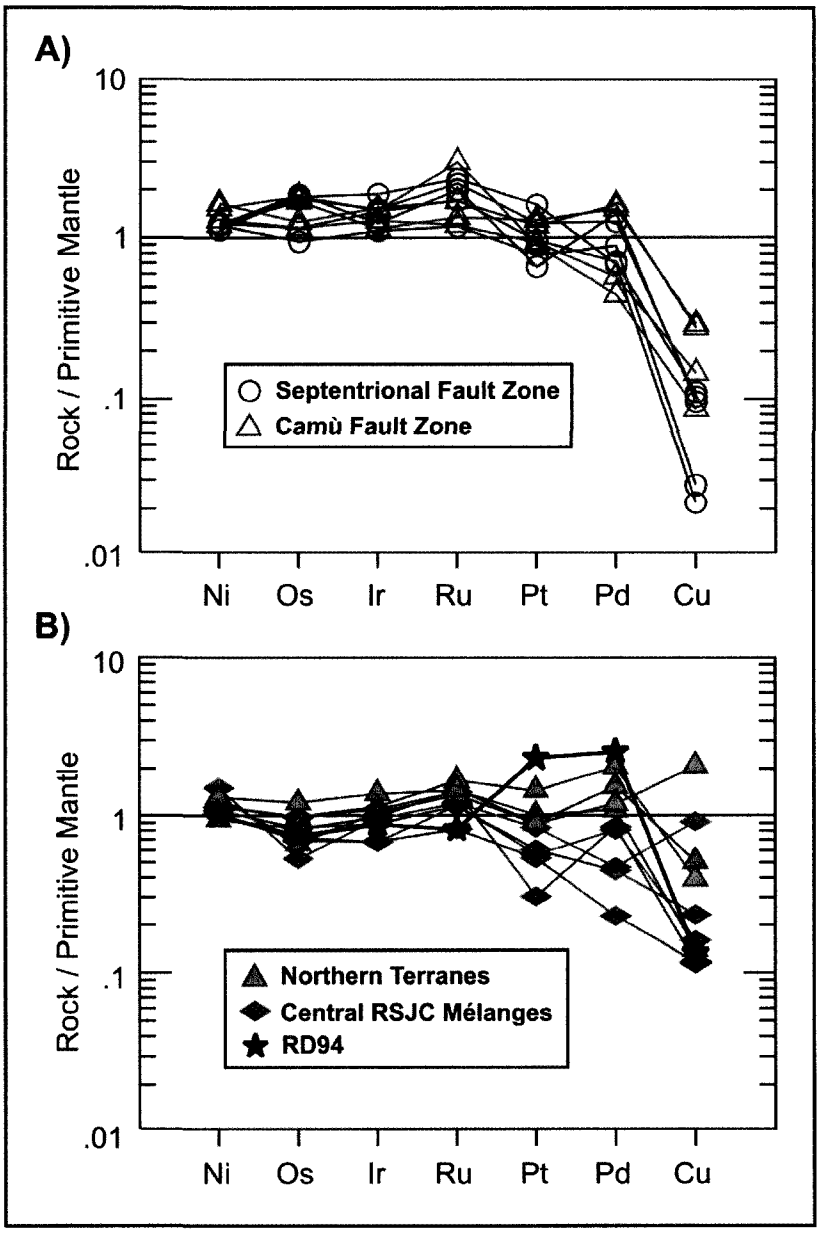


**Figure 1.8:** Primitive mantle normalized plots of PGE, Ni and Cu in serpentinites from northern Dominican Republic. Elements are placed in order of decreasing compatibility (e.g., Pearson et al., 2004). PGE values for the primitive mantle are 0.00725 times those of CI chondrite (McDonough and Sun, 1995): 3.55 ppb Os; 3.30 ppb Ir, 5.18 ppb Ru, 7.32 ppb Pt and 3.99 ppb Pd. In general, the high content in Ir-group PGEs suggests that serpentinites were initially mantle residues. **A)** Plots of data from the fault zones, showing generally flat patterns with depletion in Cu. **B)** Plots of data from the central RSJC mélanges and the northern terranes, showing flat to Pd-group PGE and Cu depleted patterns. RD94 is shown separately because of its distinctly different Pd and Pt enriched pattern (see text).

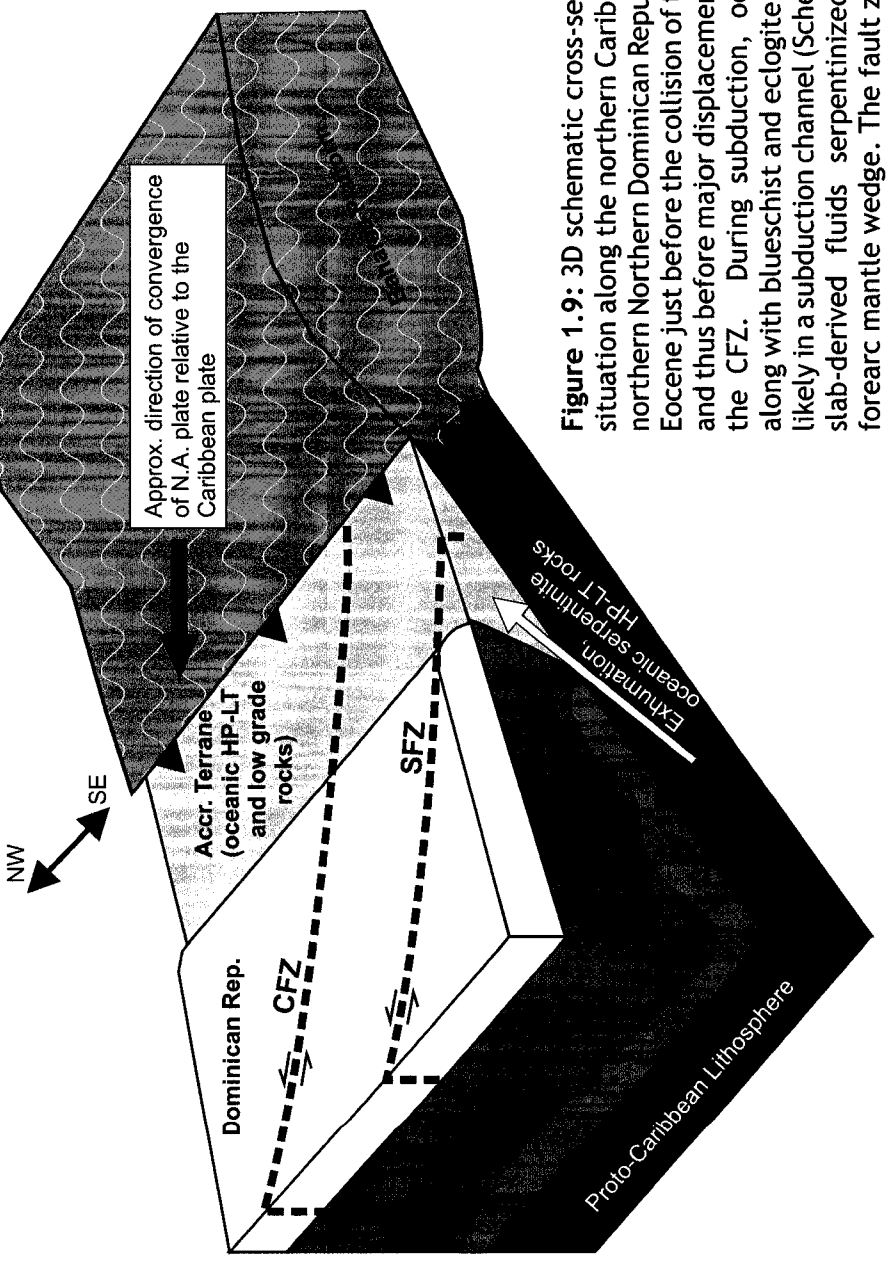


**Figure 1.9:** 3D schematic cross-section illustrating the situation along the northern Caribbean plate margin in northern Northern Dominican Republic, during the mid-Eocene just before the collision of the Bahama Platform and thus before major displacements along the SFZ and the CFZ. During subduction, oceanic serpentinites along with blueschist and eclogite were exhumed most likely in a subduction channel (Schertl et al., 2006), and slab-derived fluids serpentinized the base of the forearc mantle wedge. The fault zones, formed during collision, cut obliquely across the original trend of the subduction complex (Mann et al., 1991), which implies that they tap the serpentinized base of the mantle wedge at depth. Mantle wedge serpentinites protruded along the fault zones during collision.

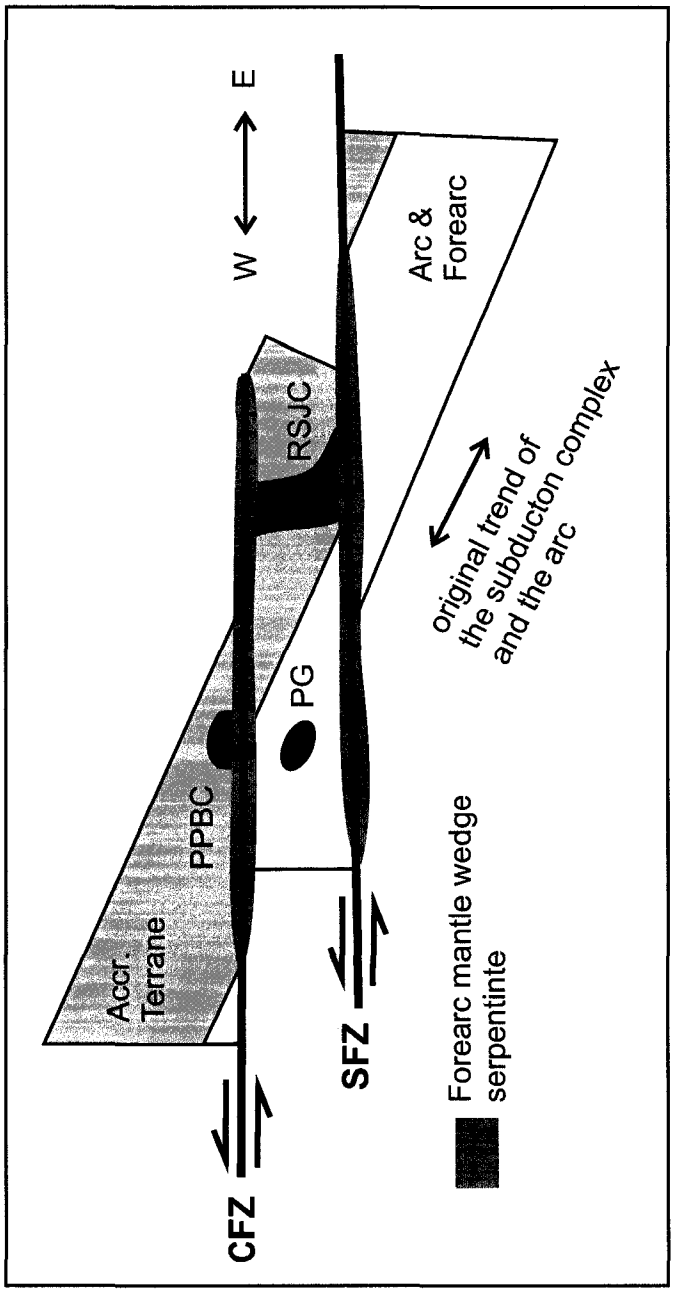


**Figure 1.10:** 2D schematic "birds-eye view" of the subduction complex after collision and displacement along the SFZ and the CFZ. The fault zones cut obliquely across accretionary and arc terranes and therefore tap the underlying mantle wedge, allowing protrusion of relatively ductile and buoyant serpentinite along the strike of the fault zones. Before collision, the Puerto Plata Basement Complex (PPBC) and the Rio San Juan Complex (RSJC) were initially continuous (Draper and Nagle, 1991). Strike-slip motion along the CFZ (~ 60 km, Draper and Nagle, 1991) causes the PPBC to migrate west, and results in the Perdro Garcia arc terrane (PG) to be located just south of the PPBC.

## Table 1.1: Seclected microprobe analyses of Cr-spinel from serpentinites from northern Dominican Republic.

| *locality* | *Northern Terranes* | | | | *Camù Fault Zone* | | | | *Septentrional Fault Zone* | | | | |
|---|---|---|---|---|---|---|---|---|---|---|---|---|---|
| *sample* | **RD4** | **RD6a** | **RD8b** | **RD31** | **RD9a** | **RD18b** | **RD6-80** | **RD6-81** | **RD45** | **RD48** | **RD34c** | **RD68** | **RD6-36a** |
| $SiO_2$ | – | 0.06 | 0.07 | 0.04 | 0.05 | 0.04 | 0.02 | 0.01 | 0.01 | – | – | – | – |
| $Al_2O_3$ | 50.28 | 34.91 | 23.18 | 24.07 | 23.07 | 27.42 | 15.84 | 29.62 | 16.04 | 19.03 | 23.24 | 27.93 | 20.62 |
| $TiO_2$ | 0.07 | 0.09 | 0.27 | 0.01 | 0.04 | 0.07 | 0.06 | 0.06 | 0.07 | 0.21 | 0.08 | 0.04 | 0.11 |
| $V_2O_3$ | *n.a.* | 0.17 | 0.25 | 0.25 | 0.25 | 0.23 | 0.25 | 0.18 | 0.27 | 0.22 | 0.28 | 0.28 | *n.a.* |
| $Cr_2O_3$ | 18.64 | 33.22 | 37.77 | 43.18 | 45.69 | 40.76 | 52.68 | 38.39 | 46.99 | 44.89 | 40.31 | 38.65 | 42.18 |
| $Fe_2O_3$ | 0.96 | 2.03 | 9.15 | 3.65 | 1.92 | 2.32 | 2.67 | 3.24 | 7.05 | 5.49 | 5.69 | 2.25 | 6.48 |
| FeO | 13.27 | 14.01 | 17.77 | 17.36 | 17.16 | 16.14 | 18.33 | 15.21 | 21.45 | 20.47 | 19.50 | 19.07 | 20.51 |
| MgO | 17.34 | 15.31 | 11.68 | 12.04 | 12.06 | 13.12 | 10.59 | 14.08 | 8.22 | 9.01 | 9.93 | 10.77 | 9.09 |
| MnO | 0.07 | 0.07 | 0.24 | 0.13 | 0.08 | 0.14 | 0.09 | 0.09 | 0.27 | 0.30 | 0.28 | 0.29 | 0.23 |
| NiO | 0.29 | 0.09 | 0.1 | 0.1 | 0.10 | 0.06 | 0.03 | 0.11 | 0.04 | *n.a.* | 0.10 | *n.a.* | 0.12 |
| ZnO | 0.27 | 0.16 | 0.19 | 0.24 | 0.21 | 0.26 | 0.22 | 0.22 | 0.67 | 0.80 | 0.77 | 0.68 | 0.53 |
| CaO | 0.01 | – | – | – | – | 0.01 | 0.01 | 0.01 | 0.01 | – | 0.03 | 0.01 | 0.03 |
| SUM | 101.20 | 100.12 | 100.67 | 101.07 | 100.63 | 100.57 | 100.79 | 101.22 | 101.09 | 100.42 | 100.21 | 99.97 | 99.90 |
| **O = 32** | | | | | | | | | | | | | |
| Si | – | 0.013 | 0.018 | 0.010 | 0.013 | 0.010 | 0.005 | 0.003 | 0.003 | – | – | – | – |
| Al | 12.673 | 9.496 | 6.743 | 6.923 | 6.681 | 7.755 | 4.769 | 8.218 | 4.901 | 5.739 | 6.859 | 8.045 | 6.203 |
| Ti | 0.011 | 0.016 | 0.050 | 0.002 | 0.007 | 0.013 | 0.012 | 0.011 | 0.013 | 0.039 | 0.014 | 0.008 | 0.021 |
| V | *n.a.* | 0.032 | 0.049 | 0.048 | 0.048 | 0.045 | 0.050 | 0.034 | 0.057 | 0.044 | 0.056 | 0.056 | *n.a.* |
| Cr | 3.152 | 6.063 | 7.371 | 8.333 | 8.876 | 7.735 | 10.637 | 7.146 | 9.630 | 9.081 | 7.981 | 7.470 | 8.513 |
| $Fe^{+3}$ | 0.154 | 0.353 | 1.700 | 0.670 | 0.355 | 0.419 | 0.513 | 0.574 | 1.375 | 1.057 | 1.072 | 0.413 | 1.245 |
| $Fe^{+2}$ | 2.373 | 2.704 | 3.667 | 3.544 | 3.527 | 3.240 | 3.915 | 2.995 | 4.651 | 4.382 | 4.084 | 3.899 | 4.378 |
| Mg | 5.529 | 5.266 | 4.296 | 4.379 | 4.416 | 4.693 | 4.030 | 4.940 | 3.175 | 3.438 | 3.706 | 3.924 | 3.460 |
| Mn | 0.013 | 0.014 | 0.051 | 0.028 | 0.017 | 0.029 | 0.018 | 0.018 | 0.058 | 0.066 | 0.059 | 0.060 | 0.051 |
| Ni | 0.050 | 0.016 | 0.021 | 0.020 | 0.021 | 0.011 | 0.006 | 0.020 | 0.009 | *n.a.* | 0.020 | *n.a.* | 0.024 |
| Zn | 0.042 | 0.027 | 0.034 | 0.044 | 0.038 | 0.046 | 0.041 | 0.038 | 0.129 | 0.152 | 0.142 | 0.123 | 0.099 |
| Ca | 0.002 | – | – | – | – | 0.004 | 0.003 | 0.003 | 0.002 | 0.001 | 0.007 | 0.004 | 0.007 |
| SUM | 23.999 | 24.000 | 24.000 | 24.001 | 23.999 | 24.000 | 23.999 | 24.000 | 24.003 | 23.999 | 24.000 | 24.002 | 24.001 |
| Cr# | 0.199 | 0.390 | 0.522 | 0.546 | 0.571 | 0.499 | 0.690 | 0.465 | 0.663 | 0.613 | 0.538 | 0.481 | 0.578 |
| $YFe^{3+}$ | 0.010 | 0.022 | 0.108 | 0.042 | 0.022 | 0.026 | 0.032 | 0.036 | 0.086 | 0.067 | 0.067 | 0.026 | 0.078 |
| XMg | 0.700 | 0.661 | 0.539 | 0.553 | 0.556 | 0.592 | 0.507 | 0.623 | 0.406 | 0.440 | 0.476 | 0.502 | 0.441 |

Cr# : Cr/(Cr+Al);
XMg : $Mg/(Mg+Fe^{2+})$;
$Y_{Fe^{3+}}$ : $Fe^{3+}/(Cr+Al+Fe^{3+})$
*n.a.*: not analysed; – : not detected

## Table 1.2: Selected analyses of olivine and orthopyroxene

| | Olivine | | |
|---|---|---|---|
| *locality* | *JCM** | | *SFZ* |
| *sample* | RD6-52a | RD94 | RD68 |
| $SiO_2$ | 40.41 | 41.45 | 41.72 |
| $Al_2O_3$ | – | – | – |
| MgO | 48.06 | 49.05 | 51.22 |
| FeO | 10.64 | 9.61 | 9.27 |
| CaO | – | 0.03 | – |
| $Cr_2O_3$ | – | *n.a.* | 0.01 |
| MnO | 0.21 | 0.11 | 0.21 |
| $TiO_2$ | 0.01 | *n.a.* | *n.a.* |
| NiO | 0.34 | 0.5 | *n.a.* |
| SUM | 99.67 | 100.75 | 102.43 |
| **O = 4** | | | |
| Si | 0.999 | 1.007 | 0.995 |
| Al | 0.000 | 0.000 | 0.000 |
| Mg | 1.771 | 1.777 | 1.821 |
| Fe | 0.220 | 0.195 | 0.185 |
| Ca | 0.000 | 0.001 | 0.000 |
| Cr | 0.000 | *n.a.* | 0.000 |
| Mn | 0.004 | 0.002 | 0.004 |
| Ti | 0.000 | *n.a.* | *n.a.* |
| Ni | 0.007 | 0.010 | *n.a.* |
| SUM | 3.001 | 2.992 | 3.005 |
| Fo (%) | 89.0 | 90.1 | 90.8 |

| | Orthopyroxene | | | |
|---|---|---|---|---|
| *locality* | *CFZ* | *SFZ* | | *JCM** |
| *sample* | RD18B | RD68 | RD34a | RD94 |
| $SiO_2$ | 57.14 | 57.22 | 57.03 | 57.48 |
| $Al_2O_3$ | 2.23 | 1.67 | 1.45 | 1.72 |
| MgO | 34.42 | 34.92 | 34.34 | 34.29 |
| FeO | 5.75 | 5.74 | 6.87 | 6.75 |
| CaO | 0.79 | 0.26 | 0.3 | 0.2 |
| $Cr_2O_3$ | 0.66 | 0.4 | 0.39 | 0.08 |
| MnO | 0.15 | 0.15 | 0.19 | 0.14 |
| $TiO_2$ | 0.02 | 0.04 | 0.02 | 0.08 |
| NiO | – | 0.04 | – | *n.a.* |
| $Na_2O$ | – | 0.01 | – | 0.01 |
| SUM | 101.16 | 100.45 | 100.59 | 100.75 |
| **O = 6** | | | | |
| Si | 1.947 | 1.959 | 1.961 | 1.967 |
| Al | 0.089 | 0.051 | 0.059 | 0.069 |
| Mg | 1.748 | 1.782 | 1.760 | 1.749 |
| Fe | 0.164 | 0.164 | 0.198 | 0.193 |
| Ca | 0.029 | 0.011 | 0.011 | 0.007 |
| Cr | 0.018 | 0.026 | 0.010 | 0.002 |
| Mn | 0.004 | 0.004 | 0.006 | 0.004 |
| Ti | 0.001 | 0.001 | 0.001 | 0.002 |
| Ni | 0.000 | 0.001 | 0.000 | *n.a.* |
| Na | 0.000 | 0.001 | 0.000 | 0.001 |
| SUM | 4.000 | 4.000 | 4.006 | 3.994 |
| Mg#** | 0.914 | 0.916 | 0.899 | 0.901 |
| En (%) | 90.1 | 91.1 | 89.4 | 89.7 |
| Fs (%) | 8.4 | 8.4 | 10.1 | 9.9 |
| Wo (%) | 1.5 | 0.6 | 0.6 | 0.4 |

* Jagua Clara Mélange (central Rio San Juan C.)

** Mg# = atomic ratio of Mg/(Mg+Fe).

*n.a.*: not analysed; –: not detected

*Table 1.3 - Bulk rock composition of serpentinites from Northern Dominican Repuublic*

| | *Northern Terranes* | | | | *Camù Fault Zone* | | | | *Central RSJC Mélanges ** | | | |
|---|---|---|---|---|---|---|---|---|---|---|---|---|
| | **RD4** | **RD6a** | **RD8b** | **RD31** | **RD9a** | **RD18b** | **RD6-80** | **RD6-81** | **RD87** | **RD89** | **RD91** | **RD94** |
| $SiO_2$ (wt%) | 39.9 | 39.3 | 39.3 | 40.5 | 41.1 | 39.7 | 41.1 | 40.7 | 41.9 | 42.2 | 42.08 | 44.72 |
| $TiO_2$ | 0.04 | 0.02 | 0.02 | 0.02 | 0.02 | 0.02 | 0.02 | 0.02 | 0.06 | 0.11 | 0.07 | 0.05 |
| $Al_2O_3$ | 1.99 | 0.9 | 1.6 | 1.44 | 0.53 | 0.69 | 0.36 | 0.61 | 3.01 | 2.69 | 2.23 | 2.51 |
| $Fe_2O_3$ (tot.) | 9.34 | 7.83 | 10.03 | 8.19 | 9.11 | 8.52 | 9.23 | 8.36 | 9.37 | 7.78 | 7.94 | 8.14 |
| MnO | 0.07 | 0.10 | 0.06 | 0.06 | 0.09 | 0.09 | 0.08 | 0.09 | 0.12 | 0.09 | 0.05 | 0.12 |
| MgO | 35.7 | 38.2 | 37.0 | 38.3 | 35.2 | 37.9 | 36.5 | 37.5 | 34.5 | 36.3 | 36.41 | 34.98 |
| CaO | 0.15 | 0.15 | 0.06 | 0.06 | 0.15 | 0.10 | 0.18 | 0.05 | 0.07 | 0.39 | 0.77 | 0.18 |
| $Na_2O$ | < 0.005 | < 0.005 | < 0.005 | < 0.005 | < 0.005 | < 0.005 | < 0.005 | < 0.005 | < 0.005 | < 0.005 | < 0.005 | < 0.005 |
| $K_2O$ | < 0.005 | < 0.005 | < 0.005 | < 0.005 | < 0.005 | < 0.005 | < 0.005 | < 0.005 | < 0.005 | < 0.005 | < 0.005 | < 0.005 |
| $P_2O_5$ | 0.01 | 0.01 | 0.01 | 0.01 | 0.01 | 0.01 | 0.01 | 0.01 | 0.01 | 0.02 | 0.01 | 0.02 |
| LOI | 14.4 | 14.4 | 12.7 | 13.8 | 15.2 | 14.8 | 14.0 | 14.4 | 11.7 | 11.8 | 12.1 | 10.0 |
| SUM | 101.8 | 101.2 | 100.9 | 102.6 | 101.8 | 102.2 | 101.7 | 101.8 | 101.0 | 101.6 | 101.9 | 100.9 |
| Co (ppm) | 107 | 109 | 112 | 97 | 120 | 110 | 92 | 91 | 99 | 83 | 97 | 92 |
| Cr | 2900 | 2380 | 2380 | 2510 | 2400 | 2910 | 2720 | 1500 | 2510 | 2710 | 2460 | 2540 |
| Ni | 2580 | 2560 | 1850 | 2250 | 3180 | 2350 | 2970 | 2510 | 2950 | 1970 | 2110 | 1970 |
| V | 62 | 36 | 24 | 31 | 54 | 38 | 33 | 26 | 64 | 67 | 51 | 50 |
| Zn | 65 | 48 | 42 | 36 | 51 | 46 | 52 | 53 | 58 | 66 | 43 | 55 |
| Pb | 0.04 | 0.04 | 0.04 | 0.07 | 0.21 | 0.02 | 0.02 | 0.14 | 0.03 | 0.47 | 0.05 | 0.08 |
| Cu | 15 | 4.2 | 62 | 12 | 8.4 | 8.8 | 2.6 | 4.4 | 27 | 4.8 | 6.9 | 4.0 |
| S | 20 | 320 | 9.3 | 19 | 6.7 | 140.0 | 8.4 | 13 | 2.4 | 2.3 | 620 | 69 |
| Os (ppb) | 2.36 | 4.29 | 2.94 | 3.48 | 4.43 | 5.96 | 6.41 | 4.09 | 1.88 | 2.57 | 2.96 | 2.62 |
| Ir | 3.45 | 4.58 | 3.22 | 3.75 | 5.05 | 3.74 | 4.87 | 4.21 | 3.13 | 2.23 | 2.93 | 2.90 |
| Ru | 6.98 | 7.53 | 7.56 | 8.66 | 8.67 | 6.89 | 15.37 | 6.16 | 6.17 | 5.97 | 5.90 | 4.22 |
| Pt | 6.53 | 7.37 | 6.54 | 10.62 | 8.67 | 9.42 | 6.55 | 6.83 | 6.13 | 4.12 | 4.42 | 17.07 |
| Pd | 6.17 | 4.33 | 4.75 | 8.19 | 6.39 | 6.02 | 1.79 | 2.30 | 1.86 | 3.22 | 1.77 | 10.19 |
| Bulk Mg# ** | 88.3 | 90.6 | 88.0 | 90.3 | 88.4 | 89.8 | 88.7 | 89.9 | 88.0 | 90.2 | 90.1 | 89.5 |

* Central Rio San Juan Mélanges, include data from the Arroyo Sabana and Jagua Clara Mélange

** Bulk Mg# = atomic (molar) Mg*100 / (Mg + total Fe)

*n.a.* : not available

*Table 1.3 - Bulk rock composition (major oxydes, major elements and PGE's) of serpentinites from Northern Dominican Repuublic (continued)*

| | *Central RSJC Mélanges (ctd.)* | | | | *SFZ - Rio Cuevas* | | | *SFZ - Loma Quita Espuela* | | | | |
|---|---|---|---|---|---|---|---|---|---|---|---|---|
| | **RD6-50c** | **RD6-52a** | **RD21a** | **RD6-54a** | **RD48** | **RD60** | **RD45** | **RD34a** | **RD34c** | **RD68** | **RD6-36a** | **RD6-36c** |
| $SiO_2$ (wt%) | 42.2 | 42.3 | 38.8 | 36.0 | 40.8 | 40.8 | 39.6 | 41.3 | 39.8 | 42.3 | 40.8 | 41.6 |
| $TiO_2$ | 0.02 | 0.11 | 0.03 | 0.04 | 0.02 | 0.02 | 0.02 | 0.03 | 0.02 | 0.02 | 0.02 | 0.02 |
| $Al_2O_3$ | 2.63 | 1.16 | 1.24 | 1.36 | 0.44 | 0.76 | 0.4 | 0.61 | 0.7 | 0.74 | 0.69 | 0.71 |
| $Fe_2O_3$ (tot.) | 8.47 | 9.89 | 11.21 | 10.71 | 7.98 | 7.72 | 8.26 | 9.76 | 8.75 | 9.19 | 8.60 | 8.84 |
| MnO | 0.14 | 0.12 | 0.14 | 0.15 | 0.05 | 0.07 | 0.07 | 0.10 | 0.12 | 0.12 | 0.09 | 0.08 |
| MgO | 36.0 | 33.9 | 36.7 | 35.4 | 39.4 | 39.2 | 38.5 | 37.3 | 38.0 | 36.0 | 37.3 | 37.5 |
| CaO | 0.10 | 3.19 | 0.09 | 3.23 | 0.08 | 0.10 | 0.09 | 0.07 | 0.48 | 0.43 | 0.39 | 0.12 |
| $Na_2O$ | < 0.005 | < 0.005 | < 0.005 | < 0.005 | < 0.005 | < 0.005 | < 0.005 | < 0.005 | < 0.005 | < 0.005 | < 0.005 | < 0.005 |
| $K_2O$ | < 0.005 | < 0.005 | < 0.005 | < 0.005 | < 0.005 | < 0.005 | < 0.005 | < 0.005 | < 0.005 | < 0.005 | < 0.005 | < 0.005 |
| $P_2O_5$ | 0.01 | 0.01 | 0.01 | 0.01 | 0.01 | 0.01 | 0.01 | 0.02 | 0.01 | 0.01 | 0.01 | 0.01 |
| LOI | 11.2 | 9.9 | 12.4 | 13.9 | 14.2 | 10.6 | 13.3 | 13.0 | 13.1 | 12.9 | 13.6 | 12.3 |
| SUM | 101.0 | 100.9 | 101.0 | 101.1 | 103.1 | 99.5 | 100.6 | 102.4 | 101.3 | 102.1 | 101.8 | 101.4 |
| Co | 95 | 110 | 89 | 105 | 98 | 102 | 98 | 120 | 110 | 110 | 106 | 108 |
| Cr | 2670 | 2400 | 3110 | 2790 | 2480 | 2710 | 2270 | 2880 | 2530 | 2780 | 3380 | 2550 |
| Ni | 2210 | 2010 | 2360 | 2330 | 2340 | 2400 | 2370 | 2390 | 2340 | 2190 | 2370 | 2380 |
| V | 46 | 81 | 44 | 51 | 23 | 47 | 27 | 25 | 33 | 30 | 44 | 39 |
| Zn | 61 | 53 | 61 | 50 | 54 | 41 | 54 | 74 | 59 | 69 | 54 | 65 |
| Pb | 0.19 | 0.01 | 0.03 | 0.31 | 0.87 | 1.4 | 1.4 | 0.68 | 0.97 | 2.9 | 1.3 | 1.3 |
| Cu | 3.4 | 3.5 | *n.a.* | *n.a.* | 2.9 | 3.1 | 1.8 | 3.3 | 0.84 | 0.66 | 3.9 | 0.71 |
| S | < 1.0 | 46 | *n.a.* | *n.a.* | 35 | 23 | 4.5 | 35 | 23 | 120 | 26 | 28 |
| Os (ppb) | 3.47 | 2.45 | *n.a.* | *n.a.* | 6.60 | 6.18 | *n.a.* | 4.07 | 3.36 | 6.38 | *n.a.* | *n.a.* |
| Ir | 3.60 | 2.25 | *n.a.* | *n.a.* | 4.05 | 4.95 | *n.a.* | 4.79 | 3.64 | 6.19 | *n.a.* | *n.a.* |
| Ru | 7.32 | 4.21 | *n.a.* | *n.a.* | 10.25 | 11.29 | *n.a.* | 8.83 | 6.06 | 12.03 | *n.a.* | *n.a.* |
| Pt | 2.21 | 3.91 | *n.a.* | *n.a.* | 4.89 | 8.99 | *n.a.* | 7.05 | 5.76 | 11.77 | *n.a.* | *n.a.* |
| Pd | 3.38 | 0.90 | *n.a.* | *n.a.* | 5.63 | 5.02 | *n.a.* | 2.84 | 3.55 | 2.73 | *n.a.* | *n.a.* |
| Bulk Mg# ** | 89.4 | 87.2 | 86.7 | 86.8 | 90.7 | 91.0 | 90.2 | 88.3 | 89.6 | 88.6 | 89.6 | 89.4 |

* Central Rio San Juan Mélanges, include data from the Arroyo Sabana and Jagua Clara Mélange

** Bulk Mg# = atomic (molar) Mg*100 / (Mg + total Fe)

*n.a.* : not available

# CHAPTER 2

# Zoned Cr-spinel in forearc serpentinites from the Cuaba Unit, Rio San Juan Complex, Hispaniola: early stages of ferritchromit alteration.

*Benoit-Michel Saumur and Kéiko H. Hattori*

Department of Earth Sciences, University of Ottawa, 140 Louis Pasteur, Ottawa, Ontario, K1N 6N5, Canada

*Manuscript in preparation for submission to a refereed journal*

**ABSTRACT**

Cr-spinels from forearc serpentinites from the Cuaba Unit (Rio San Juan Complex, northern Dominican Republic) are concentrically zoned. Cores preserve primary compositions, but are gradually altered to ferritchromit. This alteration is essentially a replacement of $Al_2O_3$ by $Fe_2O_3$ (and $Cr_2O_3$) and MgO by FeO. Released MgO and $Al_2O_3$ are taken up by chlorite nucleating at the rims of Cr-spinel and by matrix serpentine. The formation of ferritchromit and chlorite haloes has been documented in rocks that have undergone amphibolite facies metamorphism. However, our serpentinite samples do not show convincing evidence of such high-grade thermal metamorphism since they are dominated by low-grade pseudomorphic lizardite. Furthermore, ferritchromit is still high in Al and Mg compared to most other reported occurrences, and chlorite rims do not completely envelope Cr-spinels. The evidence suggests that this poorly developed ferritchromit represents the early stages of alteration of Cr-spinel, either because of low temperature metamorphism, or a short-lived event of amphibolite metamorphism.

## 2.1) INTRODUCTION

Cr-spinel has been used as a petrological indicator in a wide variety of rocks (e.g., Irvine, 1967; Dick and Bullen, 1984; Barnes and Roeder, 2001). They are especially useful in identifying the origin of serpentinites, since spinel is commonly the only primary mineral preserved after the hydration of silicate minerals. However, spinel compositions can be modified during serpentinization and subsequent metamorphism, and thus careful analysis must be carried out in order to correctly interpret spinel compositions.

"Ferritchromit", a term first coined by Spangenberg (1943) for reflective rims (showing high electron backscatter) high in Fe and relatively depleted in MgO and $Al_2O_3$ around Cr-spinel, is a common alteration product of Cr-spinel. Several mechanisms have been proposed for the formation of ferritchromit rims. Notably, Bliss and McLean (1975) showed that ferritchromit is the product of a reaction between magnetite and Cr-spinel during epidote-amphibolite facies metamorphism. Ulmer (1974) showed that ferritchromit can form as overgrowths because of Cr and Fe mobilization during low temperature serpentinization, whereas Wylie et al. (1987) showed that outward diffusion of $Fe^{3+}$ along with the dissolution of spinel cores causes the precipitation of ferritchromit rims. Furthermore, several authors consider that the formation of ferritchromit is associated with the formation of chlorite, either by reaction with primary silicates

(Beeson and Jackson, 1969; Onyeagocha, 1974), reaction with secondary serpentinite (Pinsent and Hirst, 1977), or during hydrothermal alteration (Kimball, 1990).

This contribution reports zoned spinels from serpenitinites that originated from the forearc mantle wedge (Saumur et al., *see chapter 1*). To our knowledge, ferritchromit rims are uncommon in forearc serpentinites, the only other reported occurrence being from the Omi massif, Japan (Tsujimori, 2004). We show that in our samples, spinel zoning formed during alteration and is associated with the formation of chlorite rims.

## 2.2) GEOLOGICAL SETTING AND SAMPLES

The Cuaba Unit (or Cuaba Amphibolite in earlier publications, i.e. Draper and Nagle, 1991) is the southernmost part of the Rio San Juan Complex (Fig 2.1), which is an oceanic subduction complex formed during the subduction of Proto-Caribbean lithosphere (North American plate) under the Caribbean plate between the late Cretaceous and mid-Eocene (e.g., Pindell et al., 1988). Subduction ceased in response to the oblique collision of the Bahamas Platform, and the subduction complex has since been uplifted via major strike-slip movements concentrated mostly along the Septentrional and Camú Fault zones (e.g., Mann and Gordon, 1996) which respectively form the southern and northern boundaries of the complex. The Cuaba Unit is dominantly composed of amphibolite and eclogite, both of which are interpreted to have an oceanic protolith (e.g. Abbott et al., 2006). The Cuaba Unit was later intruded by the Rio Boba Gabbro (Draper and Nagle, 1991).

Serpentinites are minor in volume in the Cuaba Unit. They have highly depleted bulk rock compositions compared to abyssal peridotites (Fig. 2.5), suggesting that they are most likely forearc mantle peridotites hydrated by slab-derived fluids. The close association of serpentinite with the Septentrional Fault Zone (SFZ) and associated Bajabonico Fault Zone suggests that the serpentinites protruded up into the crust along the fault zones during post-Eocene transpression (Saumur et al, *see chapter 1*).

Serpentinites of forearc mantle origin occur in two localities in the southern Rio San Juan Complex; along Rio Cuevas and in the Lomá Quita Espuela area (Fig. 1). Along the narrow (~ 6 m in width) stream of Rio Cuevas (RD45, RD48 and RD60), serpentinites occur as large boulders (~ 1m in size) and therefore most likely have a proximal source. Efforts to find in situ serpentinite in this area have failed due to dense vegetation. Serpentinites crop out in the Lomá Quita Espuela area northwest of Rio Cuevas (RD34, RD68, RD6-36). They form large outcrops (> 100 m), are faulted and jointed, are variably massive to

foliated, and are interpreted to form lens shaped bodies within amphibolites of the Cuaba Unit.

## 2.3) ANALYTICAL METHOD

Cr-spinels were examined with transmitted and reflected light microscopy (D.D. Hogarth Microscopy Lab, University of Ottawa). Back-scattered electron (BSE) images were collected with a Lamont 4 element solid state detector and BSE Quad Summing Amplifier (Carleton University). Mineral compositions were determined using an automated 4 spectrometer CAMEBAX MBX electron probe by the wavelength dispersive x-ray analysis method (WDX) (Carleton Univeristy). Counting times were 15 seconds per element, except for Fe (20 s) and Ni (40 s). A 15 kV accelerating potential and a 20 nA beam current were applied. The calibration standards used were pure wollastonite (Si, Ca), synthetic spinel (Al), synthetic $Cr_2O_3$ (Cr), forsterite (Mg), synthetic $MnTiO_3$ (Mn, Ti), pure vanadium metal (V), albite (Na), fayalite (Fe in silicates), synthetic $Fe_2O_2$ (Fe in oxides), tugtupite (Cl) and synthetic lithium fluoride (F). $Fe_2O_3$ contents of spinel were calculated assuming stoichiometric compositions. A total of 27 spinel grains were analysed.

## 2.4) PETROGRAPHY

All samples are dominated by pseudomorphic serpentine flakes and fine-grained magnetite. X-ray powder diffraction, Raman and microscopic studies confirm that the dominant serpentine species is lizardite. Cr-spinel is the only primary mineral preserved in most samples. Primary olivine ($Fo_{90}$) and orthopyroxene ($En_{89-91}$) are rare and present only in samples RD34a and RD68 (Saumur et al., see chapter 1). Samples RD34a and RD6-36 from Lomá Quita Espuela contain minor talc, tremolite and cummingtonite. The presence of these minerals suggests local amphibolitization. No secondary metamorphic olivine or orthopyroxene were found.

Cr-spinel is less than 1 vol. % in samples. They are highly variable in size in individual samples. Some are as small as 50 μm, but most range between 0.3 and 1.2 mm in size. Grains are subhedral to anhedral, can be slightly vermicular and may contain embayments. These grain morphologies are likely primary, as there is no evidence of grain dissolution.

### *2.4.1) Concentrically Zoned Cr-spinel*

Cr-spinel grains are zoned in most samples. In transmitted light, transluscent dark red to brown cores gradually change to opaque towards the rims. Grains with $YFe^{3+}$ ($=Fe^{3+}/[Cr+Al+Fe^{3+}]$) higher than 0.10 lack transluscent cores. The compositional data indicate that opacity is correlated with high $Fe^{3+}$. Chlorite commonly nucleates adjacent to zoned Cr-spinel grains, and partially to completely surround Cr-spinel. Cr-spinel grains also come in contact with magnetite and matrix serpentine. There is a sharp contrast between zoned Cr-spinel and magnetite observed in both BSE-images and reflected light (Figs 2.2c,2h).

The concentric zoning in Cr-spinel grains is highlighted by bright reflective ferritchromit rims (Figs 2a-d; g-h). The boundaries between cores and rims are diffuse and gradational. In general, the zoning is defined by an increase in $YFe^{3+}$ and a decrease in XMg (Fig. 2.4) from core to rim. Rims contain lower $Al_2O_3$ MgO, and ZnO, and higher $Cr_2O_3$, $TiO_2$, MnO, NiO and $V_2O_3$, and Fe compared to cores (Table 2.1). Rims plot along the ferritchromit alteration trend (e.g. Pinsent and Hirst, 1977; Fig. 2.3b-c). However, rims in this study are relatively high in Al and Mg and low in Fe compared to ferritchromit rims reported in other localities (Fig. 2.3; all previous references).

Cr-spinel cores plot in the fields of forearc mantle peridotite (Fig 2.3a-b), whereas some cores plotting slightly outside the field suggesting that they are slightly altered. Cores plotting in the forearc fields have high Cr# ($=Cr/[Cr+Al]$; 0.54-0.66) and moderate to low XMg ($=Mg/[Mg+Fe^{2+}]$; 0.47-0.40), and have low $TiO_2$ (<0.21 wt%). Some of these cores show moderate $YFe^{3+}$ (up to 0.10), which is not uncommon in Mariana forearc peridotites (e.g. Ishii et al., 1992; Ohara and Ishii; 1998). Slightly altered cores which plot outside the forearc fields have higher $YFe^{3+}$ ($=Fe^{3+}/[Cr+Al+Fe^{3+}]$; 0.11-0.22), lower XMg (down to 0.22) and moderately high $TiO_2$ (0.15-1.07 wt%). Such cores have similar compositions to ferritchromit rims. For all cores, MnO (0.15 - 0.47 wt%) and ZnO (0.46 - 0.95 wt%) are fairly low compared to spinels from ultramafic rocks affected by amphibolites metamorphism (Santti et al, 2006; Barnes, 2000).

Chlorites in contact with spinel are subhedral and are high Mg clinochlores (XMg = 0.94-0.96) containing significant $Cr_2O_3$ (1.24 - 3.01 wt%). Chlorite blades overprint matrix serpentine (Fig. 2.2b), suggesting that it likely replaced serpentine. Magnetite has end member compositions (Fig 2.3). Chlorite and magnetite are commonly intergrown when located on the edge of rims of Cr-spinel, forming a symplectite-like texture, which suggests that the two minerals are contemporaneous.

Several grains of Cr-spinel show polygonal fractures that intersect at constant angles within grains (Fig. 2a-2d), suggesting a crystallographic control on fracture formation. These are most likely partings along [111] which are common in Cr-spinel (Deer, Howie and Zussman, 1992). The fractures are commonly filled with chlorite. $Fe_2O_3$ and FeO contents of Cr-spinel adjacent to the fractures are slightly elevated (Fig 2.2d-2g), and parting appears to overprint zoning (Fig. 2.2a).

### *2.4.2) Weakly zoned Cr-spinel in sample RD68*

Sample RD68 is not as extensively hydrated compared to other samples since primary olivine and orthopyroxene are observed. Cr-spinel grains in this sample are dark red under transmitted light and zoning is not apparent under the microscope. Grains are anhedral and primary grain morphologies are preserved. Cr#'s are low (0.48 - 0.55), and within cores, there is a weak zoning defined by minor variations in Cr# (0.54-0.56; Fig. 2f). In addition to this, there is a sharp change in composition at the rims (Fig 2e-f) defined by a slight decrease in XMg and a slight increase in Cr#. However, $YFe^{3+}$ values are consistently low within grains (0.03-0.05), and ferritchromit is not present at the rims (Fig 2.3b, c). Furthermore, no chlorite is found around Cr-spinels. Magnetite rimming spinel has close to end member compositions ($YFe^{3+}$ = 0.97; XMg = 0) and is compositionally identical to magnetite dusts in the serpentine matrix.

## 5) DISCUSSION

### *2.5.1) Primary compositions of spinel*

Cr-spinel cores are likely primary or very close to primary in composition, considering their low $YFe^{3+}$ and $TiO_2$ content. Cr-spinels coexist with pure magnetite in the groundmass, and since magnetite was stable during the serpentinitzation of olivine and orthopyroxene (Evans and Frost, 1975), Cr-spinels must be inherited from precursor primary conditions. Furthermore, core compositions of coarsely grained Cr-spinel are similar within samples, confirming that they likely retained their primary compositions. The Cr-spinel cores show refractory compositions, which is consistent with refractory bulk rock compositions (Fig. 2.5), and the two suggest that these serpentinites were originally forearc mantle peridotites hydrated by slab-derived fluids at the base of the mantle wedge (Saumur et al., see chapter 1).

### *2.5.2) Alteration of Cr-spinel*

Alteration of Cr-spinel took place in two stages. The first stage of alteration involved a replacement of Mg by Fe in spinel during serpentinization (e.g., Barnes, 2000). This is expressed in sample RD68. $Fe^{2+}$ is released during the hydration of olivine to form serpentine and this $Fe^{2+}$ is incorporated in Cr-spinel.

The second stage of alteration resulted in the formation of chlorite with Al and Mg from Cr-spinel. Al and Mg in spinel were replaced by $Fe^{3+}$ and $Fe^{2+}$, forming ferritchromit, and is essentially a "cation for cation" replacement since Cr-spinels preserve their original shapes. Ferritchromit and chlorite are alteration products, since zoning appears to be controlled by an alteration gradient perpendicular to grain boundaries and fractures, and because chlorite only nucleates around such concentrically altered grains. The close spatial relationship between concentrically zoned spinels and chlorite suggests that Al was released during chromite alteration and was taken up by chlorite, and $Fe^{3+}$ replaced Al in spinel, producing ferritchromit. The high content of $Cr_2O_3$ in chlorite also suggests a genetic association with Cr-spinel. Aluminum released during ferritchromit formation could potentially be incorporated in serpentine as well, since lizardite can take up significant Al content (Caruso and Chernosky, 1979).

Cr-spinels with chlorite coronas are reported by Pinsent and Hirst (1977) from the Blue River Ultramafic Body in British Columbia, Canada. They suggest that that ferritchromit and chlorite formed by a reaction involving Cr-spinel, serpentine and brucite, and state that $Fe_2O_3$ and FeO replace $Al_2O_3$ and MgO. We envisage a similar process, except for the lack of brucite in our samples. Other workers have also reported a similar relationship: Fleet et al. (1993) suggested that chlorite formation is contemporaneous with ferritchromit alteration, and Mellini et al. (2005) noted that Al liberated by ferritchromit favours the transformation of lizardite to chlorite. A similar model of "cation for cation" replacement has been proposed by Beeson and Jackson (1969). However, their model involves primary silicates reacting with Cr-spinel producing ferritchromit and chlorite. This is inapplicable here because primary silicates were serpentinized prior to or during $Fe^{3+}$-Al exchange. This is known because chlorite overprints serpentinite and chlorite is intergrown with magnetite. Furthermore, the sharp contact between magnetite rims and Cr-spinel (Fig. 2.2e-h), and the preservation of original shapes of Cr-spinel grains suggests that the two did not react to produce a diffuse ferritchromit zone as described by Bliss and MacLean (1975). Dissolution of Cr-spinel

grains and the formation of ferritchromit overgrowths via various processes (e.g., Wylie et al., 1987; Ulmer, 1974), is also inapplicable.

Grains with intense parting have homogeneous composition probably because of the relative ease that alteration fluids could penetrate into the interiors of grains. Parting overprints zoned Cr-spinels (Fig 2.2a), suggesting that fracturing took place after alteration, and is possibly related to the deformation of the Cr-spinels.

### *2.5.3) Reaction producing ferritchromit and chlorite*

In the balanced reaction found below, the alteration of Cr-spinel to ferritchromit is considered to be essentially a 1:1 cation exchange. Cr-spinel, ferritchromit and chlorite compositions were taken from analyses on grain RD48-TRA (Figs. 2.2g,h; Tables 2.1-2) and assumes that serpentine has ideal compositions:

$$1\ (Mg_{0.45},\ Fe_{0.55})(Cr_{0.56},\ Al_{0.39},\ Fe^{3+}_{0.05})_2\ O_4\ \textit{(PRIM. SPINEL)}$$
$$+\ 0.22\ Mg_3[Si_2O_5](OH)_4\ \textit{(SERPENTINE)}$$
$$+\ 0.09\ FeFe_2O_4\ \textit{(MAGNETITE)}$$
$$+\ 0.22\ H_2O + 0.08\ FeO + 0.06\ Cr_2O_3 + 0.09\ SiO_2\ \textit{(FLUID)}$$
$$=$$
$$1\ (Mg_{0.32},\ Fe_{0.68})(Cr_{0.60},\ Al_{0.26},\ Fe^{3+}_{0.14})_2O_4\ \textit{("EARLY" FERRITCHROMIT)}$$
$$+\ 0.08\ (Mg_{0.8},\ Fe_{0.04},\ Al_{0.12},\ Cr_{0.04})_{12}(Al_{0.22},\ Si_{0.78})_8O_{20}(OH)_{16}\ \textit{(CHLORITE)}$$

Magnetite is likely involved in the reaction since it is the likely most source of $Fe^{3+}$. $Fe^{3+}$ may also have been brought by fluids, in which case the reaction would be consistent with minor breakdown of magnetite. The ferritchromit is classified as "early", because further alteration would produce ferritchromit more depleted in Al and Mg and richer in Fe (see section 2.5.4).

The reaction gives interesting insights on the mobility of Cr. Minor Al-Cr exchange occurs in both the first and second stages of alteration. Cr is generally considered immobile and its distribution is controlled by local abundances (Evans and Frost, 1975) so therefore variations in Cr may at least in part be primary. However, some Cr is likely liberated during serpentinization of pyroxenes. Since significant Al can be taken up by lizardite, small amounts of Cr-Al exchange can potentially occur at low grades. Furthermore, Kimball (1990) showed that the breakdown of Cr-spinel to form chlorite could result in a slight enrichment of Cr in the spinel because of Al-Cr partitioning.

However, our spinels lack evidence of breakdown, since primary shapes are preserved. Nonetheless, since Cr content changes only slightly from core to rim, and because only a small input of $Cr_2O_3$ is necessary to produce the observed zoning, a small-scale breakdown of Cr-spinel may have occurred, liberating Cr incorporated by ferritchromit and chlorite. This would suggest that the alteration is not exactly a 1:1 transformation of spinel to ferritchromit, yet this remains a valid approximation because of the small amount of Cr involved.

The reaction assumes that all Mg and Al were incorporated in chlorite. This is not the case because, as discussed earlier, some Fe-Mg and Cr-Al exchange occurs at lower grades during the first stages of alteration before the formation of ferritchromit and chlorite. Therefore, the amount of chlorite produced and the amount of serpentine consumed in this reaction are maximum values.

### *2.5.4) Conditions of ferritchromit alteration*

Molibization of divalent cations begins at low metamorphic grades and during serpentinzation (e.g., Barnes, 2000). However, serpentinization alone is considered insufficient to produce ferritchromit rims, as many workers consider that further heating is required (e.g., Rost, 1961; Cerny, 1968; Bliss and MacLean, 1975). In sample RD68, which is the least hydrated sample, spinels are unzoned in $YFe^{3+}$, whereas all other samples show ample evidence of mobilization of $Fe^{3+}$. Therefore, all samples, with the exception of RD68, were likely heated to a certain degree.

Most workers have shown that the mobilization of trivalent cations in Cr-spinel producing ferritchromit requires heating up to amphibolite conditions (e.g., Bliss and MacLean, 1975, Pinsent and Hirst, 1977; Barnes, 2000; Tsujimori et al., 2004; Santti et al., 2006). However, most of our samples do not show evidence of thermal metamorphism at amphibolite conditions. All samples are dominated by lizardite, which is stable up to temperatures as high as 300°C (Evans, 2004). Furthermore, characteristic metamorphic minerals such as secondary olivine and enstatite are absent. Minerals stable in amphibolite grades such as tremolite, talc and cummingtonite are present in samples RD34 and RD6-36, yet their occurrence is only local. However, talc is also a mineral formed during early serpentinization (Evans, 1977; Bach et al., 2004) and therefore is not an indicator for high T. Tremolite is stable at upper greenschist grades (Evans, 1977) and can thus be an indicator of slight heating.

Well-developed ferritchromit contains low $Al_2O_3$ and MgO down to nil (e.g., Santti et al, 2006; Liipo et al., 1995, and previously mentioned references). Barnes and Roeder (2001) showed that typical ferritchromit rims in the global database plot along the Cr-$Fe^{3+}$ join in Cr-$Fe^{3+}$-Al triangular plots. Among others, Pinsent and Hirst (1977) and Bliss and MacLean (1975) showed that ferritchromit gradually changes into Cr-bearing magnetite by incorporating $Fe_2O_3$ and FeO during alteration. This is a well-known alteration trend in metamorphic spinels at amphibolite grades (Fig 2.3b-c). In contrast, most of the ferritchromit rims from Cuaba Unit serpentinites still contain substantial Al and Mg (Fig 2.3c). $YFe^{3+}$ is always below 0.35, and $TiO_2$, ZnO, and MnO are also fairly low compared to typical ferritchromit rims from amphibolite terranes (e.g. Barnes 2000; Santii et al., 2006). This suggests that this Cr-spinel zoning represents the early stages of ferritchromit alteration.

Furthermore, chlorite coronas around Cr-spinel typically form at amphibolite grades (e.g. O'Hanley, 1996; Pinsent and Hirst, 1977). However, in our case, chlorite rarely completely envelops entire Cr-spinel grains, suggesting that the conditions for chlorite rim formation have barely been attained. The reaction presented in the above section (section 2.5.3), highlights the fact that very little chlorite is produced with poorly developed "early" ferritchromit. The production of evolved ferritchromit favours the release of Al and Mg and the development of chlorite coronas.

We suggest that the occurrence of poorly developed ferritchromit, along with incomplete chlorite haloes, the dominance of lizardite and the general lack of evidence for thermal metamorphism suggest that amphibolite conditions were not reached, suggesting that Fe-Al diffusion in Cr-spinel may become significant at temperatures lower than previously estimated. Ferritchromit rims are well developed at amphibolite grades and temperatures of at least 500°C (e.g., Barnes, 2000). However, Kimball (1990) showed that zoning in Cr# during hydrothermal alteration occurs at temperatures as low as 400°C, which is in upper greenschist conditions and close the upper stability limit of lizardite. Standish et al. (2002) also report ferritchromit formed at temperatures below 500°C. It is therefore possible that $Fe^{3+}$-Al exchange starts at temperatures near 300°C, but would not be sufficiently hot to produce "evolved" ferritchromit rims.

Alternatively, amphibolite or near-amphibolite conditions may have been reached, but for only a very short period of time, since lizardite is metastable in the stability field of antigorite (Dungan, 1977). This would be consistent with the local occurrence of tremolite and cummingtonite.

In any case, further metamorphism of these serpentinites would have allowed the recrystallization of lizardite to antigorite, and would have encouraged the formation of "evolved" ferritchromit rims and complete chlorite coronas. Furthermore, the lack of $Fe^{3+}$ mobilization in sample RD68 confirms previous interpretations suggesting that serpentinization alone is not enough to produce ferritchromit and that heating event of some magnitude is required.

### *2.5.5) Possible processes causing ferritchromit alteration*

Serpentinites from the Cuaba Unit protruded through the forearc mantle along the Septentrional Fault Zone in response to collision of the Caribbean plate with the Bahamas Platform (Saumur et al., see chapter 1). The interiors of mantle wedges are relatively hot compared to their bases near the slab (e.g. Peacock, 1996). Therefore, during protrusion, serpentinites could be heated for a short period of time during their passage through the hotter interior of the mantle wedge. They would be later cooled once shallow mantle or crustal levels were reached. Alternatively, formation of ferritchromit and chlorite could be related to contact metamorphism associated with the intrusion of the Rio Boba Gabbro.

## 2.6) CONCLUSIONS

Cr-spinel shows compositional zoning with high $Fe^{2+}$ and $Fe^{3+}$ and a slight increase of Cr towards rims. The zoning is explained by two stages of alteration: the first is essentially a replacement of MgO by FeO, and the second is additional replacement of MgO by FeO along with replacement of $Al_2O_3$ by $Fe_2O_3$ (and $Cr_2O_3$), with released MgO and $Al_2O_3$ consumed by newly formed chlorite. However, because ferritchromit rims are still rich in Al and Mg, and because chlorite coronas are poorly developed, this alteration represents the early stages of alteration of primary Cr-spinels. It occurred either at metamorphic grades lower than most reported occurrences of ferritchromit, or in response to a short lived thermal metamorphic event. This study illustrates that primary ratios of divalent and trivalent cations can be slightly modified at temperatures below those of amphibolite grades, and therefore one must be cautious when interpreting Cr-spinel compositions even in only slightly metamorphosed serpentinites.

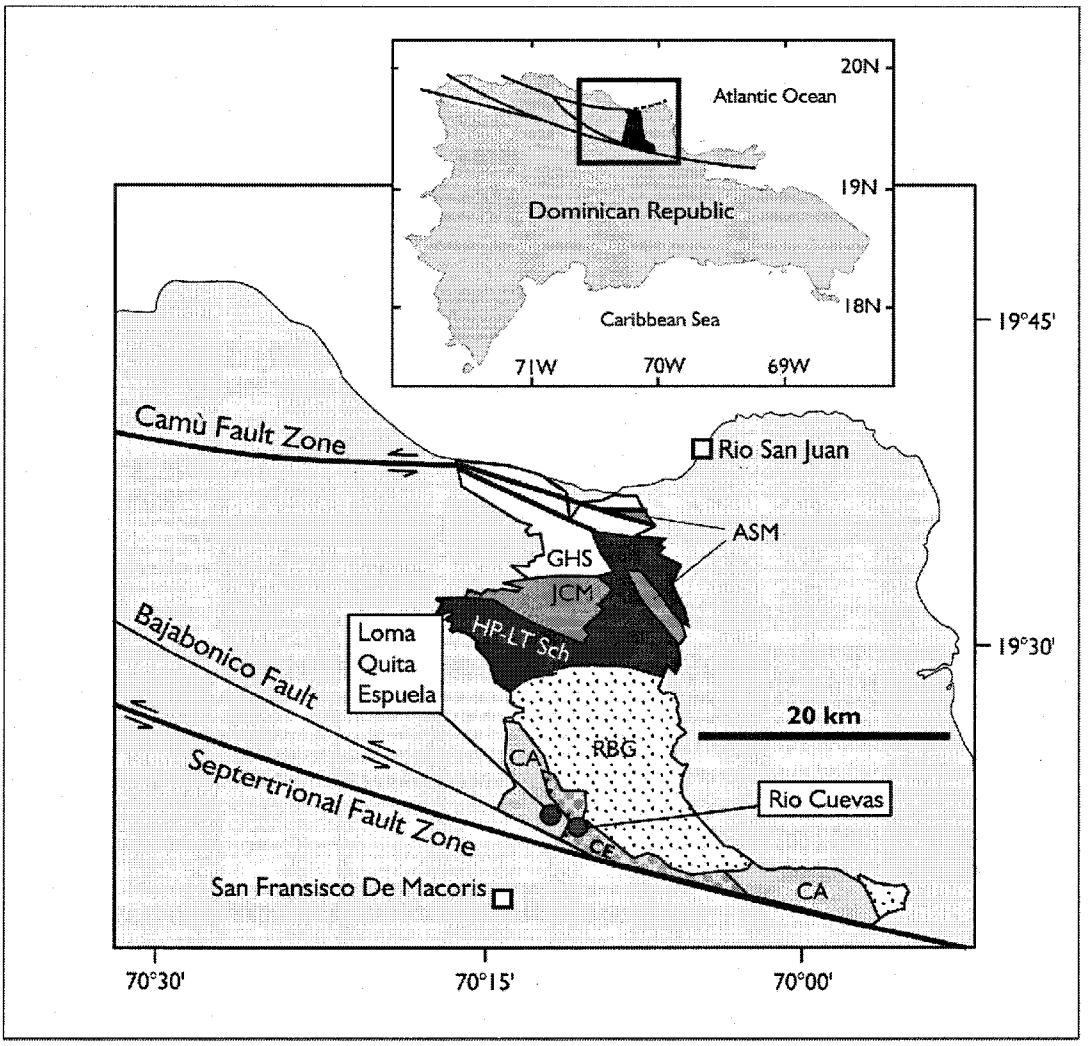


**Figure 2.1** Rio San Juan Complex, northern Dominican Republic. The northern part of the complex is composed of low temperature serpentinites (Gaspar Hernanzez serpentinites; GHS) two blueschist and eclogite bearing serpentinite mélanges (Jagua Clara Mélange - JCM and Arroyo Sabana Mélange - ASM) and a coherent HP-LT schist unit. The southern part of the complex is composed of the Cuaba Unit (Amphibolites - CA; Eclogites CAE), and is intruded by the Rio Boba Gabbroic Unit to the north (RBG). Two localities form the study area: Rio Cuevas and Loma Quita Espuela. Modified from Draper and Nagle (1991) and Abbott et al. (2006).

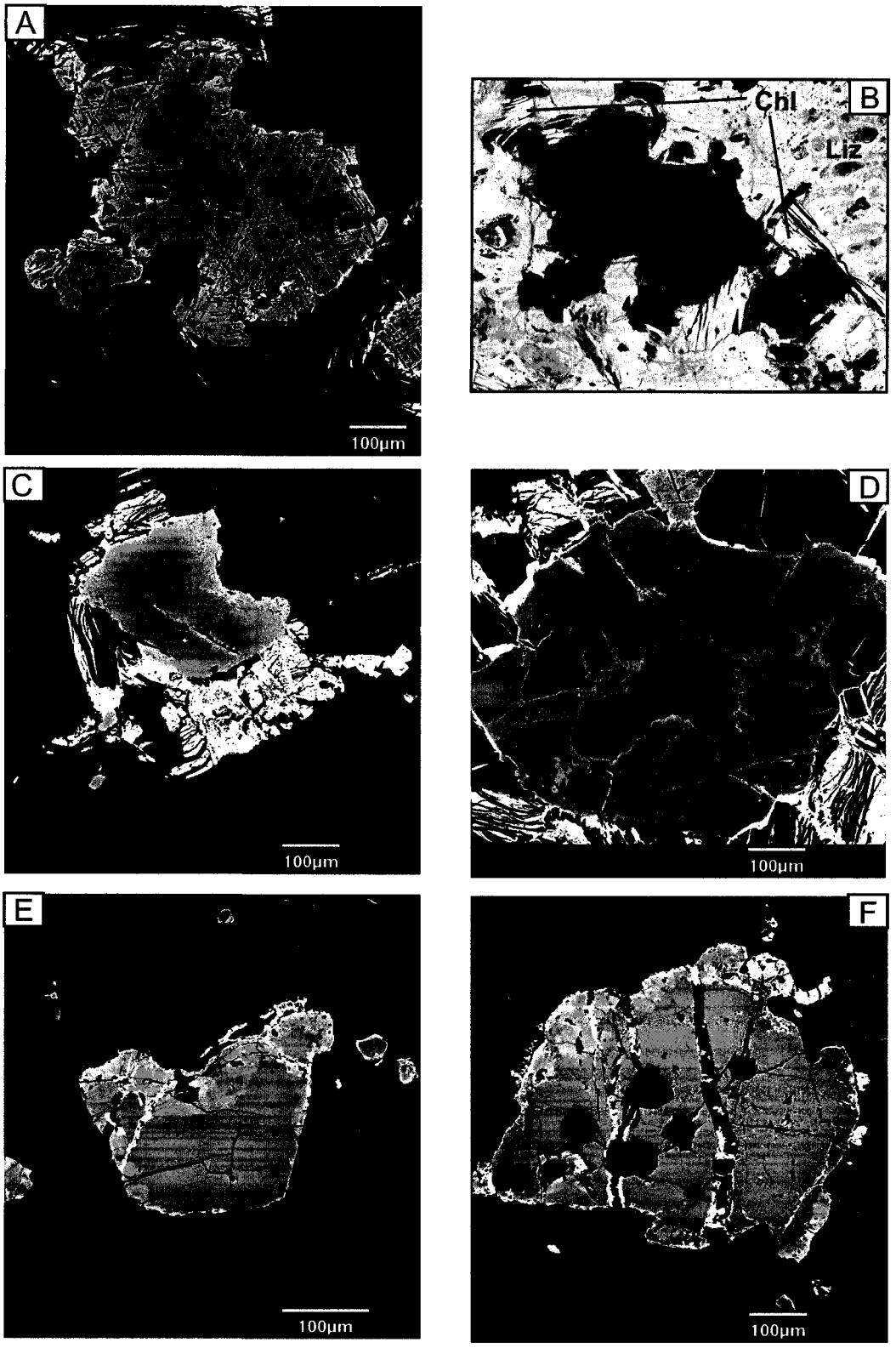


**Figure 2.2**

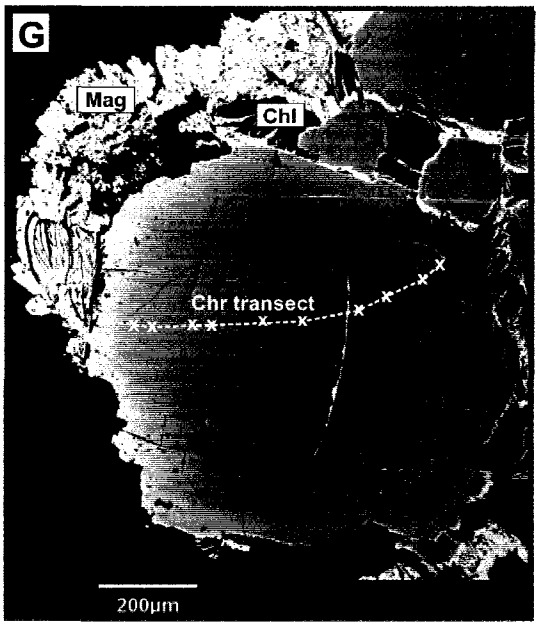


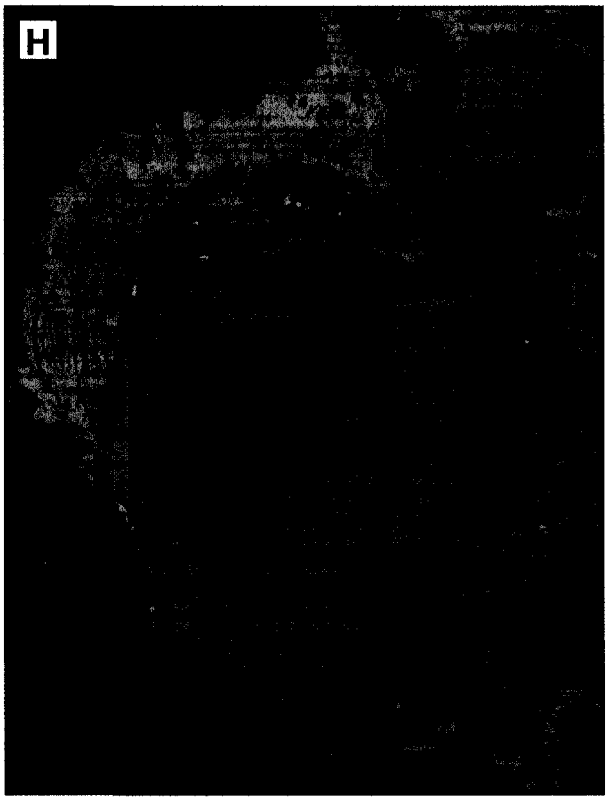


**Figure 2.2 (continued)**

**Figure 2.2 A)** BSE-image, Sample RD34c, gradually zoned Cr-spinel cut by polygonal partings. **B)** Transmitted light photomicrograph of the Cr-spinel grain shown in Fig. 2a, plane polarised light. Note the chlorite (clear, high relief) around the Cr-spinel which overprints serpentine and its intergrowth with magnetite (symplectite). **C)** BSE-image of Cr-spinel showing graduate zoning and Cr-spinel showing gradual zoning and a sharp compositional contrast with magnetite overgrowths. Magnetite is intertwined with chlorite (black). The matrix is lizardite (black in the image). Sample RD48. **D)** BSE-image, Sample RD48, gradually zoned Cr-spinel, with overgrowths of magnetite and chlorite. Note the relationship between zoning and grain boundaries and parting. The center of the grain is filled with well crystallized chlorite and lizardite **E)** BSE-image, sample RD68, Cr-spinel showing sharp contrast between core and slightly altered rim. **F)** BSE-image, sample RD68, weakly zoned core of Cr-spinel and a sharp contrast with bright magnetite overgrowths. **G)** BSE-image, Gradually zoned Cr-spinel on which transect was carried out. Magnetite and chlorite were identified. **H)** Reflected light photomicrograph, uncrossed polars. Note the sharp boundary between Cr-spinel and magnetite overgrowths.

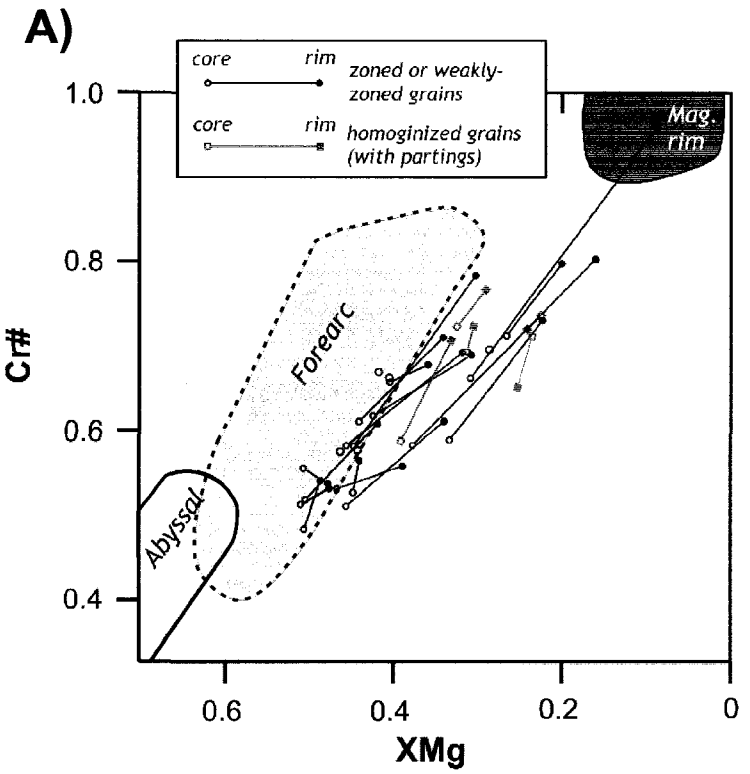
A)
core
rim
zoned or weakly-zoned grains
core
rim
homoginized grains (with partings)
Mag. rim
Forearc
Abyssal
Cr#
1.0
0.8
0.6
0.4
0.6
0.4
0.2
0
XMg

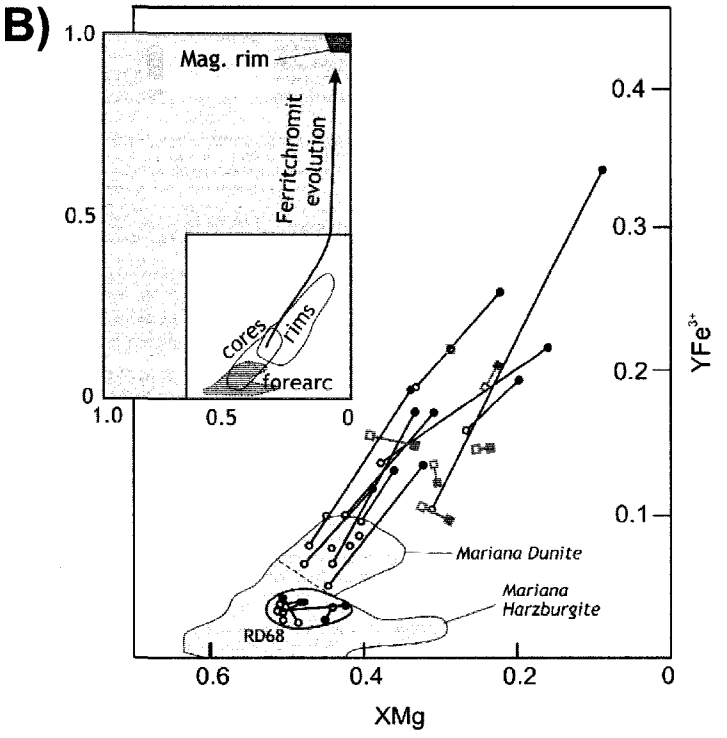
B)
1.0
Mag. rim
Ferritchromit evolution
0.5
0
1.0
0.5
0
cores
rims
forearc
0.4
0.3
0.2
0.1
YFe3+
Mariana Dunite
Mariana Harzburgite
RD68
0.6
0.4
0.2
0
XMg

**Figure 2.3**

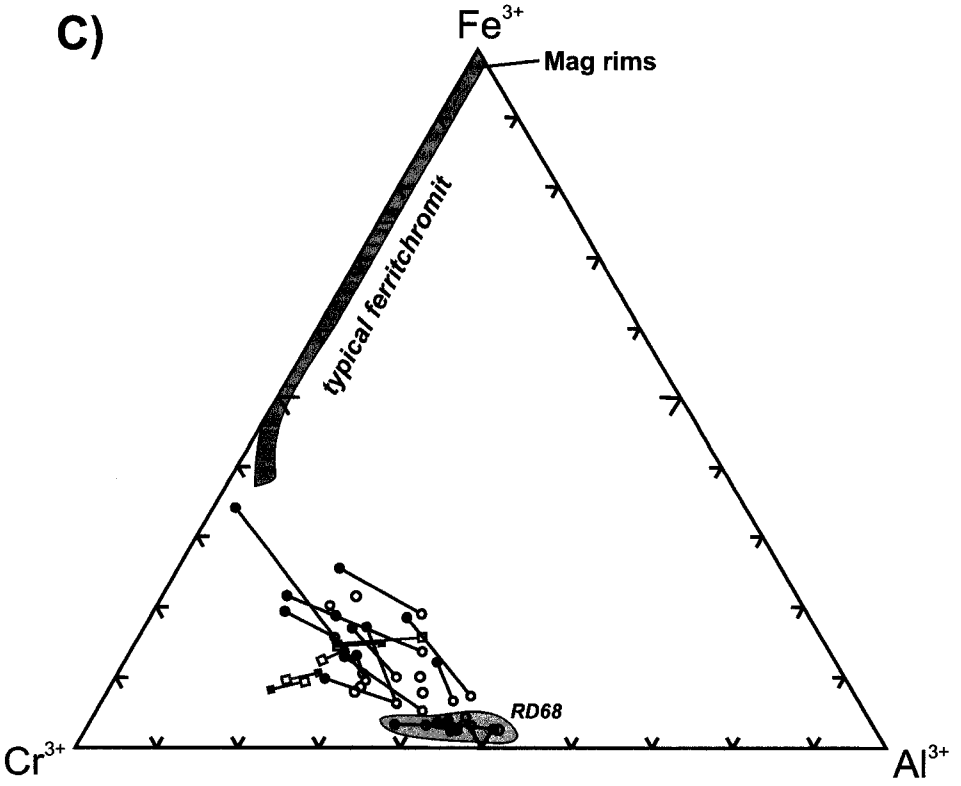


**Figure 2.3)** Composition of cores and rims of zoned Cr-spinels. Open circles are cores of grains and filled circles represent grain rims. Grains with penetrative partings are shown in light grey and with squares instead of circles (see legend on top of fig. A). One "core-rim" pair represents one grain. **A)** Cr# vs XMg, **B)** YFe3+ vs. XMg and **C)** ternary diagram of Cr-Fe3+-Al. Note the enrichment in Fe at the expense of Al and Mg. Nevertheless, cores and rims are low in Fe compared to typical ferritchromit rims. Also, in figure C, a slight enrichment in Cr is noted. Magnetites from this study are low in Cr and consequently plot in the fields of "mag rims" (in low temperature serpentinites, Evans and Frost, 1975). The forearc fields are based on data from spinel from peridotites from Mariana Forearc (Ishii et al., 1992) and the field of abyssal peridotites is taken from Dick and Bullen (1984). Typical ferritchromit alteration trends (Fig. B) and compositions (Fig. C) are from Barnes and Roeder (2001), Pinsent and Hirst (1977) and Liipo et al. (1995).

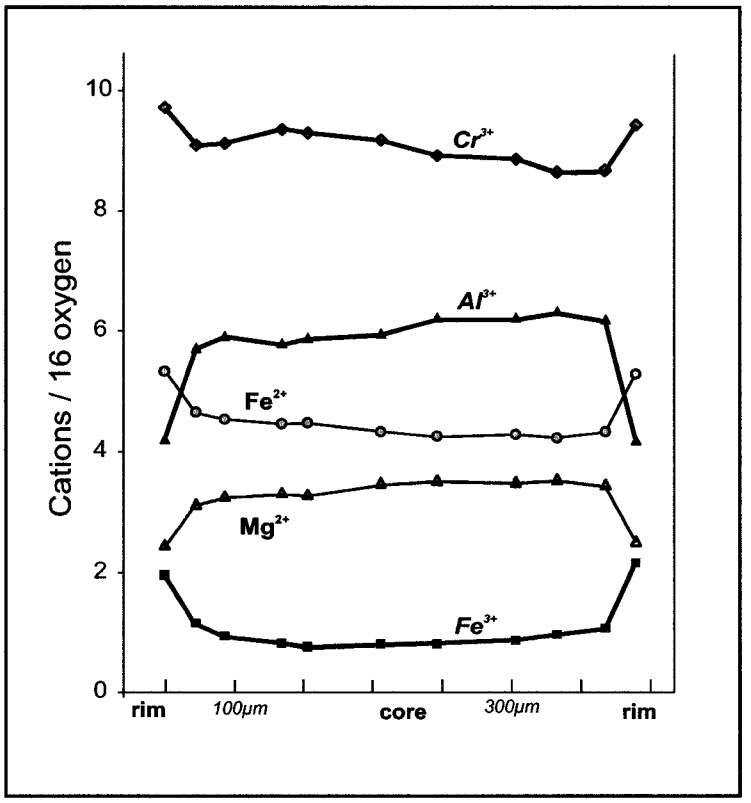


**Figure 2.4)** Compositional transect of Cr-spinel grain from sample RD48 (fig 2g-h). Fe3+ contents were determined assuming stoichiometry is respected.

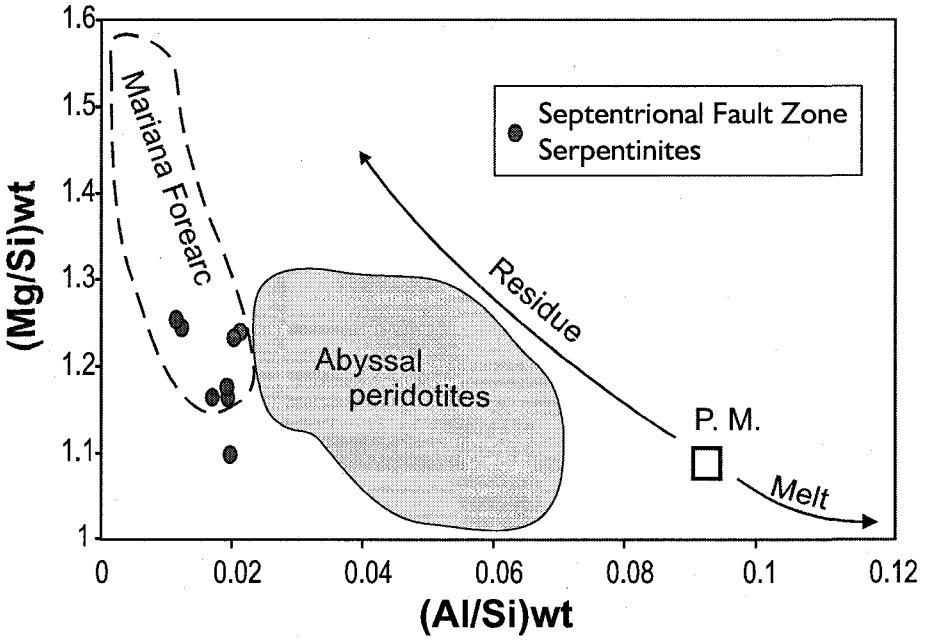


**Figure 2.5)** Mg/Si vs. Al/Si bulk rock weight ratios of Cuaba Unit (Septentrional Fault Zone) serpentinites. The compositional variations expected during partial melting are shown with arrows. Depletion is similar to Forearc Peridotites from the Mariana Forearc (Ishii et al., 1992; Parkinson and Pearce, 1998). Diagram is modified from Saumur et al. (in prep.) and Guillot and Hattori (2007). The field of abyssal peridotite is defined by data compiled by Niu (2004), with outlier values removed. Primitive mantle values (P.M.) are from McDonough and Sun (1995).

## Table 2.1) Representative Cr-spinel and magnetite compositions

| sample | slightly zoned RD48-T | | | slightly zoned RD34C-1 | | zoned - Fe rich core RD34A-K | | chromite with partings RD60-2 | | weakly zoned 68B-4-1 | |
|---|---|---|---|---|---|---|---|---|---|---|---|
| | core chromite | rim ferritchr | magnetite near chro | core chromite | rim ferritchr | core Fe-chro | rim ferritchr | core ferritchr | rim ferrtichr | core chromite | rim chromite |
| $SiO_2$ | 0.04 | 0.12 | 0.81 | – | – | 0.52 | 0.13 | – | 0.06 | 0.01 | – |
| $Al_2O_3$ | 20.71 | 13.22 | 0.03 | 23.24 | 20.06 | 15.22 | 1.21 | 12.3 | 10.49 | 25.26 | 24.61 |
| $TiO_2$ | 0.06 | 0.23 | – | 0.08 | 0.14 | 0.15 | 0.95 | 0.28 | 0.17 | 0.02 | 0 |
| $V_2O_3$ | 0.16 | 0.23 | – | 0.28 | 0.32 | 0.25 | 0.32 | 0.55 | 0.44 | 0.25 | 0.3 |
| $Cr_2O_3$ | 43.99 | 44.36 | 0.82 | 40.31 | 38.28 | 44.68 | 41.86 | 48.21 | 50.86 | 40.73 | 42.74 |
| $Fe_2O_3$ | 4.48 | 10.65 | 65.58 | 5.69 | 9.7 | 8.33 | 23.71 | 8.39 | 7.56 | 3.62 | 2.15 |
| FeO | 20.11 | 23.44 | 31.54 | 19.5 | 21.87 | 24.54 | 29.26 | 23.69 | 24.51 | 18.85 | 19.82 |
| MgO | 9.25 | 6.32 | 0.12 | 9.93 | 7.86 | 6.19 | 1.58 | 6.33 | 5.67 | 10.78 | 10.08 |
| MnO | 0.27 | 0.42 | 0.05 | 0.28 | 0.37 | 0.46 | 0.79 | 0.58 | 0.45 | 0.31 | 0.31 |
| NiO | 0.07 | 0.12 | – | 0.1 | 0.14 | 0.14 | 0.18 | n.a. | n.a. | n.a. | n.a. |
| ZnO | 0.82 | 0.71 | – | 0.77 | 0.68 | 0.95 | 0.47 | 0.46 | 0.47 | 0.53 | 0.64 |
| CaO | 0.01 | 0.01 | 0.03 | 0.03 | – | 0.19 | 0.01 | 0.03 | 0.02 | – | – |
| TOTAL | 99.97 | 99.83 | 98.98 | 100.21 | 99.42 | 101.62 | 100.47 | 100.82 | 100.7 | 100.36 | 100.65 |
| **O = 32** | | | | | | | | | | | |
| Si | 0.01 | 0.031 | 0.251 | – | – | 0.136 | 0.037 | – | 0.06 | 0.002 | – |
| Al | 6.214 | 4.194 | 0.009 | 6.859 | 6.134 | 4.703 | 0.418 | 3.878 | 3.353 | 7.337 | 7.177 |
| Ti | 0.011 | 0.047 | – | 0.014 | 0.027 | 0.03 | 0.21 | 0.056 | 0.035 | 0.004 | 0 |
| V | 0.033 | 0.049 | – | 0.056 | 0.066 | 0.052 | 0.077 | 0.118 | 0.096 | 0.049 | 0.06 |
| Cr | 8.853 | 9.442 | 0.201 | 7.981 | 7.853 | 9.264 | 9.752 | 10.201 | 10.905 | 7.934 | 8.361 |
| $Fe^{+3}$ | 0.858 | 2.157 | 15.288 | 1.072 | 1.894 | 1.645 | 5.258 | 1.69 | 1.543 | 0.67 | 0.4 |
| $Fe^{+2}$ | 4.282 | 5.278 | 8.17 | 4.084 | 4.746 | 5.382 | 7.21 | 5.302 | 5.558 | 3.883 | 4.102 |
| Mg | 3.511 | 2.534 | 0.057 | 3.706 | 3.039 | 2.42 | 0.696 | 2.525 | 2.29 | 3.96 | 3.719 |
| Mn | 0.058 | 0.097 | 0.012 | 0.059 | 0.082 | 0.102 | 0.198 | 0.131 | 0.103 | 0.064 | 0.064 |
| Ni | 0.014 | 0.026 | – | 0.02 | 0.03 | 0.031 | 0.042 | n.a. | n.a. | n.a. | n.a. |
| Zn | 0.154 | 0.141 | – | 0.142 | 0.129 | 0.184 | 0.102 | 0.091 | 0.093 | 0.097 | 0.117 |
| Ca | 0.004 | 0.002 | 0.01 | 0.007 | – | 0.053 | 0.002 | 0.008 | 0.006 | – | – |
| Cr# | 0.59 | 0.69 | 0.96 | 0.54 | 0.56 | 0.66 | 0.96 | 0.72 | 0.76 | 0.52 | 0.54 |
| $YFe^{3+}$ | 0.05 | 0.14 | 0.99 | 0.07 | 0.12 | 0.11 | 0.34 | 0.11 | 0.10 | 0.04 | 0.03 |
| XMg | 0.45 | 0.32 | 0.01 | 0.48 | 0.39 | 0.31 | 0.09 | 0.32 | 0.29 | 0.50 | 0.48 |

Cr# = Cr / (Cr + Al); $YFe^{3+}$ = Fe3+/($Fe^{3+}$+Cr+Al); XMg = Mg/(Mg+$Fe^{2+}$)

n.a.; not analysed; – : below detection limit

ferritchr = ferritchromit; Fe-chro: Iron rich chromite core

$Fe_2O_3$ content was calculated assuming stoichiometric compositions

## Table 2.2) Representative chlorite compositions

| | 636B-C-7 | 636B-B-4 | 636C-1-1 | 48- tra-19 | 34A-K-5 |
|---|---|---|---|---|---|
| $SiO_2$ | 32.48 | 31.24 | 32.13 | 32.42 | 31.56 |
| $Al_2O_3$ | 16.59 | 17.1 | 15.98 | 13.93 | 17.55 |
| $TiO_2$ | 0.11 | 0.1 | – | – | – |
| $Cr_2O_3$ | 1.24 | 1.82 | 2.04 | 3.01 | 1.79 |
| FeO | 3.06 | 3.52 | 3.84 | 2.79 | 3.65 |
| MgO | 32.6 | 32.52 | 33.71 | 33.59 | 33.4 |
| CaO | – | 0.01 | 0.01 | 0 | 0.01 |
| Cl | 0.03 | 0.02 | n.a. | 0.04 | n.a. |
| F | 0.22 | 0.17 | 0.14 | 0.04 | n.a. |
| TOTAL | 86.33 | 86.5 | 87.85 | 85.83 | 87.97 |
| | | | | | |
| **Formula Basis O = 28** | | | | | |
| Si | 6.18 | 5.97 | 6.06 | 6.24 | 5.93 |
| Al | 1.82 | 2.03 | 1.94 | 1.76 | 2.07 |
| SUM | 8.00 | 8.00 | 8.00 | 8.00 | 8.00 |
| | | | | | |
| Al | 1.91 | 1.83 | 1.62 | 1.40 | 1.81 |
| Ti | 0.02 | 0.01 | – | – | – |
| Cr | 0.19 | 0.28 | 0.31 | 0.46 | 0.27 |
| Fe | 0.49 | 0.56 | 0.61 | 0.45 | 0.57 |
| Mg | 9.25 | 9.27 | 9.48 | 9.64 | 9.35 |
| Ca | – | 0.00 | 0.00 | 0.00 | 0.00 |
| SUM | 11.85 | 11.95 | 12.01 | 11.95 | 12.00 |
| | | | | | |
| Cl | 0.01 | 0.01 | n.a. | 0.02 | n.a. |
| F | 0.13 | 0.10 | 0.08 | 0.01 | n.a. |
| | | | | | |
| SUM | 0.14 | 0.11 | 0.08 | 0.04 | n.a. |
| | | | | | |
| XMg | 0.95 | 0.94 | 0.94 | 0.96 | 0.94 |

XMg = Mg/(Mg+Fe)
n.a.: not analysed; –: below detection limit

# CHAPTER 3

## Petrology and geochemistry of garnet peridotites and corundum-bearing garnet wehrlites from Rio Cuevas

*A report by B.-M. Saumur, Dept. Earth Sciences, Univ. Ottawa*

### 3.1) INTRODUCTION

Ultra-high pressure (UHP) terranes are common worldwide in areas of continental collision (e.g., Liou et al., 2004; Brueckner and Medaris, 2000), yet UHP-rocks have only been described in only two oceanic subduction complexes: in the Higashi-araishi peridotite body of the Sanbagawa metamorphic belt, Japan (e.g. Mizukami and Wallis, 2005; Enami et al., 2004), and in the southern Rio San Juan Complex of Dominican Republic (Abbott et al., 2005; 2006; 2007). In both cases, the UHP rocks are garnet bearing ultramafic rocks, a rock type synonymous with UHP metamorphic conditions since garnet is known to be the stable aluminium phase at mantle depths greater than ~50 km (e.g., O'Hara et al., 1971).

Garnet peridotites and garnet clinopyroxenites occur within the southern part of Rio San Juan Complex, within the Cuaba Amphibolites (or Cuaba Unit) in a zone rich in variably retromorphosed eclogite (Abbott et al., 2005; Fig 3.1). The unit was formed between the Cretaceous and the mid-Eocene during the south-westward subduction of the Proto-Caribbean lithosphere under the Caribbean Plate, and the unit was exhumed in response to post-Eocene transpression (e.g., Mann and Gordon, 1991; Draper and Nagle, 1991). The Cuaba Unit was originally interpreted as fore-arc basement (Draper and Nagle, 1991), but the occurrence of retromorphosed eclogites implies an oceanic protolith, and accordingly later publications consider the Cuaba Unit to have an oceanic origin (e.g., Abbott et al., 2005).

Abbott et al. (2005; 2007) argue for a cumulate origin for the garnet peridotites and garnet clinopyroxenites from Dominican Republic. They interpret that the magmas were generated at UHP-conditions at the base of the lithosphere, and therefore that spinel, garnet and corundum are magmatic, arguing that the evolution from garnet peridotite to garnet clinopyroxenite to corundum bearing garnet clinopyroxenite forms a constrained but well defined liquid line of descent. This model of UHP-magma paragenesis producing ultramafic cumulates is contentious, since most occurrences of garnet peridotites worldwide are interpreted to have low-pressure protoliths (i.e. plagioclase or spinel bearing peridotites or gabbros formed from melts) affected by subducition zone prograde metamorphism (i.e. Sanbagawa, Enami et al., 2004), as garnet peridotites originating from deep mantle levels, or mantle spinel peridotites heated by upwelling astenosphere (e.g., Brueckner and Medaris, 2000). Furthermore, more than one process can be at play in a given subduction complex. For example, Kornprobst et al. (1990) report 2 types of garnet bearing clinopyroxenites from Beni Bousera, Morocco: the first were generated by high-pressure magma fractionation where garnet and corundum are primary magmatic aluminous phases (similar model to Abbott et al., 2005), and the second were generated at low pressures where Ca-plagioclase was the primary aluminous phase and subduction zone metamorphism eventually formed garnet.

In this report, I focus mostly on bulk rock and trace element geochemistry of the garnet peridotites that we sampled in Rio Cuevas. Abbott et al. (2005; 2006) have yet to report any bulk rock chemistry and such data can obviously provide significant information on the origin of these rocks. Furthermore, a petrographic study and preliminary mineral analyses are also included. Ultimately, these results will be used to determine the origin of garnet peridotites from the southern Rio San Juan Complex, and to see if they support either the UHP-magma genesis model of Abbott et al. (2005) or another alternative model.

## 3.2) METHODS

Mineral compositions were determined using an automated 4 spectrometer CAMEBAX MBX electron probe (Carleton University) by the wavelength dispersive x-ray analysis method (WDX). Counting times were 15 seconds per element, except for Fe (20 s) and Ni (40 s). A 15 kV accelerating potential and a 20 nA beam current were applied. The calibration standards used were pure wollastonite (Si, Ca), synthetic spinel (Al), synthetic $Cr_2O_3$ (Cr), forsterite (Mg), synthetic $MnTiO_3$ (Mn, Ti), pure vanadium metal (V),

albite (Na), fayalite (Fe in silicates) and synthetic $Fe_2O_2$ (Fe in oxides). $Fe_2O_3$ contents of spinel were determined assuming that stoichiometry is respected.

Major and minor element concentrations were determined using a Phillips PW 2400 X-ray fluorescence spectrometer (University of Ottawa) after fusing bulk rock powder with a flux composed of 78.5% lithium tetraborate ($Li_2B_4O_7$) and 21.5% lithium metaborate ($LiBO_2$). Platinum group element (PGE) concentrations were determined by isotopic dilution techniques using a mixed spike of $^{101}Ru$, $^{105}Pd$, $^{190}Os$, $^{191}Ir$ and $^{194}Pt$. PGEs were pre-concentrated in a Ni-sulphide bead, which was dissolved in 6N HCl, and the filtrate was dissolved in concentrated $HNO_3$. Mass ratios were determined using an Agilent HP 4500 inductively coupled plasma mass spectrometer (ICP-MS) (University of Ottawa). Blanks were 0.002-0.007 ng Ir/g flux, 0.002-0.006 ng Os/g flux, 0.07-16 ng Pt/g flux and 0.03-0.9 ng Pd/g flux and 0.002-0.007 ng Ru/g flux. These values are negligible compared to amounts in samples and thus blank corrections were not applied to the results.

Nd and Sm concentrations were determined by adding a solution enriched in $Nd^{148}$ and $Sm^{149}$ to sample powders. These were digested with HF-$HNO_3$, and an alkali column was used to separate Nd and Sm from LREE. Trace element data were obtained from ACME Laboratories (Vancouver), where bulk samples were digested in HF-$HNO_3$-$HClO_4$-HCl and were run with an ICP-MS.

## 3.3) PETROLOGY

A grand total of 10 samples were collected from Rio Cuevas (Table 3.1, Figure 3.2a). All peridotites occur as boulders between 1-4 me in size. The Rio Cuevas stream is at most 6 meters wide and very shallow, and therefore boulders were not transported great distances. Abbott et al. (2005) interpret that the boulders did not come from one large body but from several smaller bodies within the eclogites of the Cuaba Unit. All samples are undeformed and coarse grained. Outcrops on the side of the river are eclogite or retromorphosed eclogite (amphibolite), or post-Eocene limestone. In addition to peridotites, a wide variety of boulders are found in the river, namely fresh eclogite, retromorphosed eclogite (amphibolite, occasionnally with preserved garnet) and serpentinite (RD45, RD48 and RD60, see chapter 1).

Samples RD40, RD61, RD62, RD62b, RD63 and RD6-13b are **garnet peridotites**. Orthopyroxene is not present and therefore, based on the classification of Le Maître

(1989) and on modal olivine content, they can be classified as wehrlites (olivine >40%) or olivine clinopyroxenites (olivine < 40%)[1].

Pink garnet forms grains as large as 1.5 cm in diameter and are subhedral to anhedral. They contain inclusions of euhedral green spinel and green hornblende. Garnet is often rimmed by 0.5 to 5 mm thick secondary green rims composed of fine grained amphibole and spinel forming a kelyphitic texture ("kelyphite rims", Fig. 3.2b, 3.3d-e). Kelyphite can often completely replace garnet. Fresh garnet forms between 5% and 10% of the rocks, but if we assume that fine grained kelyphite was originally garnet, this number increases up to 40% before secondary alteration. Garnets appear to be granoblastic, since individual hexagonal-shaped garnet grains within granoblasts are occasionally rimmed by green spinel (Fig. 3.3d-e). Garnet granoblasts contain inclusions of fine grained hornblende (clinopyroxene hydrated by secondary alteration) and spinel.

Green spinel (<3%) forms euhedral to subhedral grains, occurs as inclusions in garnet granoblasts and appears to rim original garnet grains (Fig 3.3d-e). They occur as fine grains in kelyphite and also elsewhere in the rock in contact with clinopyroxene.

Clinopyroxene (10-15%) can form large (up to 5 mm) crystals which exhibit spectacular twinning under crossed polars (Fig 3.3f). Clinopyroxene is subhedral to anhedral, and is often replaced by secondary magnesiohornblende. Before secondary hydration, clinopyroxene formed probably between 30-40% of the rock.

Olivine (30-40%) is present in variable amounts within the rock and does not seem to share mutual grain contacts with garnet (Fig 3.3a). Grains are large (< 4 mm), euhedral and are partially serpentinized. A cumulate texture with large cpx originally described by Abbott et al. (2005) is occasionally discernable, yet because of secondary serpentinization is often difficult to observe.

RD50 and RD51 are similar in mineralogy but are distinguished by Crn inclusions (0.2 to 1 mm in size) in garnet (Fig 3.3b-c) and are therefore **Crn-bearing garnet wehrlite.**[2] Corundum is surrounded by spinel and brown amorphous material rich in Ca (Fig 3.3c, see table 3.3 for analysis of Crn and associated phases).

---

[1] Based on classification by Le Maître (1989), rocks where olivine is under 40% are not peridotites and should technically be called garnet pyroxenites. However, because the modal proportion is close to or just under 40% and can locally change within boulders, and to simplify the text, I refer to garnet wehrlites and garnet olivine clinopyroxenites together as garnet peridotites. Furthermore, this simplification is useful since "garnet clinopyroxenites" described by Abbott et al. (2005) contain no olivine whatsoever. A clear distinction is therefore made between the rocks in this study and those described by Abbott et al. (2005).

[2] More recent thin sections (Dec. 2007) show that RD40 also is a Crn-bearing garnet wehrlite.

RD57 is devoid of garnet and spinel and is composed of anhedral clinopyroxene partially altered to magnesiohornblende (25%) and olivine (75%), and is therefore a **wehrlite**. RD59 is a **dunite** composed of 90% olivine and 10% magnesiohornblende. In both samples, olivine is crosscut by secondary serpentine. RD57 contains trace secondary chlorite, and both RD57 and RD59 contain highly altered Cr-spinel. Both samples preserve a cumulate texture.

### 3.4) MINERAL CHEMISTRY

Preliminary mineral analyses are available in appendix D.8 and are summarized in Table 3.2. Olivine in all samples is relatively low in magnesium ($Fo_{74-83}$) compared to typical olivine from mantle residues (i.e., $Fo_{90-92}$; Arai, 1994). Olivines in dunite (RD59) have the highest Mg content, followed by the wehrlite (RD57) and finally the aluminous garnet bearing peridotites. Clinopyroxene compositions are similar in all samples, with XMg (= atomic ratio of $Mg/[Mg+Fe^{2+}]$) between 0.86 and 0.90, and their compositions are similar to clinopyroxenes from other arc-related ultramafic intrusions (Fig. 3.3a-b). Spinels are extremely aluminum rich and XMg varies between 0.50 and 0.62. Spinels occurring as inclusions within garnet, in kelyphitic rims and in the Cpx matrix appear to all have similar compositions within the same sample. Such Al-spinels are common in metamorphosed ultramafic rocks (Evans, 1977; Barnes and Roeder, 2001). Garnets are relatively rich in the almandine end member (Fig. 3.3c) and those from samples RD51, RD62 and RD63 have similar compositions to Grt-peridotites from the Sanbagawa metamorphic belt (Enami et al., 2004).

### 3.5) BULK ROCK COMPOSITIONS

In similar fashion to other Grt-bearing ultramafic rocks interpreted to be cumulates (i.e. Higashi-Akaishi, Enami et al., 2004; Beni Bousera, Kornprobst et al., 1990), bulk rock compositions in CaO, $Al_2O_3$ and $TiO_2$ systematically increase with decreasing MgO content (Table 3.4, Fig 3.8), and MgO and FeO are positively correlated. All samples are depleted in compatible elements such as Ni, Mg, Cr and Co relative to primitive mantle values (Fig. 3.5 and 3.6). With the exception of RD59 and RD57, samples are enriched in incompatible Al and Ca relative to primitive mantle compositions (Fig. 3.6). They have bulk rock compositions distinctly different from mantle residues (Fig. 3.6) and thus the evidence suggests that all samples are indeed cumulates. The "garnet-less" rocks (RD57 and RD59) are the most depleted samples, whereas RD62 (vein sample) has

the most evolved compositions (Fig 3.5). Furthermore, all samples appear are slightly depleted in high field strength elements (HFSE) such as Ti, Y, and Zr (Fig. 3.7). A negative Zr anomaly is best observed in figure 3.5. Finally, all samples are considerably high in Sr abd Ba compared to primitive mantle values (figure 3.5).

All peridotites are low in compatible Ir-group PGEs and high in compatible Pd-group PGEs (Table 3.7; Fig 3.9, 3.10). In peridotites samples containing garnet, counts for Ir were extremely low and in the case of garnet peridotites, they are below the limits of detection. Ir values are likely not that low in reality and analytical problems may be to blame for these anomalous results. It is possible that the garnets did not fuse very well during sample firing, and that this affected the recovery of Ir. Nevertheless, low concentrations of Os and Ru together with high concentrations of Pd-Group PGEs suggest that Ir concentrations are of an order similar to Os and Ru and present at slightly lower concentrations than RD57 and RD59. Because Ir-group PGEs are compatible and Pd-group PGEs are incompatible during mantle melting (e.g., Brenan et al., 2005), the observed concentrations suggest an origin from a melt.

REE concentrations are quite low, and for some elements concentrations provided by ACME labs were below their limits of detection (Table 3.6). With the exception of RD62, Ce (0.32-1.26 times chondrite), Sm (0.33 - 1.48 times chrondrite) and Nd (0.6 - 2.13 times chrondrite) are close to or under chondritic values.

## 3.6) DISCUSSION

### *3.6.1) Defining the Magmatic Suite*

Bulk rock compositions depleted in compatible elements and low concentrations in Ir-group PGEs clearly show that the peridotites were crystallized from a melt. This is supported by forsterite content between 74% and 84% in olivines, which are uncommon in mantle residues, and cumulate textures preserved in some samples.

Abbott et al. (2005) describe three types of garnet peridotite in Rio Cuevas:

- Garnet peridotite, which is the most common lithology
- Garnet clinopyroxenite, devoid of olivine
- Corundum bearing garnet clinopyroxenite, devoid of olivine as well, and found in cm to dm scale veins cutting boulders of Grt-clinopyroxenite, and are therefore a UHP equivalent of pegmatite.

RD40, RD61, RD62, RD62b, RD63 and RD6-13b are garnet peridotites and our observations are similar to those by Abbott et al. (2005). We unfortunately have not

sampled any rock where olivine is absent. However, these authors have sampled areas east of Rio Cuevas that we did not have the chance to visit. Nevertheless, our study suggests that we observe three rock types that were not previously described: dunite (RD59), wehrlite (RD57) and Crn-bearing garnet wehrlite (RD50-51).

All the peridotites are interpreted to all be part of the same magmatic suite. Dunite (RD59), and later wehrlite (RD57) were the first cumulates formed, and RD62, taken from a vein, represents the most evolved melt. All other samples are of intermediate evolution between these two extremes. This is supported by the evolving compositions of olivine: dunite contains olivine with the highest forsterite content (81.9% to 83.6%), followed by wehrlite (81.0 to 81.6%) and finally aluminum rich peridotites (74.2 to 79.0%). Furthermore, all samples plot in a linear array in Al2O3 vs. Feo/MgO space (Fig. 3.8), which suggests that all samples are potentially from the same magmatic system. Moreover, all samples record similar retrograde hydration (hornblende replacing clinopyroxene and mesh serpentine replacing olivine), suggesting they all have the same origin and have undergone similar retrograde paths.

Wehrlite and dunite have perhaps been ignored in past studies because they lack a significant aluminous phase indicative of UHP conditions. However, because of the reasons mentioned above, they are likely genetically related to the aluminous peridotites and represent the earliest cumulates in the same magmatic suite. Cumulates with such mineralogy are ignored by Abbott et al. (2007) in their description of the theoretical magmatic suite produced at UHP conditions.

### *3.6.2) Origin of the cumulates*

Ultramafic cumulates could have three possible origins: in addition to a UHP-magma origin, they could have been generated at lower pressures (i.e. shallow mantle levels), either as arc cumulates subsequently brought near the subduction plane by subduction induced mantle corner flow, or as oceanic cumulates formed by fractionation at a mid-oceanic ridge which were later subducted.

Clinopyroxene compositions negate an oceanic origin for the cumulates, since compositions are similar to those from the arc-related Quetico ultramafic intrusions (Pettigrew and Hattori, 2006) and Alaskan ultramafic intrusions (Rublee, 1994; Helmy and El Mahallawi, 2003), and are quite different from clinopyroxenes in mid-oceanic ridge settings (Fig 3.3b). The negative Zr anomaly also supports a supra-subduction zone origin.

At this point, it is difficult to determine with certainty if the grt-peridotites were generated at low or high pressures:

- Grt-peridotites produced at high-pressures tend to have FeO/MgO which strongly increases at constant $Al_2O_3$ because such a trend required the early precipitation of an Al-Mg rich phase (Kornprobst et al., 1990). Our samples do not plot on this trend Fig 3.8). Indeed, the evolution of the suite in $Al_2O_3$ vs FeO/MgO (mol %) space shows a rapid enrichment in $Al_2O_3$. The trend is parallel to Grt-Crn-peridotites from Beni Bousera, Morocco (Kornprobst et al., 1990) and fractionated gabbros from the Oman Ophiolite (e.g., Boudier and Coleman, 1981), suggesting that fractionation at low-pressures can give the observed trends. However, our samples are not high enough in $Al_2O_3$ infer this with great confidence (Fig 3.8).
- Sr/Nd ratios are very high (72-175). Kornprobst et al., (1990) interpret that such high values are consistent with plagioclase rich cumulates because of the large plagioclase/melt partition coefficient of Sr. However RD59 and RD57 have no significant aluminum phase, yet have high values, suggesting that this ratio may not be the best proxy for a low-pressure plagioclase rich origin of the cumulates because of the mobility of Sr during alteration.
- High values of Ba compared to primitive mantle are also observed, yet Ba is also mobile during alteration.

If these rocks were generated in a shallow arc environment, plagioclase (or spinel) must have been the original Al-phase, and the garnet bearing assemblages must have been formed by prograde metamorphism. However, plagioclase crystallization is commonly suppressed in the early stages of crystallization of arc magmas due to high partial pressures of $H_2O$, but is known to occur after substantial crystallization of olivine and clinopyroxene (Gaetani et al., 1993). In our case, only one boulder of dunite and one of wehrlite were found. If large amounts of dunite and wehrlite were formed, one should observe many blocks in the field as well. However, it is possible that other dunites or wehrlite blocks were not exhumed in the same fashion as garnet peridotites, that they were not preserved during exhumation, or that they occur somewhere else in the Cuaba Unit and do not crop out in Rio Cuevas. Furthermore, because of our admitted bias for garnet peridotite exploration during fieldwork, these rocks may have been somewhat looked over. Nevertheless, the presence of dunite and wehrlite, together with high modal proportions of olivine and clinopyroxene in garnet peridotites and Crn-bearing

garnet wehrlites, suggests that such extensive crystallization olivine may indeed have occurred, and may also explain high FeO/MgO (Fig 3.8).

In summation, data presented here confirms that these cumulates were generated somewhere in the supra-subduction zone mantle. The depth at which they initially crystallized remains unknown.

### *3.6.3) Corundum: Arguments for a Metamorphic Origin*

Abbott et al. (2005) interpret that Crn was the latest phase produced in the magmatic evolution of the suite. In both their samples, and in samples from this study, Crn occurs as inclusions in garnet, and they state that Crn was produced by a reaction between spinel and a magmatic liquid according to the following equilibrium, which is only stable at UHP conditions:

$$Spl + Liq = Cpx + Grt + Crn \quad (1)$$

Intuitively, because Crn are inclusions in Grt, one would think that another way of forming this would be for Crn to be present before or during garnet crystallization. Furthermore, our occurrences of corundum are in direct conflict with two important observations from Abbott et al. (2005). Firstly, they state "Crn inclusions in Garnet occur where olivine is locally absent". Secondly, they state that corundum-bearing rock only occurs in veins cutting through Grt-clinopyroxenite. Both these observations allowed for the interpretation that Crn-bearing rocks are the equivalent of evolved peridotites for UHP magmas. However, our sampling from vein material did not yield corundum- bearing rock. Furthermore, and more importantly, our Crn-bearing garnet wehrlites (RD50 and RD51) were taken from boulders, contain abundant olivine (corundum and olivine are in the same thin section!), and are only of intermediate evolution within the whole magmatic suite (Fig 3.5, 3.8, 3.10). This evidence suggests that the occurrence of corundum as inclusions in garnet is not ubiquitous with highly evolved melt fractions as interpreted by Abbott et al. (2005; 2007).

In figure 3.3c corundum is completely enclosed by spinel, and appears to be slightly altered to a brownish Ca-Si rich material (liquid?). This can be interpreted to represent the opposite of reaction (1), since Grt and Crn (and Cpx, present as inclusions in garnet, but is now hydrated to form hornblende) appear to be reacting to produce Spl and Liq. The highest P-T assemblage would therefore be Spl +Liq. Moreover, this is consistent with spinel rimming individual garnet grains within the garnet granoblasts (figure 3.3d-e).

Furthermore, granoblastic texture in garnet is usually interpreted as a metamorphic texture.

In summation, contrary to interpretations by Abbott et al. (2005, 2007), prograde metarmophism appears to have played a major role in the generation of these UHP rocks which implies that plagioclase was initially present as a magmatic phase. Crn can be produced during prograde recrystallization of an ultramafic cumulate by reactions such as Grt + Spl + Pl = Cpx + Crn (Kornprobst et al., 1990) or Pl + Spl = Cpx + Crn (Morfin, pers. comm.). Consequently, Crn must have been included in Grt during further prograde metamorphism, at conditions favouring Grt as the stable aluminous phase.

### *3.6.4) Exhumation and Relationship with Serpentinites*

The incorporation of garnet peridotites with continental or oceanic material brought down to HP or UHP conditions is common worldwide (e.g. Liou et al., 2004). In the case of the Dominican Republic occurrence, they are found within a large eclogitic body and thus incorporation in eclogite likely occurred at depth. Abbott et al. (2006) propose that reverse flow, as modeled by Gerya et al. (2002), likely caused exhumation of Grt-peridotites along with eclogites. Recently, Gorczyk et al. (2007) suggested that a serpentinite rich subduction channel, formed of serpentinized mantle wedge, contributed to the exhumation of the UHP rocks in Dominican Republic. However, there is no field evidence for this: there is no serpentinite mélange exposed in the area and serpentinite boulders found in Rio Cuevas are composed of pseudomorphic low temperature lizardite (Saumur et al., *see chapter 1*). Nonetheless, the lack of field evidence does not negate this model, but I wish to emphasize on the fact that if this subduction channel exists, it does not crop out in the Cuaba Unit. However, Septentrional Fault Zone serpentinites may have contributed to the late stages of exhumation in response to post-Eocene transpression (Saumur et al., *see chapter 1)*.

## 3.7) CONCLUDING REMARKS

The geochemical evidence shown in this report, along with olivine and clinopyroxene compositions, confirms interpretations by Abbott et al. (2005, 2007) that the garnet peridotites have an igneous and have a supra-subduction zone origin. However, the occurrence of corundum in garnet wehrlite contradicts the foundation of the UHP-magma paragenesis model, and petrographic observations confirm that corundum and garnet are not primary magmatic phases and that prograde metamorphism occurred.

In light of these preliminary results, it is clear that models brought forward by Abbott et al. (2005) need to be modified or at the very least refined. However, further analyses must be carried out to propose with certainty a depth at which the magma crystallized in the supra-subduction zone mantle (low-pressure sub-arc magma vs. UHP magma, and all possibilities in between...).

**Acknowledgements**

From the University of Ottawa, I would like to thank Monika Wilk-Alemany and Mahmood Salman for analytical assistance, Ron Hartree for XRF analyses and Gerorge Mrazek for polished section preparation. Furthermore, I wish to thank Peter Jones from Carleton University for his assistance on the microprobe, and the people at ACME Laboratories INC. (Vancouver) for their services. Brian Cousens is thanked for helpful suggestions. Special thanks go to Dr. Tony Fowler, who provided helpful comments when I was scratching my head with petrography.

Furthermore, special thanks to Fabien Deschamps, Ph.D. candidate at Université J.F. Grenoble, for allowing me to use his preliminary mineral analyses from sample RD51 which he carried out on the microprobe at Université Clermont-Ferrand. Also, thanks to Samuel Morfin for providing his Masters defense presentation, which gave valuable insights for the writing of this report.

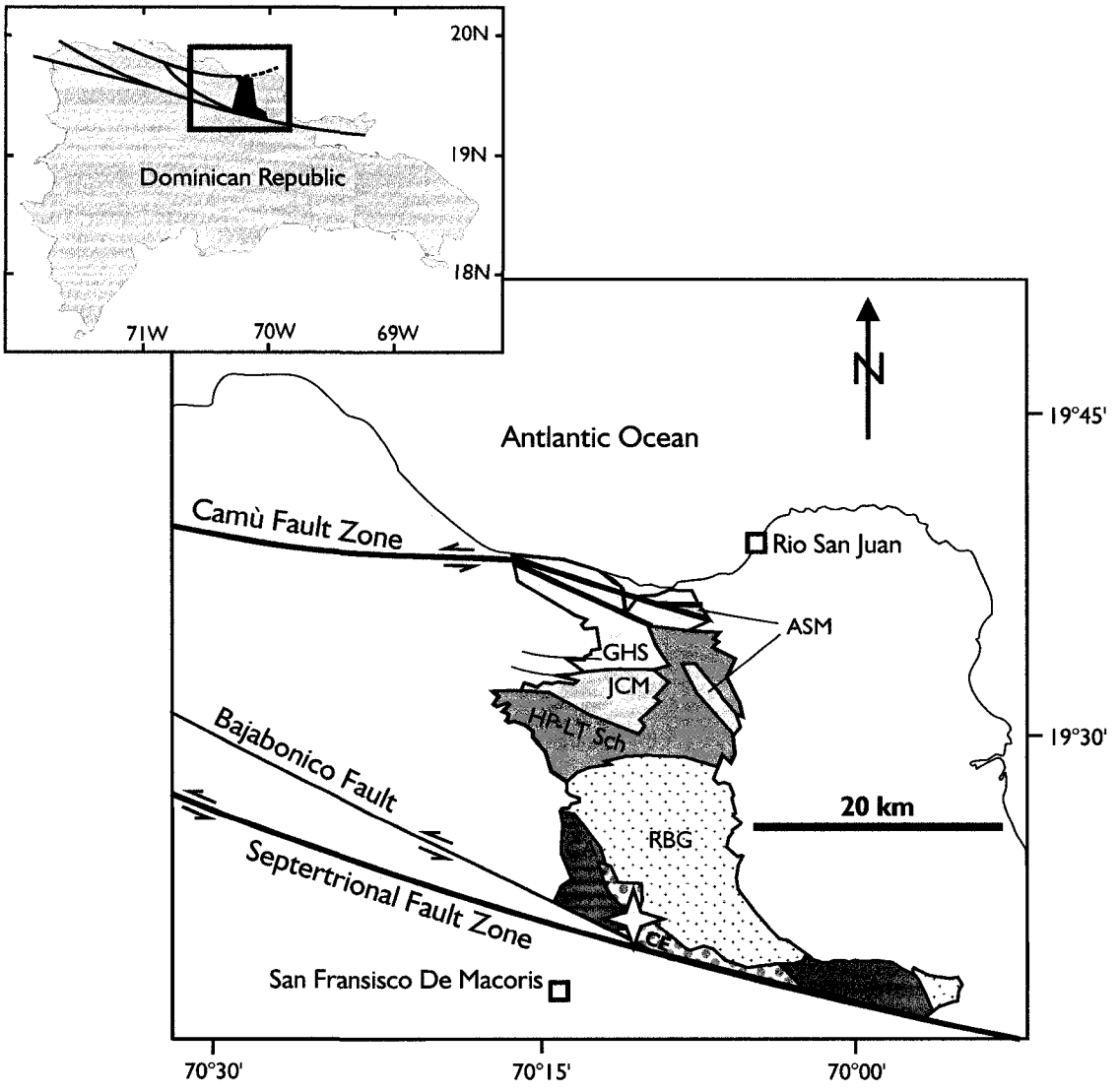


**Figure 3.1)** Map of the Rio San Juan Complex in northern Dominican Republic (see detailed description in chapter 1, regional geology, and Figure 1.2). This chapter focuses on a section of the Cuaba Amphibolite (CA) which is dominated by partially retrograded eclogite (CE). Garnet peridotites are concentrated in a restricted zone in the small stream of Rio Cuevas (yellow star). Map modified from Abbott et al. (2006) and Draper and Nagle (1991).

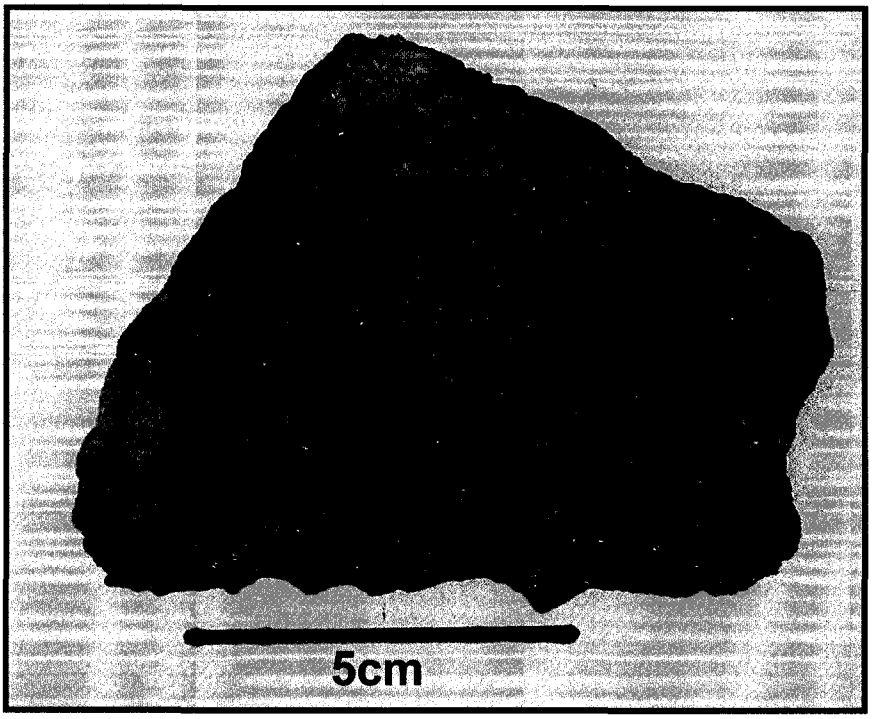


**Figure 3.2)** A) Stéphane Guillot sampling vein from garnet peridotite boulder, Rio Cuevas (RD62); February 2005 (photo by Kéiko Hattori) B) Example of hand sample of garnet peridotite (RD61). Note large pink garnet on the left side with thick fine grained amphibole rich kelyphitic rim. Black matrix is mostly olivine, light green is clinopyroxene or amphibole.

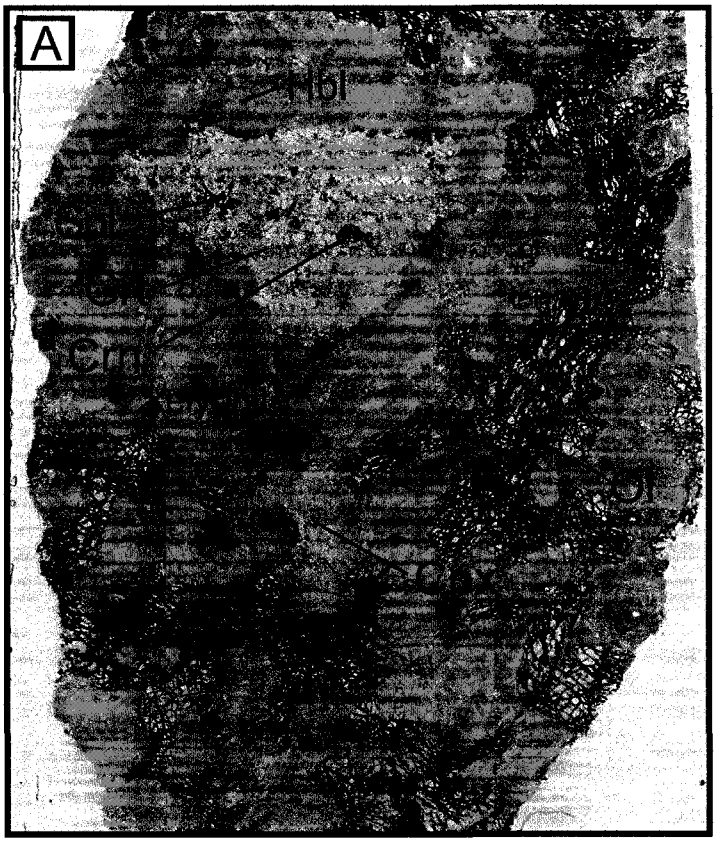
A
Hbl
Crn
Pl
1cm

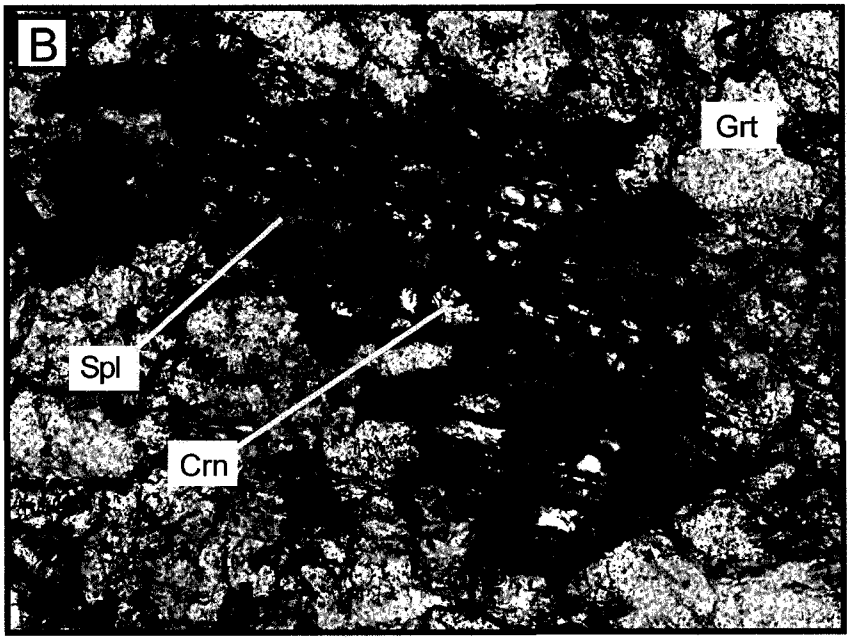
B
Grt
Spl
Crn
0.5mm

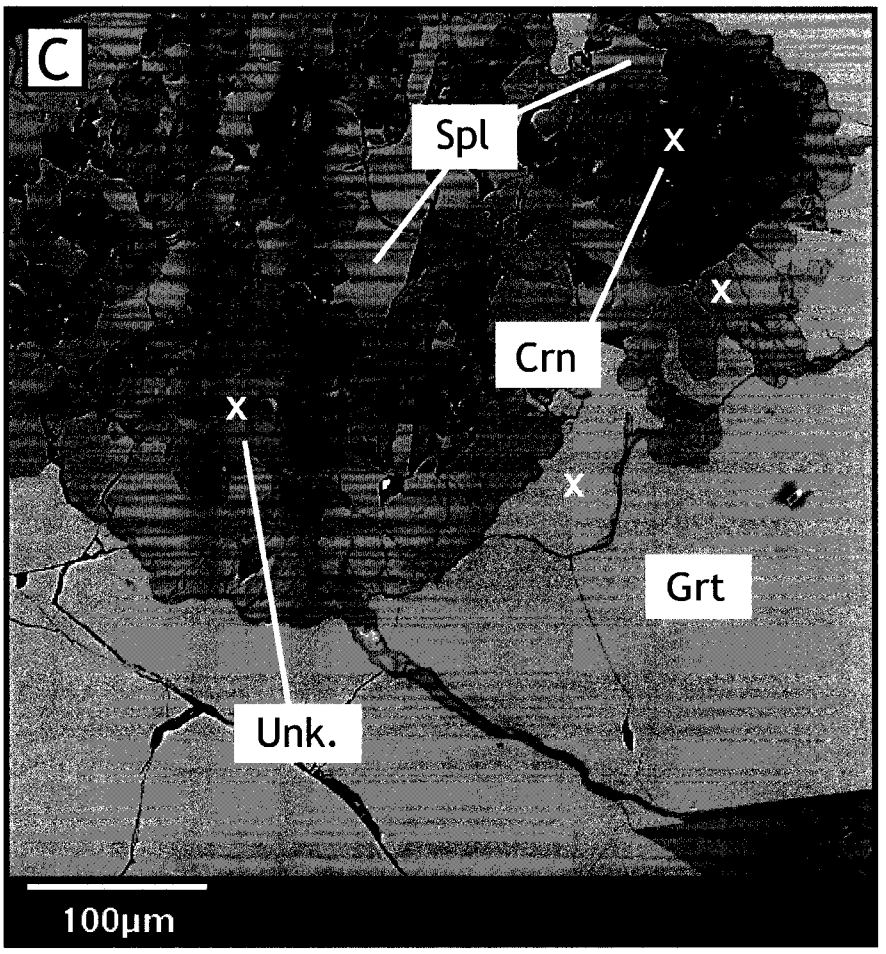
C
Spl
x
x
Crn
x
x
Grt
Unk.
100µm

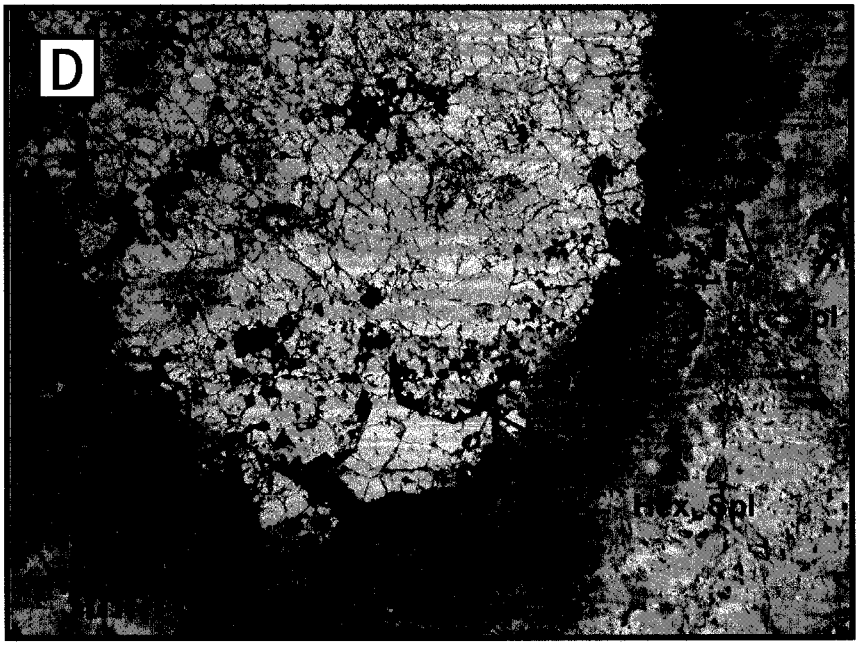
D
Hex. Spl

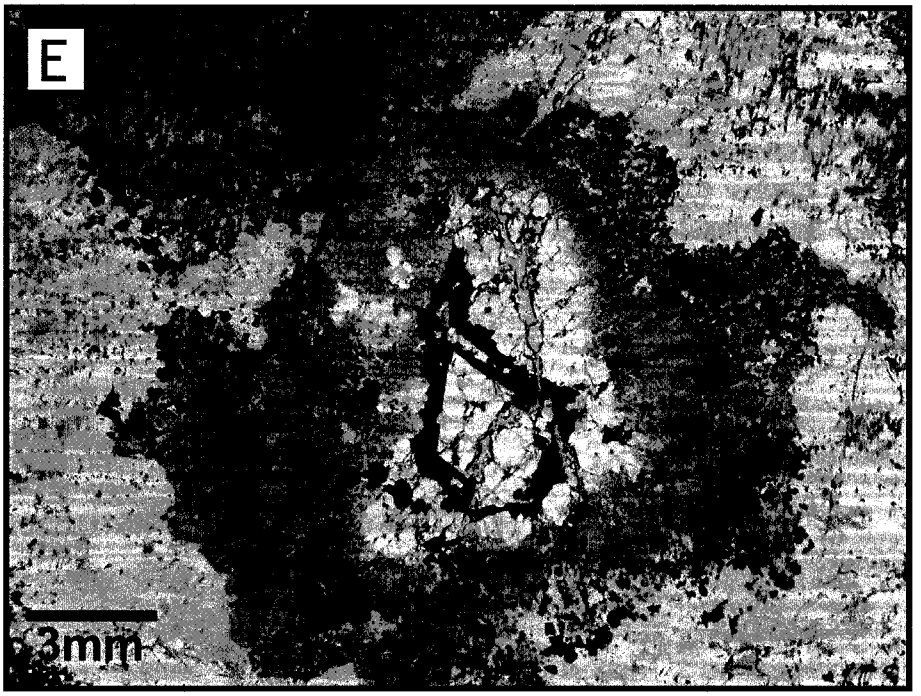
E
3mm

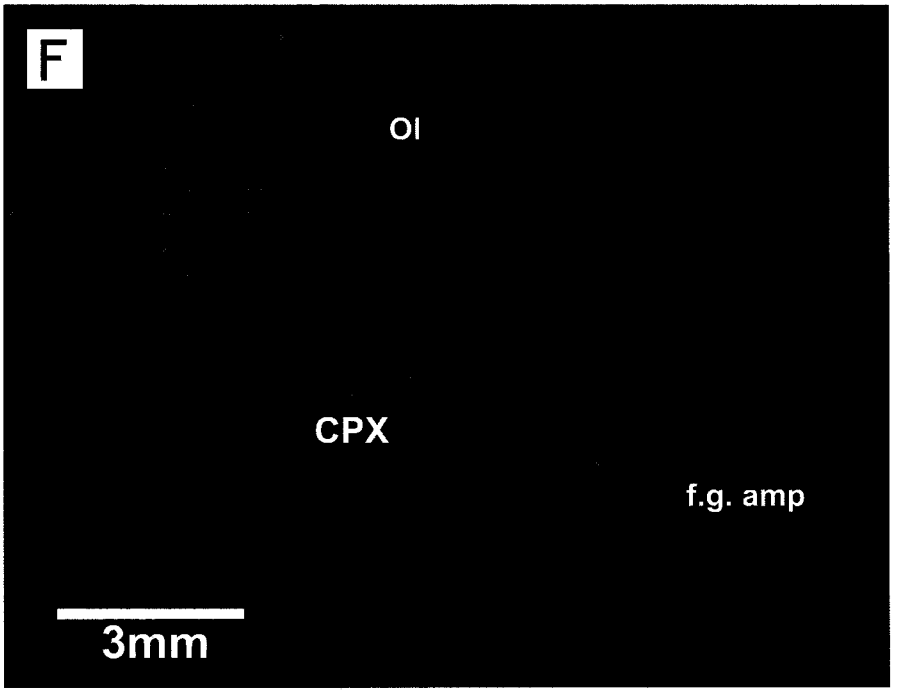
F
Ol
CPX
f.g. amp
3mm

**Figure 3.3)** Various photos of garnet peridotites. **A)** Photo (taken with scanner) of thin section RD51. Garnet only has a very thin kelyphitic rim in this case. Note that olivine and garnet do not share mutual grain boundaries. **B)** RD51, Photomicrograph of corundum inclusion at high magnification (x50) with plane polarized light. **C)** RD50, Back-scattered electron image of Crn, Spl, Grt and an unknown Ca-rich material (Unk.), which could be melt generated by the reaction Crd+Ol+CPX = Spl + Liq (see discussion, section 6.3). Spl and Crn are inclusions in Grt. Note that spinel forms a corona around corundum. "X"'s represent areas where analyses were done on the probe. Analyses are given in table 3.3. **D and E)** RD6-13b, Granoblastic garnet with thick kelyphitic rim and spinel inclusions. Note the hexagonal shape and straight outline of spinel, suggesting that it is forming the outline of original garnet grains part of the granoblast. Also, note circular fine grained spinels in kelyphite. FOV 5mm, plane polarized light. Blue tint is because of carbon coating. **F)** RD51, groundmass and cumulate texture, photomicrograph taken with crossed polars. Note large 5mm zoned clinopyroxene, large olivine and fine grained amphibole rich matrix.

**Fig 3.4**

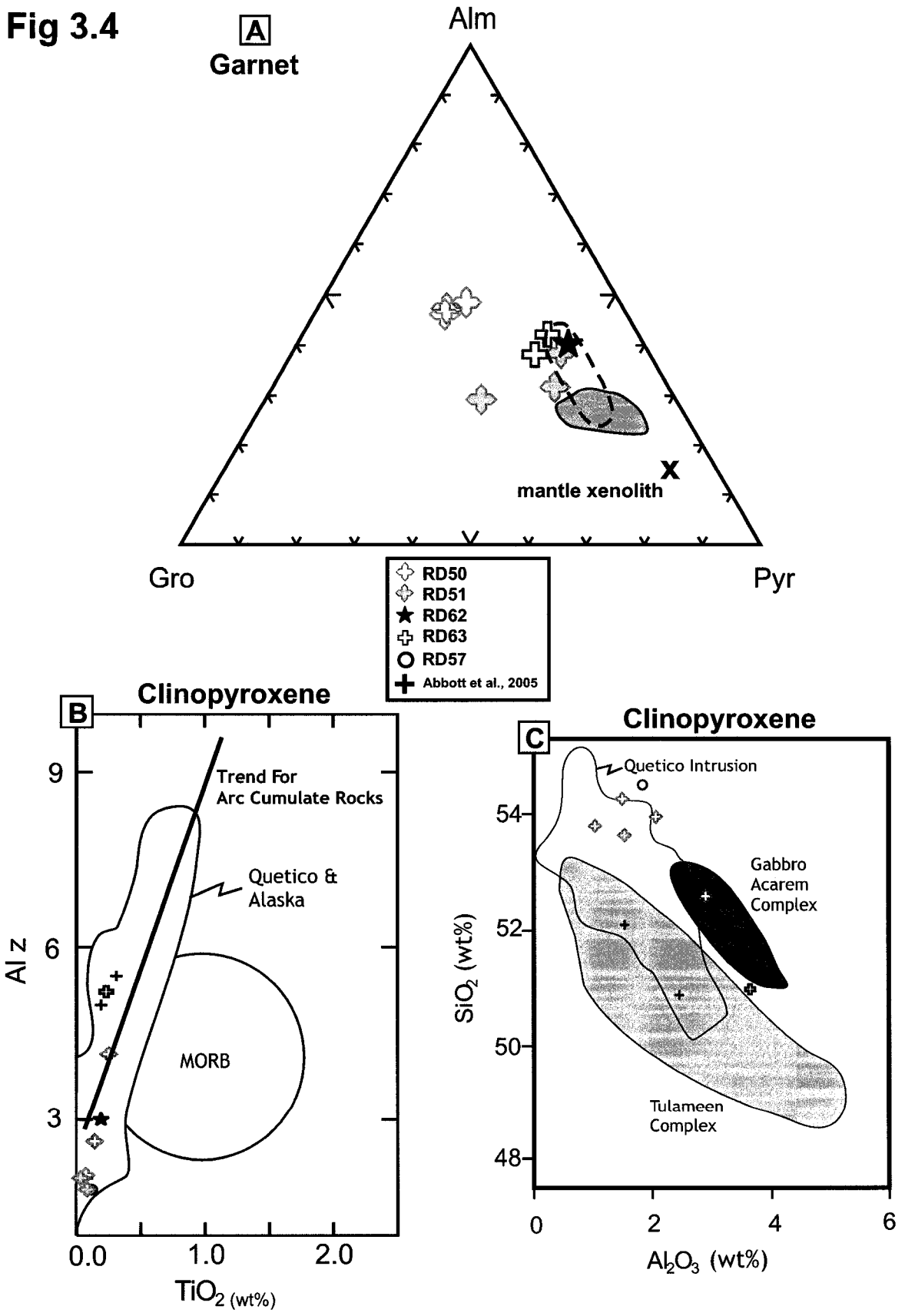
A
Garnet
Alm
Gro
Pyr
mantle xenolith
RD50
RD51
RD62
RD63
RD57
Abbott et al., 2005
B
Clinopyroxene
Trend For
Arc Cumulate Rocks
Quetico &
Alaska
MORB
Al z
TiO2 (wt%)
C
Clinopyroxene
Quetico Intrusion
Gabbro
Acarem
Complex
Tulameen
Complex
SiO2 (wt%)
Al2O3 (wt%)

**Figure 3.4)** Compositions of Garnet and Clinopyroxene. A) Garnet compositions Analyses were taken from within the same grain with the exception of RD63. Note the high content in almandine and the variation in composition in RD51. "X" is a pyrope garnet from a mantle xenolith, South Arfica (Carswell and Dawson, 1970). The blue field are garnet data from Beni Beroussa garnet pyroxenites (Kornprobst et al, 1990) and the colourless field (with dotted line) represents the range of composition of garnet of samples from the Sambagawa belt (Enami et al., 2004). **B and C)** Clinopyroxene compositions of peridotites from Rio Cuevas. Black crosses are data from Rio Cuevas peridotites from Abbott et al. (2005; 2006). The figures are modified from Pettigrew and Hattori (2006) and Le Bas (1962). Data from the Quetico ultramafic intrusion are from Pettigrew and Hattori (2006), whereas data from the Tulameen complex and the Akarem complex, which are Alaskan ultramafic intrusions, are from Rublee (1994) and Helmy and El Mahallawi (2003) respectively. All three of these are considered to have an arc-derived origin. In figure B, "Alz" is defined and the percentage of Al in the tetrahedral sites. Clinopyroxenes from Rio Cuevas have similar compositions as those from Alaskan and Quetico intrusions. In figure C, they plot in a steeply sloping array characteristic of pyroxenes from hydrous arc magmas (Loucks, 1990) and are quite different in composition compared to MORB clinopyroxenes.

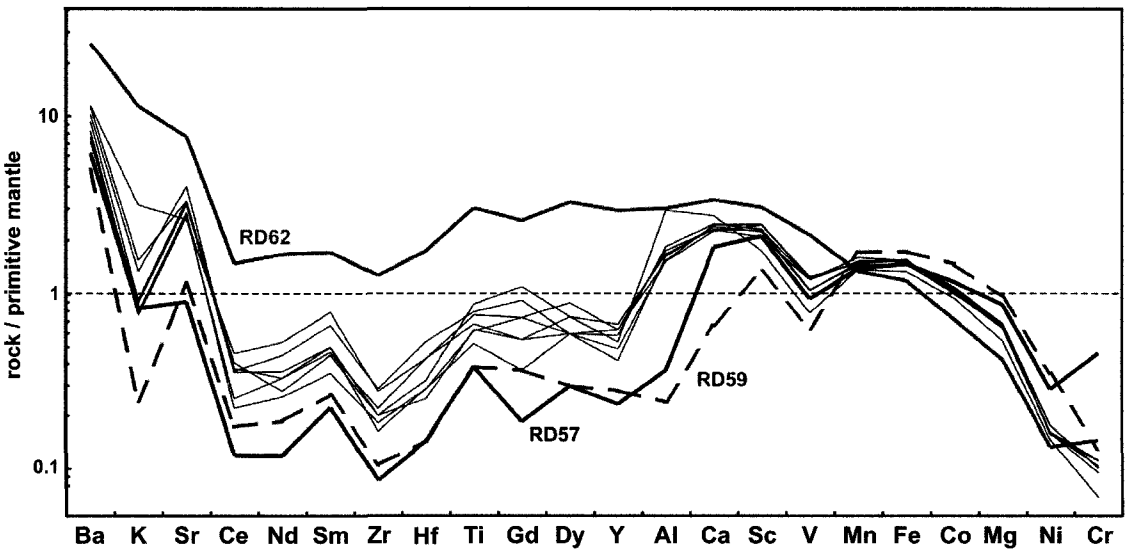


**Figure 3.5)** Primitive mantle normalized bulk rock composition of Rio Cuevas peridotites. Elements are sorted roughly with increasing compatibility. RD62 shows the highest enrichment in incompatible elements. RD57 and RD59, the "garnet-less" samples, are the most depleted in incompatible elements, and are the most enriched in compatible elements. Primitive mantle compositions are from McDonough and Sun (1995).

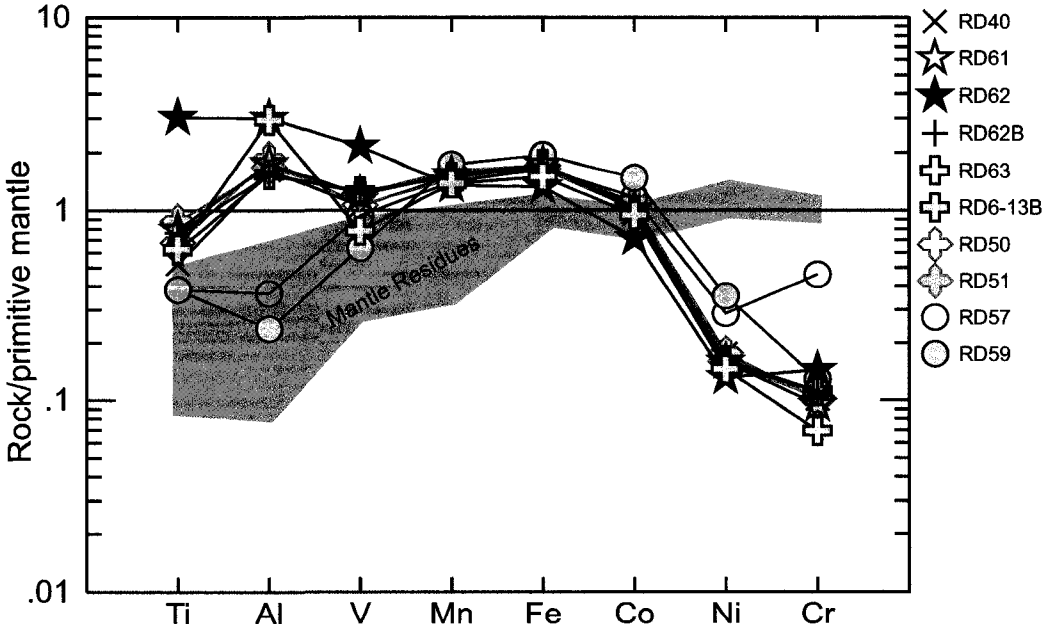


**Figure 3.6)** Primitive mantle normalized immobile elements. Most samples are enriched in incompatible Al, Ti and V and depleted in Cr and Ni. RD57 and RD59 do not contain garnet yet depletion in compatible elements. The patterns of Rio Cuevas peridotites are quite different from those of mantle residues (mantle residue data from Guillot et al., 2001; Niu et al., 2004 and chapter 1 of this volume). Primitive mantle values are from McDonough and Sun (1995).

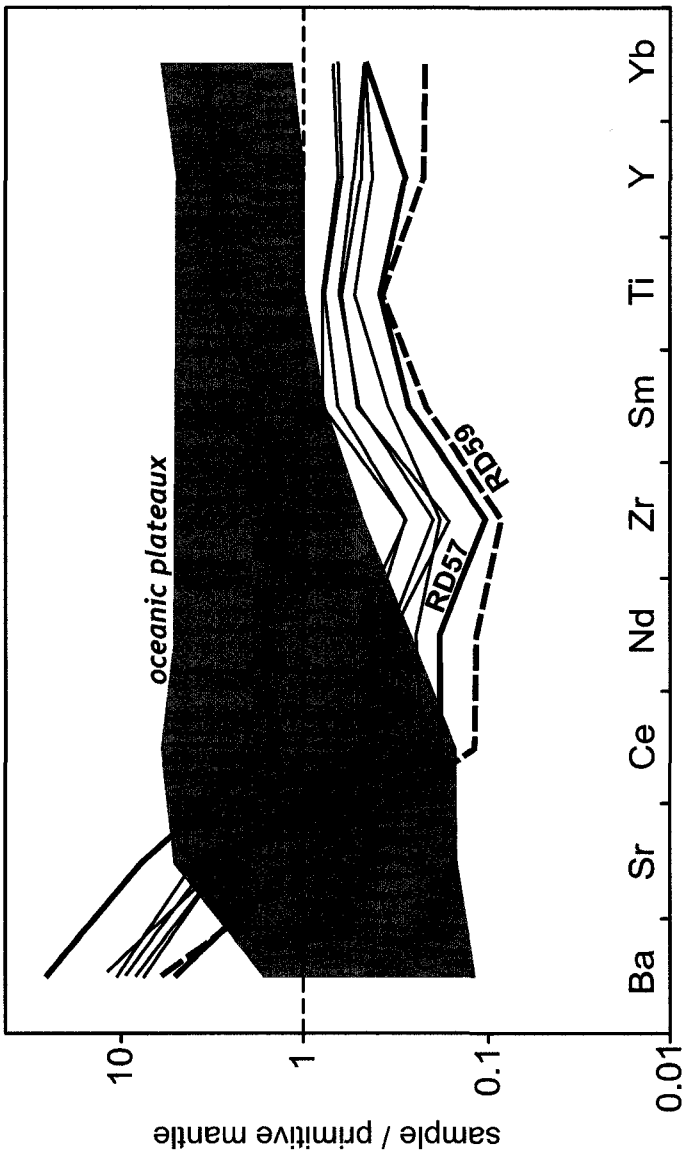


**Figure 3.7)** Primitive mantle normalized elements with a focus on high field strength elements (modified from Hattori et al., submitted). With the exception of RD62, Ti, Sm, Zr, Y and Yb are much lower than values from oceanic cumulates from plateaus and oceanic islands. Cumulate data are from Guillot et al. (2000), Kerr et al. (2004) and Révillon et al. (2000). Primitive mantle values are from McDonough and Sun (1995).

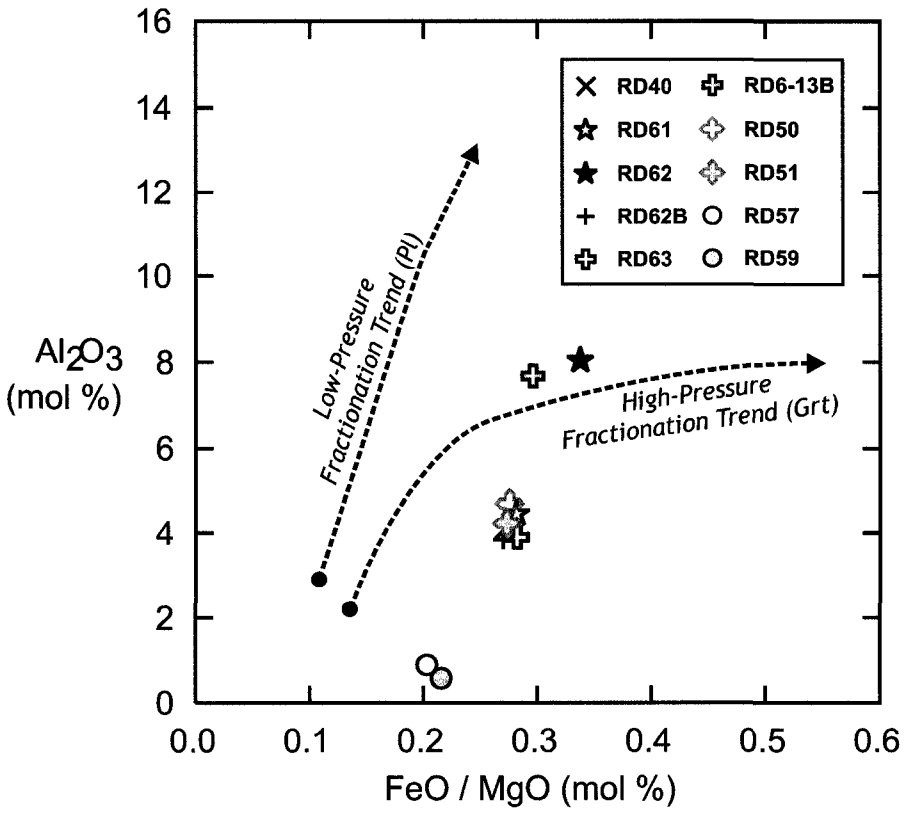


**Figure 3.8)** Whole rock $Al_2O_3$ (mol%) vs. FeO/MgO (mol%) (modified from Kornprobst et al., 1990). The low-pressure trend is defined by data from garnet bearing meta-gabbros from Morocco (Kornprobst et al., 1990) and Oman ophiolitic gabbros (Boudier and Coleman, 1981), and is caused by precipitation of plagioclase, producing high Al for restricted FeO/MgO in residual melts. The high-pressure trend is defined by Moroccan garnet peridotites generated at UHP conditions (Kornprobst et al., 1990) because Al-Mg bearing silicates (garnet or cpx) are precipitated early, which produces the flatter trend. We note that Dominican samples plot in an array parallel to the low-pressure trend, but have higher FeO/MgO ratios and are lower in $Al_2O_3$.

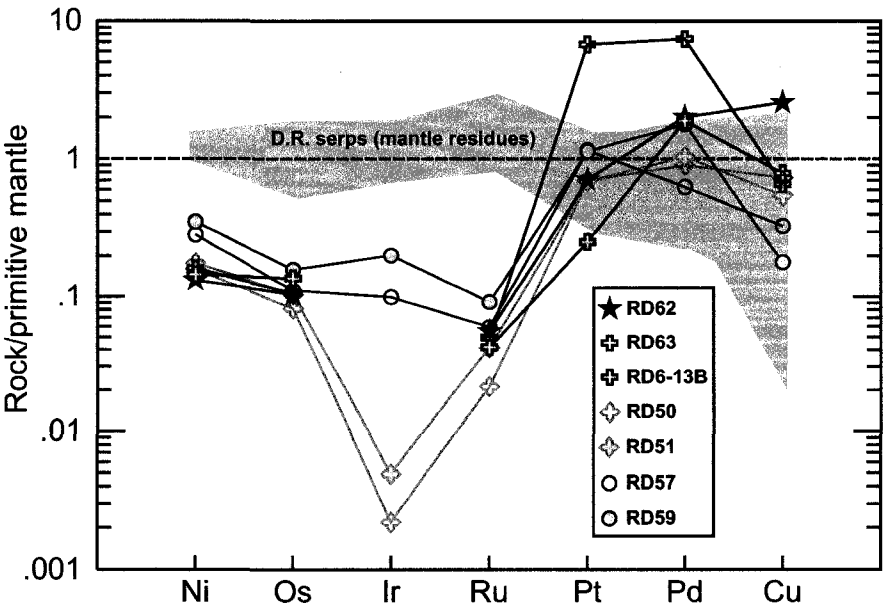


**Figure 3.9)** Primitive mantle normalized PGE concentrations. Samples are depleted in Ir-group PGEs and have Pd-group PGE concentrations similar of higher than primitive mantle. Note that Ir is below detection limit for samples RD62, RD63 and RD6-13b, and extremely low for samples RD50 and RD51 (see text). PGE contents are distinctly different than serpentinites originating from mantle residues from northern Dominican Republic (i.e. chapter 1). PGE values for the primitive mantle are 0.00725 times those of CI chondrite (McDonough and Sun, 1995): 3.55 ppb Os; 3.30 ppb Ir, 5.18 ppb Ru, 7.32 ppb Pt and 3.99 ppb Pd.

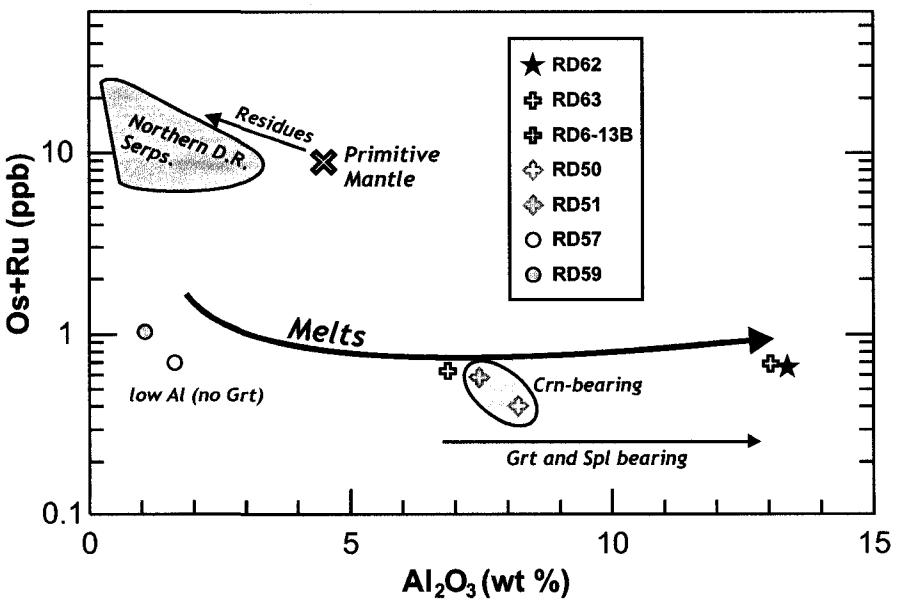


**Figure 3.10)** Os+Ru vs. $Al_2O_3$. Low Ir-group PGE concentrations are characteristic of melts, whereas residues (such as northern D.R. serpentinites, chapter 1) have high contents of Ir-group PGEs. Increasing $Al_2O_3$ reflects the evolution of the residual melt. Note that corundum bearing garnet peridotites do not represent the most evolved melts.

**Table 3.1)** GPS coordinates (datum NAD 27 Cuba) and description of peridotite samples from Rio Cuevas

| Sample | Field Season | Easting | Northing | Description | Rock type |
|---|---|---|---|---|---|
| **RD40** | 2005 | 375736.5 | 2140178.5 | Boulder (~ 1 m) | Grt-Spl Wehrlite |
| **RD50** | 2005 | 375795.5 | 2140917.4 | Boulder (~ 4 m) | Crn bearing Grt-Spl-Wehrlite |
| **RD51** | 2005 | 375795.5 | 2140917.4 | Boulder (~ 2 m) | Crn-bearing Grt-Spl-Wehrlite |
| **RD57** | 2005 | 375828.9 | 2140412.1 | Boulder | Wehrlite (75% olivine) |
| **RD59** | 2005 | 375904.5 | 2140533.9 | Boulder | Dunite (90% olivine) |
| **RD61** | 2005 | 375807.0 | 2140636.9 | Boulder | Grt-Spl Olivine Clinopyroxenite |
| **RD62** | 2005 | 375770.4 | 2140643.7 | Vein cutting boulder | Grt-Spl-Wehrlite |
| **RD62b** | 2005 | 375770.4 | 2140643.7 | Vein cutting boulder | Grt-Spl-Olivine Clinopyroxenite |
| **RD63** | 2005 | 375708.3 | 2140699.9 | Boulder (~ 3 m) | Grt-Spl-Olivine Clinopyroxenite |
| **RD6-13** | 2006 | 375792.5 | 2141105.4 | Boulder (~ 3 m) | Grt-Spl-Olivine Clinopyroxenite |

**Table 3.2)** Summary of preliminary mineral analyses (olivine, clinopyroxene, spinel and garnet). See appendix D.8 for complete dataset of of mineral compositions

| | | Olivine | | Clinopyroxene | | Green spinel | | | Garnet | | | | |
|---|---|---|---|---|---|---|---|---|---|---|---|---|---|
| **sample** | **rock type** | **Fo (%)** | **#gr.** | **XMg** | **#gr.** | **YAl** | **XMg** | **#gr.** | **Alm (%)** | **Gro (%)** | **Pyr (%)** | **XMg** | **#gr.** |
| **RD50** | Crd Grt-wehr | 74.2 - 75.9 | 4 | 0.88 - 0.90 | 2 | 0.96 - 0.99 | 0.50 - 0.54 | 4 | 44.1 - 45.1 | 24.1 - 29.1 | 22.8 - 21.3 | 0.32 - 0.34 | 2 |
| **RD51*** | Crd Grt-wehr | 77.7 - 78.9 | 3 | 0.89 | 2 | 0.99 | 0.59 - 0.60 | 1 | 37.6 - 28.5 | 14.8 - 32.7 | 47.8 - 36.3 | 0.55 - 0.60 | 1 |
| **RD62** | Grt-wehrlite | 76.4 | 1 | 0.86 | 1 | 0.97 | 0.62 | 1 | 37.4 | 12.1 | 43.6 | 0.54 | 1 |
| **RD63** | Grt-CPXite | 76.3 - 77.1 | 2 | 0.87 | 1 | not available | | | 35.7 - 40.5 | 18.5 - 15.0 | 39.4 - 40.6 | 0.50 - 0.52 | 2 |
| **RD57** | wehrlite | 81.0 - 81.6 | 2 | 0.89 | 1 | | | | | | | | |
| **RD59** | dunite | 81.9 - 83.6 | 4 | | | | | | | | | | |

#gr. = number of grains analysed
XMg = atomic ratio of $Mg/(Mg+Fe^{2+})$
YAl = atomic ratio of $Al / (Al + Cr + Fe^{3+})$
* Analyses carried out at Université Clermont-Ferrand

**Table 3.3)** Mineral analyses associated with figure 3.3c

| | Garnet | Spinel | Corundum | Unknown |
|---|---|---|---|---|
| analysis # | **RD50-A-4** | **RD50-A-2** | **RD50-A-1** | **RD50-A-3** |
| $SiO_2$ | 38.64 | – | – | 21.08 |
| $TiO_2$ | 0.01 | 0.02 | – | 0.11 |
| $Al_2O_3$ | 21.91 | 64.16 | 103.32 | 25.45 |
| $Fe_2O_3$ | 1.81 | 1.39 | – | – |
| $Cr_2O_3$ | – | 0.05 | – | 0.02 |
| FeO | 19.63 | 22.44 | 0.51 | 0.66 |
| MnO | 1.14 | 0.21 | 0.03 | 0.05 |
| MgO | 5.4 | 13.00 | – | – |
| CaO | 12.35 | 0.02 | 0.07 | 41.84 |
| NiO | n.a. | 0.05 | n.a. | – |
| $Na_2O$ | – | n.a. | – | – |
| $K_2O$ | – | n.a. | – | – |
| F | n.a. | n.a. | n.a. | 0.09 |
| TOTAL | 100.89 | 101.34 | 103.93 | 89.3 |
| **Total O** | **24** | **32** | | |
| Si | 5.916 | 0 | | |
| Ti | 0.001 | 0.003 | | |
| Al | 3.955 | 15.768 | | |
| Cr | – | 0.008 | | |
| $Fe^{+3}$ | 0.209 | 0.218 | | |
| $Fe^{+2}$ | 2.514 | 3.914 | | |
| Mg | 1.232 | 4.04 | | |
| Mn | 0.148 | 0.037 | | |
| Ni | – | 0.008 | | |
| Ca | 2.026 | 0.004 | | |
| **tot. cations** | **16** | **24** | | |
| Alman | 42.47 | | | |
| Andra | 5.27 | | | |
| Gross | 28.93 | | | |
| Pyrop | 20.81 | | | |
| Spess | 2.5 | | | |
| XMg | 0.33 | 0.51 | | |
| YAl | | 0.99 | | |
| YFe3+ | | 0.01 | | |

**Table 3.4)** Major oxide composition

| oxide | source of data | | RD40 | RD50 | RD51 | RD57 | RD59 | RD61 | RD62 | RD62b | RD63 | RD6-13B |
|---|---|---|---|---|---|---|---|---|---|---|---|---|
| $SiO_2$ | XRF - Ott | (%) | 41.93 | 42.05 | 41.83 | 41.18 | 38.71 | 41.83 | 43.68 | 42.36 | 42.14 | 41.69 |
| $Al_2O_3$ | XRF - Ott | | 7.25 | 8.2 | 7.46 | 1.63 | 1.06 | 7.81 | 13.36 | 6.8 | 6.86 | 13.04 |
| CaO | XRF - Ott | | 8.45 | 8.74 | 8.18 | 6.51 | 2.36 | 8.15 | 11.97 | 7.98 | 8.64 | 9.71 |
| $K_2O$ | XRF - Ott | | 0.023 | 0.026 | 0.045 | 0.024 | 0.007 | 0.027 | 0.329 | 0.091 | 0.022 | 0.039 |
| MgO | XRF - Ott | | 25.79 | 24.24 | 25.51 | 32.89 | 36.41 | 24.92 | 15.95 | 25.69 | 25.08 | 20.51 |
| MnO | XRF - Ott | | 0.203 | 0.197 | 0.217 | 0.189 | 0.233 | 0.207 | 0.182 | 0.204 | 0.201 | 0.186 |
| $Na_2O$ | XRF - Ott | | 0.16 | 0.25 | 0.22 | <0.005 | <0.005 | 0.2 | 0.87 | 0.2 | 0.16 | 0.44 |
| $P_2O_5$ | XRF - Ott | | 0.02 | 0.02 | 0.02 | 0.01 | 0.01 | 0.02 | 0.1 | 0.02 | 0.02 | 0.02 |
| $Fe_2O_3$ (tot) | XRF - Ott | | 13.867 | 13.234 | 13.81 | 13.249 | 15.571 | 13.905 | 10.67 | 13.732 | 14.022 | 12.036 |
| $TiO_2$ | XRF - Ott | | 0.105 | 0.136 | 0.176 | 0.077 | 0.077 | 0.159 | 0.608 | 0.153 | 0.124 | 0.126 |
| S | ACME | | <0.04 | 0.06 | <0.04 | <0.04 | <0.04 | 0.04 | 0.04 | <0.04 | 0.04 | 0.04 |
| LOI | XRF - Ott | | 1.9 | 3 | 2.1 | 4.56 | 7.22 | 2.7 | 1.46 | 3.63 | 2.95 | 1.8 |
| | | **SUM** | 99.7 | 100.2 | 99.6 | 100.3 | 101.7 | 100.0 | 99.2 | 100.9 | 100.3 | 99.6 |

*Detection limits available in Appendices B.5 and F.4*

**Table 3.5)** Trace element composition

| element | source of data | | RD40 | RD50 | RD51 | RD57 | RD59 | RD61 | RD62 | RD62b | RD63 | RD6-13B |
|---|---|---|---|---|---|---|---|---|---|---|---|---|
| Ba | ACME | (ppm) | 31 | 33 | 51 | 13 | 13 | 40 | 153 | 44 | 33 | 45 |
| Co | XRF - Ott | | 112 | 106 | 115 | 123 | 155 | 106 | 75 | 109 | 105 | 99 |
| Cr | XRF - Ott | | 266 | 271 | 264 | 1208 | 338 | 248 | 378 | 290 | 292 | 181 |
| Ni | XRF - Ott | | 344 | 312 | 346 | 560 | 694 | 312 | 259 | 307 | 317 | 285 |
| V | XRF - Ott | | 86 | 87 | 100 | 77 | 52 | 99 | 176 | 102 | 103 | 64 |
| Zn | XRF - Ott | | 51 | 71 | 79 | 56 | 73 | 90 | 71 | 94 | 70 | 63 |
| Mo* | ACME | | 0.26 | 0.2 | 0.1 | <.05 | 0.13 | 0.08 | 0.07 | <.05 | 0.06 | 0.3 |
| Cu | ACME | | 9.21 | 21.89 | 16.35 | 9.92 | 5.39 | 14.18 | 76.91 | 13.35 | 19.68 | 23.52 |
| Pb | ACME | | 2.59 | 2 | 3.15 | 1.01 | 1.03 | 2.3 | 2.66 | 2.61 | 2.64 | 1.93 |
| As* | ACME | | 0.7 | 0.8 | 1.6 | 0.6 | <.2 | 0.7 | 1.2 | 0.7 | 0.7 | 1.1 |
| Sr | ACME | | 56 | 56 | 66 | 15 | 21 | 65 | 152 | 52 | 52 | 72 |
| Cd | ACME | | 0.08 | 0.08 | 0.08 | 0.04 | 0.04 | 0.09 | 0.1 | 0.09 | 0.09 | 0.09 |
| Sb* | ACME | | 0.05 | 0.03 | 0.04 | 0.02 | 0.02 | 0.02 | 0.03 | 0.02 | <.02 | 0.04 |
| Zr | ACME | | 1.9 | 2.3 | 2.1 | 0.9 | 1.1 | 3 | 13.4 | 2.9 | 1.7 | 2.1 |
| Sn* | ACME | | 0.2 | 0.1 | <0.1 | 0.1 | <0.1 | 0.1 | 0.2 | 0.1 | 0.1 | 0.1 |
| Sc | ACME | | 36.3 | 37.5 | 37 | 34.2 | 21.9 | 33.8 | 49.5 | 39.4 | 39.7 | 28.4 |
| Y | ACME | | 1.8 | 2.5 | 2.9 | 1 | 1.2 | 2.7 | 12.6 | 2.7 | 2.1 | 2.3 |
| Hf | ACME | | 0.08 | 0.12 | 0.09 | 0.04 | 0.04 | 0.15 | 0.49 | 0.12 | 0.08 | 0.07 |
| Li | ACME | | 1.8 | 2 | 2 | 1.7 | 1 | 2 | 3.4 | 2.2 | 1.5 | 2.2 |
| Rb* | ACME | | 0.8 | 0.7 | 1 | 0.6 | 0.2 | 0.7 | 5.5 | 1.4 | 1.3 | 1.4 |
| Nb* | ACME | | 0.07 | 0.09 | 0.07 | <0.04 | 0.05 | 0.05 | 0.61 | 0.09 | <0.04 | <0.04 |
| Cs* | ACME | | 0.1 | 0.1 | 0.1 | 0.1 | 0.1 | 0.1 | 0.1 | 0.1 | 0.2 | 0.1 |
| Ga | ACME | | 3.8 | 4.34 | 5.11 | 1.79 | 1.4 | 4.43 | 8.16 | 4.27 | 4.6 | 5.88 |
| Ag | ACME | | 0.12 | 0.08 | 0.09 | 0.09 | 0.10 | 0.07 | 0.12 | 0.10 | 0.11 | 0.07 |

*Detection limits available in Appendices B.5 and F.4*

** Values are very close to detection limits*

**Table 3.6)** REE concentration of peridotites from Rio Cuevas

| element | source of data | | RD40 | RD50 | RD51 | RD57 | RD59 | RD61 | RD62 | RD62b | RD63 | RD6-13B |
|---|---|---|---|---|---|---|---|---|---|---|---|---|
| La* | ACME | (ppm) | 0.2 | 0.3 | 0.3 | 0.1 | 0.1 | 0.2 | 0.8 | 0.3 | 0.2 | 0.3 |
| Ce | ACME | | 0.37 | 0.63 | 0.68 | 0.2 | 0.29 | 0.61 | 2.5 | 0.77 | 0.42 | 0.6 |
| Pr* | ACME | | 0.1 | 0.1 | 0.1 | <0.1 | <0.1 | 0.1 | 0.4 | 0.1 | 0.1 | 0.1 |
| Nd | ICP-MS Ott | | 0.32 | 0.41 | 0.35 | 0.15 | 0.23 | 0.56 | 2.1 | 0.67 | 0.41 | 0.45 |
| Sm | ICP-MS Ott | | 0.14 | 0.19 | 0.18 | 0.09 | 0.11 | 0.27 | 0.7 | 0.32 | 0.20 | 0.20 |
| Eu* | ACME | | 0.1 | 0.1 | 0.1 | <0.1 | <0.1 | 0.1 | 0.3 | 0.1 | 0.1 | 0.1 |
| Gd | ACME | | 0.2 | 0.3 | 0.6 | 0.1 | 0.2 | 0.5 | 1.4 | 0.4 | 0.4 | 0.3 |
| Tb* | ACME | | <0.1 | 0.1 | 0.1 | <0.1 | <0.1 | 0.1 | 0.2 | 0.1 | 0.1 | 0.1 |
| Dy | ACME | | 0.4 | 0.4 | 0.5 | 0.2 | 0.2 | 0.4 | 2.2 | 0.6 | 0.4 | 0.5 |
| Ho* | ACME | | 0.1 | 0.1 | 0.1 | <0.1 | 0.1 | 0.1 | 0.5 | 0.1 | 0.1 | 0.1 |
| Er* | ACME | | 0.2 | 0.3 | 0.3 | 0.1 | 0.1 | 0.3 | 1.5 | 0.3 | 0.3 | 0.3 |
| Tm* | ACME | | <0.1 | <0.1 | <0.1 | <0.1 | <0.1 | <0.1 | 0.2 | <0.1 | <0.1 | <0.1 |
| Yb | ACME | | 0.2 | 0.3 | 0.3 | 0.1 | 0.2 | 0.3 | 1.5 | 0.3 | 0.2 | 0.2 |
| Lu* | ACME | | <0.1 | <0.1 | <0.1 | <0.1 | <0.1 | 0.1 | 0.2 | 0.1 | <0.1 | <0.1 |

*Detection Limits available in Appendix B.5*
** Values are very close to detection limits*

**Table 3.7)** PGE concentration of peridotites from Rio Cuevas

| element | source of data | | RD50 | RD51 | RD57 | RD59 | RD62 | RD63 | RD6-13B |
|---|---|---|---|---|---|---|---|---|---|
| Os | ICPMS - Ott | (ppb) | 0.29 | 0.37 | 0.39 | 0.56 | 0.37 | 0.38 | 0.48 |
| Ir | ICPMS - Ott | | 0.01 | 0.02 | 0.33 | 0.67 | <0.01 | <0.01 | <0.01 |
| Ru | ICPMS - Ott | | 0.11 | 0.21 | 0.31 | 0.47 | 0.29 | 0.25 | 0.21 |
| Pt | ICPMS - Ott | | 5.07 | 5.03 | 8.47 | 8.30 | 5.17 | 49.13 | 1.86 |
| Pd | ICPMS - Ott | | 3.58 | 4.13 | 2.51 | 7.07 | 8.04 | 29.34 | 7.48 |

*Detection Limit: 0.01 ppb, Information on precision is in Appendix F.1*

# SUMMARY OF CONCLUSIONS

## *CHAPTER 1*

- Two types of serpentinite are recognized in the subduction complex of northern Dominican Republic: hydrated abyssal peridotites and hydrated forearc mantle wedge peridotites.
- Hydrated abyssal peridotites occur in HP-LT serpentinite mélanges and low grade serpentinite terranes. They are by far the most abundant type of serpentinite, suggesting that there was abundant serpentinized abyssal peridotite in the subducted Proto-Caribbean slab, which is consistent with its formation at a slow-spreading ridge. Mélanges containing clasts of HP rocks likely represent a subduction-channel developed during the subduction of Proto-Caribbean oceanic lithosphere, and these results highlight that oceanic serpentinite may play an important role in the exhumation of HP rocks.
- Highly refractory hydrated forearc mantle wedge peridotites occur along major strike-slip fault zones that formed during collision of the Bahamas Platform. Forearc serpentintes were hydrated at the base of the mantle wedge at shallow levels, and their association with late strike-slip faults shows that ductile serpentinites from different mantle domains were brought to the surface from the base of the mantle wedge along the Septentrional (SFZ) and Camù (CFZ) Fault Zones which cross-cut the forearc mantle.
- Such an occurrence of forearc mantle wedge serpentinite, to our knowledge, has yet to have been reported in other subduction complexes. Serpentinites are reported along major faults in other subduction zones and therefore protrusion of mantle wedge serpentinites may in fact be a common process for the exhumation of forearc material and be important in the late stages of exhumation of metamorphic rocks and the seismic behaviour of fault zones.

## *CHAPTER 2*

- Cr-spinel from the SFZ shows compositional zoning with high $Fe^{2+}$ and $Fe^{3+}$ and a slight increase of Cr towards rims. The zoning is explained by two stages of alteration: the first is essentially a replacement of MgO by FeO, and the second is

additional replacement of MgO by FeO along with replacement of $Al_2O_3$ by $Fe_2O_3$ (and $Cr_2O_3$), with released MgO and $Al_2O_3$ consumed by newly formed chlorite.

- Because ferritchromit rims are still rich in Al and Mg, and because chlorite coronas are poorly developed, this alteration represents the early stages of alteration of primary Cr-spinels. It occurred either at metamorphic grades lower than most reported occurrences of ferritchromit, or in response to a short lived thermal metamorphic event. Primary ratios of divalent and trivalent cations can be slightly modified at temperatures below those of amphibolite grades, and therefore one must be cautious when interpreting Cr-spinel compositions even in only slightly metamorphosed serpentinites.
- Nevertheless, a heating event was necessary to cause the observed Cr-spinel zoning. This event is either associated with the protrusion of SFZ serpentinites through the hot centre of the mantle wedge, or with contact metamorphism from the Rio Boba Gabbro.

*CHAPTER 3*

- Garnet peridotites from the southern part of the Rio San Juan Complex have bulk rock compositions and mineral chemistries confirming their cumulate origin. Furthermore, clinopyroxene compositions are similar to those from arc cumulates, negating the possibility that these rocks were originally oceanic cumulates (i.e., they are not from the Proto-Caribbean side).
- In contrast to findings by Abbott et al. (2005), corundum was not generated in pegmatitic UHP-magmas. Corundum forms inclusions in garnet, and is present in rocks of intermediate magmatic evolution, suggesting that corundum was formed in a precursor stage at lower metamorphic grades.
- Preliminary evidence suggests that subduction zone prograde metamorphism contributed to the evolution of these rocks.

# REFERENCES

Abbott, R.N., Jr., Broman, B.N., and Draper, G., 2007, UHP Magma Paragenesis Revisited, Olivine Clinopyroxenite and Garnet-Bearing Ultramafic Rocks from the Cuaba Gneiss, Rio San Juan Complex, Dominican Republic: International Geology Review, v. 49, p. 572-586.

Abbott, R.N., Jr., Draper, G., and Broman, B.N., 2006, P-T path for ultrahigh pressure garnet ultramafic rocks of the Cuaba Gneiss, Rio San Juan Complex, Dominican Republic: International Geology Review, v. 48, p. 778-790.

Abbott, R.N., Jr., Draper, G., and Keshav, S., 2005, UHP magma paragenesis, garnet peridotite, and garnet clinopyroxenite; an example from the Dominican Republic: International Geology Review, v. 47, p. 233-247.

Abbott, R.N., Jr., Draper, G., and Keshav, S., 2001, Garnet peridotite found in the Greater Antilles: Eos, Transactions, American Geophysical Union, v. 82, p. 381.

Allen, DE and Seyfried, W.E., Jr., 2003, Compositional controls on vent fluids from ultramafic-hosted hydrothermal systems at mid-ocean ridges: An experimental study at 400 C, 500 bars. Geochim. Cosmochim. Acta, 67: 1531-1542.

Arai, S., 1994, Characterization of spinel peridotites by olivine-spinel compositional relationships; review and interpretation: Chemical Geology, v. 113, p. 191-204.

Auzende, A.L., Daniel, I., Reynard, B., Lemaire, C., and Guyot, F., 2004, High-pressure behaviour of serpentine minerals; a Raman spectroscopic study: Physics and Chemistry of Minerals, v. 31, p. 269-277.

Auzende, A.-L., 1999, Pétrologie et Microstructures des Serpentinites HP-BT de Cuba Central; Mémoire de D.E.A. (unpublished thesis), Université Blaise Pascal - Clermont-Ferrand II, 52 pp.

Bach, W., Garrido, C.J., Paulick, H., Harvew, J., and Rosner, M., 2004, Seawater-peridotite interactions; first insights from ODP Leg 209, MAR 15 degrees N, Geochemistry, Geophysics, Geosystems - G (super 3), vol.5, no.9, 22 pp.

Barnes, S.J., and Roeder, P.L., 2001, The range of spinel compositions in terrestrial mafic and ultramafic rocks: Journal of Petrology, v. 42, p. 2279-2302.

Barnes, S.J., 2000, Chromite in komatiites; II, Modification during greenschist to mid-amphibolite facies metamorphism: Journal of Petrology, v. 41, p. 387-409.

Beeson, M.H., and Jackson, E.D., 1969, Chemical composition of altered chromites from the Stillwater complex, Montana: American Mineralogist, v. 74, p. 1084-1100.

Benton, L.D., Ryan, J.G., and Tera, F., 2001, Boron isotope systematics of slab fluids as inferred from a serpentine seamount, Mariana Forearc: Earth and Planetary Science Letters, v. 187, p. 273-282.

Best, M.G., and Christiansen, E.H., 2001, Igneous Petrology, 458 pp., Blackwell Science, Oxford, UK.

Bliss, N.W., and MacLean, W.H., 1975, The paragenesis of zoned chromite from central Manitoba, Geochimica et Cosmochimica Acta, Volume 39, p. 973-990.

Boudier, F., and Coleman, R.G., 1981, Cross section through the peridotite in the Samail ophiolite, southeastern Oman Mountains: Journal of Geophysical Research, v. 86, p. 2573-2592.

Bowin, C.O., Nalwalk, A.J., and Hersey, J.B., 1966, Serpentinized peridotite from the north wall of the Puerto Rico Trench: Geological Society of America Bulletin, v. 77, p. 257-269.

Brenan J.M., W.F.McDonough, R. Ash (2005) An experimental study of the solubility and partitioning of iridium, osmium and gold between olivine and silicate melt, Earth Planet. Sci. Lett., 237, 855-872

Brown, E.H., Wilson, D.L., Armstrong, R.L., and Harakal, J.E., 1982, Petrologic, structural, and age relations of serpentinite, amphibolite, and blueschist in the Shuksan Suite of the Iron Mountain-Gee Point area, North Cascades, Washington: Geological Society of America Bulletin, v. 93, p. 1087-1098.

Brocher, T.M., T. Parsons A.M. Trehu, C.M. Snelson and M.A. Fisher (2003) Seismic evidence for widespread serpentinized forearc upper mantle along the Cascadia margin, Geology, 31, 267-270.

Brueckner, H.K., and Medaris, L.G., 2000, A general model for the intrusion and evolution of "mantle" garnet peridotites in high-pressure and ultra-high-pressure metamorphic terranes: Journal of Metamorphic Geology, v. 18, p. 123-133.

Bucher, K., and Frey, M., 2002, Petrogenesis of metamorphic rocks, 7th edition, Berlin, Spriger, p. 341.

Cannat, M., Mevel, C., Maia, M., Deplus, C., Durand, C., Gente, P., Agrinier, P., Belarouchi, A., Dubuisson, G., Humler, E., and Reynolds, J., 1995, Thin crust, ultramafic exposures, and rugged faulting patterns at the Mid-Atlantic Ridge (22 degrees -24 degrees N): Geology, v. 23, p. 49-52.

Carswell, D.A., and Dawson, J.B., 1970, Garnet peridotite xenoliths in South African kimberlite pipes and their petrogenesis: Contributions to Mineralogy and Petrology, v. 25, p. 163-184.

Caruso, L.J., and Chernosky, J.V., Jr., 1979, The stability of lizardite, in Wicks, F.J., ed., The Canadian Mineralogist, vol.17, Part 4, p. 757-769.

Cerny, P., 1968, Comments on serpentinization and related metasomatism: American Mineralogist, v. 53, p. 1377-1385.

D'Antonio, M., and Kristensen, M.B., 2004, Serpentine and brucite of ultramafic clasts from the South Chamorro Seamount (Ocean Drilling Program Leg 195, Site 1200); inferences for the serpentinization of the Mariana forearc mantle: Mineralogical Magazine, v. 68, p. 887-904.

Deer, W.A., Howie, R.A., and Zussman, J., 1992, An introduction to the rock-forming minerals, 2nd edition; Harlow, Pearson Prentice Hall, pp.696.

Dick, H.J.B., and Bullen, T., 1984, Chromian spinel as a petrogenetic indicator in abyssal and alpine-type peridotites and spatially associated lavas: Contributions to Mineralogy and Petrology, v. 86, p. 54-76.

Dobson, D.P., Meredith, P.G., Boon, S.A., Simulation of subduction zone seismicity by dehydration of serpentine. Science, 298: 1407-1410

Dolan, J.F., Mullins, H.T., and Wald, D.J., 1998, Active tectonics of the north-central Caribbean; oblique collision, strain partitioning, and opposing subducted slabs: Special Paper - Geological Society of America, v. 326, p. 1-61.

Draper, G. and Nagle, F., 1991, Geology, structure, and tectonic development of the Rio San Juan Complex, northern Dominican Republic: Special Paper - Geological Society of America, v. 262, p. 77-95.

Dungan, M.A., 1977, Metastability in serpentine-olivine equilibria: American Mineralogist, v. 62, p. 1018-1029.

Escuder-Viruete, J. and Pérez-Estaún, A., 2006, Subduction related P-T path for eclogites and garnet glaucophanites from the Samaná Peninsula Basement Complex : International Journal of Earth Sciences (Geol Rundsch), v. 95, p. 995-1017

Enami, M., Mizukami, T., and Yokoyama, K., 2004, Metamorphic evolution of garnet-bearing ultramafic rocks from the Gongen area, Sanbagawa Belt, Japan: Journal of Metamorphic Geology, v. 22, p. 1-15.

Evans, B.W., 2004, The serpentinite multisystem revisited; chrysotile is metastable: International Geology Review, v. 46, p. 479-506.

Evans, B.W., 1977, Metamorphism of alpine peridotite and serpentinite: Annual Review of Earth and Planetary Sciences, v. 5, p. 397-447.

Evans, B.W., and Frost, B.R., 1975, Chrome-spinel in progressive metamorphism; a preliminary analysis, Geochimica et Cosmochimica Acta, Volume 39, p. 959-972.

Federico, L., Crispini, L., Scambelluri, M. and Capponi, G., 2007, Ophiolite mélange zone records exhumation in a fossil subduction channel : Geology, v. 35, no. 6, p. 499-502

Fleet, M.E., Angeli, N. and Pan, Y., 1993, Oriented chlorite lamellae in chromite from the Pedra Branca mafic-ultramafic complex, Ceara, Brazil, American Mineralogist, vol.78, no.1-2, p.68-74.

Fryer, P., Wheat, C.G., and Mottl, M.J., 1999, Mariana blueschist mud volcanism; implications for conditions within the subduction zone: Geology, v. 27, p. 103-106.

Gaetani, G.A., Grove, T.L., and Bryan, W.B., 1993, The influence of water on the petrogenesis of subduction-related igneous rocks: Nature, v. 365, p. 332-334.

Gerya, T.V., Stoeckhert, B., and Perchuk, A.L., 2002, Exhumation of high-pressure metamorphic rocks in a subduction channel; a numerical simulation: Tectonics, v. 21, p. no.6, 19.

Giunta, G., Beccaluva, L., and Siena, F., 2006, Caribbean Plate margin evolution: constraints and current problems, Geologica Acta, vol. 4, no. 1-2, p. 265-278

Gorczyk, W., Guillot S., Gerya, T.V., Hattori, K.H., 2007, Asthenospheric upwelling, oceanic slab retreat and exhumation of UHP mantle rocks: insights from Greater Antilles: Geophysical Research Letters, in press.

Groppo, C., Rinaudo, C., Cairo, S., Gastaldi, D., and Compagnoni, R., 2006, Micro-Raman spectroscopy for a quick and reliable identification of serpentine minerals from ultramafics: European Journal of Mineralogy, v. 18, p. 319-329.

Gueddari, K., Piboule, M., and Amosse, J., 1996, Differentiation of platinum-group elements (PGE) and of gold during partial melting of peridotites in the lherzolitic massifs of the Betico-Rifean range (Ronda and Beni Bousera), in Menzies, M.A., Bodinier, J.L., Frey, F., Gervilla, F., and Kelemen, P., eds., Chemical Geology, Volume 134, p. 181-197.

Guillot, S., Hattori, K.H., and de Sigoyer, J., 2000, Mantle wedge serpentinization and exhumation of eclogites; insights from eastern Ladakh, Northwest Himalaya: Geology, v. 28, p. 199-202.

Guillot, S., Hattori, K.H., de Sigoyer, J., Naegler, T., and Auzende, A.-L., 2001, Evidence of hydration of the mantle wedge and its role in the exhumation of eclogites: Earth and Planetary Science Letters, v. 193, p. 115-127.

Hanor, J.S., 1979, The sedimentary genesis of hydrothermal fluids, in Barnes, H.L., ed.: New York, John Wiley & Sons.

Hattori, K.H., Wallis, S., Enami, M. and Mizukami, T. 2007; Subduction of garnet peridotites from subarc mantle due to large-scale mantle flow, recorded by the Higashi-Akaishi ultramafic body in the Sanbagawa metamorphic belt, Japan; submitted to Geology

Hattori, K.H., and Guillot, S., 2007, Geochemical Characterization of serpentinites associated with high to ultra-high pressure metamorphic rocks in the Alps, Cuba and Himalayas and the recycling of elements in subduction zones: Geochemistry, Geophysics and Geosystems (in press).

Hattori, K., Takahashi, Y., Guillot, S. and Johanson, B. 2005, Occurrence of Arsenic (V) in fore-arc mantle serpentinites: X-ray absorption spectroscopy study. Geochimica et Cosmochimica Acta. vol 69, pp.5585-5596.

Hattori, K.H., and Cameron, E.M., 2004, Utilizing the high mobility of palladium in exploration for platinum group element mineralization: Evidence from the Lac des Iles area, Canada. Economic Geology, vol. 99, no. 1, p.157-171

Hattori, K.H., and Guillot, S., 2003, Volcanic fronts form as a consequence of serpentinite dehydration in the forearc mantle wedge: Geology, v. 31, p. 525-528.

Helmy, H.M., El Mahallawi, M.M., 2003. Gabbro Akarem mafic-ultramafic complex, Eastern Desert, Egypt: a late Precambrian analogue of Alaskan-type Complexes: Mineralogy and Petrology 77, 85-108.

Hinchey, J.G. and Hattori, K.H., 2005, Magmatic mineralization and hydrothermal enrichment of the High Grade Zone at the Lac des Iles palladium mine, northern Ontario, Canada. Mineralium Deposita, vol. 40, pp. 13-23.

Hinchey, J.G., Hattori, K.H. and Lavigne, M.J., 2005, Geology, Petrology, and Controls on PGE Mineralization of the Southern Roby and Twilight Zones, Lac des Iles Mine, Canada, Economic Geology; January 2005; v. 100; no. 1; p. 43-61.

Hinchey, J.G., 2005, The geology and palladium mineralization of the southern Roby, Twilight, and high grade zones of the Lac des Iles Mine, western Superior Province of Canada. Unpublished Ph.D. thesis, University of Ottawa, Canada, pp. 156.

Hofmann, A.W., Jochum, K.P., Seufert, M., and White, W.M., 1986, Nb and Pb in oceanic basalts; new constraints on mantle evolution: Earth and Planetary Science Letters, v. 79, p. 33-45.

Hyndman, R.D., and Peacock, S.M., 2003, Serpentinization of the forearc mantle: Earth and Planetary Science Letters, v. 212, p. 417-432.

Irvine, T.N., 1967, Chromian spinel as a petrogenetic indicator; Part 2, Petrologic applications: Canadian Journal of Earth Sciences = Journal Canadien des Sciences de la Terre, v. 4, p. 71-103.

Irwin, W.P. and Barnes, I., 1975. Effect of geologic structure and metamorphic fluids on seismic behavior of the San Andreas fault system in central and northern California. Geology, 3: 713-716.

Ishii, T., Robinson, P.T., Maekawa, H., Fiske, 1992, Petrological studies of peridotites from diapiric serpentinite seamounts in the Izu-Ogasawara-Mariana forearc, Leg 125, in Fryer, P., Pearce, J.A., Stokking, L.B., et al. eds., Proceedings of the Ocean Drilling Program, Scientific Results, v. 125, p. 445-485.

Iturralde-Vinet, M.A., and Lidiak, E.G., 2006, Foreword: Caribbean Tectonic, Magmatic, Metamorphic and Stratigraphic Events: Inplications for Plate Tectonics. Geologica Acta, vol. 4, no. 1-2, p. 1-5.

James, K.H., 2006, Arguments for and against a Pacific origin of the Caribbean Plate: discussion, finding for an inter-American origin. Geologica Acta, vol. 4, no. 1-2, p. 279-302.

Jaques, A.L., and Green, D.H., 1980, Anhydrous melting of periodotite at 0-15 Kb pressure and the genesis of tholeiitic basalts. *Contributions to Mineralogy and Petrology, vol.73, no.3,* p. 287-310

Joyce, J., 1991, Blueschist metamorphism and deformation on the Samana Peninsula; a record of subduction and collision in the Greater Antilles: Special Paper - Geological Society of America, v. 262, p. 47-76.

Kamimura, A., Kasahara, J., Shinohara, M., Hino, R., Shiobara, H., Fujie, G., and Kanazawa, T., 2002, Crustal structure study at the Izu-Bonin subduction zone around 31 degrees N; implications of serpentinized materials along the subduction plate boundary, in Cummins, P.R., Kodaira, S., and Ruff, L., eds., Physics of the Earth and Planetary Interiors, v.132, p. 105-129.Kubo, K., 2002, Dunite formation processes in highly depleted peridotite; case study of the Iwanaidake Peridotite, Hokkaido, Japan: Journal of Petrology, v. 43, p. 423-448.

Kornprobst, J., Piboule, M., Roden, M., and Tabit, A., 1990, Corundum-bearing garnet clinopyroxenites at Beni Bousera (Morocco); original plagioclase-rich gabbros recrystallized at depth within the mantle?: Journal of Petrology, v. 31, p. 717-745.

Kimball, K.L., 1990, Effects of hydrothermal alteration on the compositions of chromian spinels: Contributions to Mineralogy and Petrology, v. 105, p. 337-346.

Kretz, R., 1995, Geochemistry (XRF) Laboratory Biannual Report, U. Ottawa, unpublished, 3 pp.

Lagabrielle, Y., and M. Cannat, (1990) Alpine Jurassic ophiolites resemble the modern central Atlantic basement, Geology, 18, 319-322.

Le Bas, M.J., 1962, The role of aluminum in igneous clinopyroxenes with relation to their parentage: American Journal of Science, v. 260, p. 267-288.

Le Maître, R.W., 1989, A classification of igneous rocks and glossary of terms. Oxford, Blackwell Science

Lewis, J.F., Draper, G., Bourdon, C., Bowin, C., Mattson, P.O., Maurrasse, F., Nagle, F., and Pardo, G., 1990, Geology and tectonic evolution of the northern Caribbean margin, in Dengo, G., and Case, J.E., eds.: Boulder, Geol. Soc. Am.

Liipo, J.P., Vuollo, J.I., Nykanen, V.M., and Piirainen, T.A., 1995, Zoned Zn-rich chromite from the Naataniemi serpentinite massif, Kuhmo greenstone belt, Finland: The Canadian Mineralogist, v. 33, p. 537-545.

Liou, J.G., Tsujimori, T., Zhang, R.Y., Katayama, I., and Maruyama, S., 2004, Global UHP metamorphism and continental subduction/collision; the Himalayan model: International Geology Review, v. 46, p. 1-27.

Loubet, M., and Allegre, C.J., 1982, Trace elements in orogenic lherzolites reveal the complex history of the upper mantle: Nature, v. 298, p. 809-814.

Maekawa, H., Shouzui, M., Ishii, T., Fryer, P., and Pearce, J.A., 1993, Blueschist metamorphism in an active subduction zone: Nature, v. 364, p. 520-523.

Mann, P., and Gordon, M.B., 1996, Tectonic uplift and exhumation of blueschist belts along transpressional strike-slip fault zones: Geophysical Monograph (Subduction Top to Bottom), v. 96, p. 143-154.

Mann, P., Draper, G., and Lewis, J.F., 1991, An overview of the geologic and tectonic development of Hispaniola: Special Paper - Geological Society of America, v. 262, p. 1-28.

Mann, P., Burke, K.C., and Matumoto, T., 1984, Neotectonics of Hispaniola; plate motion, sedimentation, and seismicity at a restraining bend: Earth and Planetary Science Letters, v. 70, p. 311-324.

McCollom, T.M., and Seewald, J.S., 2001, A reassessment of the potential for reduction of dissolved CO2 to hydrocarbons during serpentinization of olivine. Geochimica et Cosmochimica Acta, vol. 65, no. 21, p. 3769-3778.

McDonough, W.F., and Sun, S.S., 1995, The composition of the Earth: Chemical Geology, v. 120, p. 223-253.

Mellini, M., Rumori, C. and Viti, C., 2005, Hydrothermally reset magmatic spinels in retrograde serpentinites; formation of "ferritchromit" rims and chlorite aureoles. Contributions to Mineralogy and Petrology, vol.149, no.3, pp.266-275

Meschede, M., and Frisch, W., 1998, A plate-tectonic model for the Mesozoic and early Cenozoic history of the Caribbean Plate: Tectonophysics, v. 296, p. 269-291.

Mével, C., 2003 Serpentinization of abyssal peridotites at mid-ocean ridges. Comptes Rendus Geoscience, 335, 825-852.

Michael, P.J., and Bonatti, E., 1985, Peridotite composition from the North Atlantic; regional and tectonic variations and implications for partial melting: Earth and Planetary Science Letters, v. 73, p. 91-104.

Mizukami, T., and Wallis, S.R., 2005, Structural and petrological constraints on the tectonic evolution of the garnet-lherzolite facies Higashi-akaishi peridotite body, Sanbagawa Belt, SW Japan: Tectonics, v. 24, p. no.6, 17.

Mysen, B.O., and Kushiro, I., 1977, Compositional variations of coexisting phases with degree of melting of peridotite in the upper mantle, American Mineralogist, vol.62, no.9-10, p. 843-856.

Niu, Y., 2004, Bulk-rock major and trace element compositions of abyssal peridotites: Implications for mantle melting, melt extraction and post-melting processes beneath mid-ocean ridges, J. Petrol., 45, 2423-2458.

Niu, Y. and Hekinian, R., 1997, Spreading-rate dependence of the extent of mantle melting beneath ocean ridges: Nature, v. 385, p. 326-329.

O'Hanley, D.S., 1996, Serpentinites, Oxford Monographs on Geology and Geophysics, v. 34, pp. 277.

O'Hara, M.J., Richardson, S.W., and Wilson, G., 1971, Garnet-Peridotite Stability and Occurrence in Crust and Mantle: Contributions to Mineralogy and Petrology, v. 32, p. 48-68.

Ohara, Y. and Ishii, T., 1998, Peridotites from the southern Mariana forearc: Heterogeneous fluid supply in the mantle wedge: The Island Arc, v. 7, p. 541-558

Okamura, H., Arai, S., and Kim, Y.U., 2006, Petrology of fore-arc peridotite from the Hahajima Seamount, the Izu-Bonin Arc, with special reference to chemical characteristics of chromian spinel: Mineralogical Magazine, v. 70, p. 15-26.

Onyeagocha, A.C., 1974, Alteration of Chromite from the Twin Sisters Dunite, Washington: American Mineralogist, v. 59, p. 608-612.

Ozawa, K., 1983, Evaluation of olivine-spinel geothermometry as an indicator of thermal history for peridotites, Contributions to Mineralogy and Petrology, v. 82, no. 1, p. 52-65.

Page, B.M., Thompson, G.A. and Coleman, R.G., 1998. Late Cenozoic tectonics of the central and southern Coast Ranges of California. Geological Society America Bulletin, 110: 846-876.

Parkinson, I.J., and Pearce, J.A., 1998, Peridotites from the Izu-Bonin-Mariana forearc (ODP Leg 125); evidence for mantle melting and melt-mantle interaction in a supra-subduction zone setting: Journal of Petrology, v. 39, p. 1577-1618.

Peacock, S.M., 1996, Thermal and petrologic structure of subduction zones: Geophysical Monograph (Subduction Top to Bottom), v. 96, p. 119-133.

Pearson, D.G., Irvine, G.J., Ionov, D.A., Boyd, F.R., and Dreibus, G.E., 2004, Re-Os isotope systematics and platinum group element fractionation during mantle melt extraction; a study of massif and xenolith peridotite suites, in Reisberg, L., Alard, O., Lorand, J.-P., and Ohnenstetter, M., eds., Chemical Geology, v. 208, p. 29-59.

Pettigrew, N.T., and Hattori, K.H., 2006, The Quetico intrusions of western Superior Province; Neo-Archean examples of alaskan/ural-type mafic-ultramafic intrusions: Precambrian Research, v. 149, p. 21-42.

Pindell, J.L., Kennan, L., Stanek, K.P., Maresch, W.V. and Draper, G., 2006, Foundations of gulf of Mexico and Caribbean evolution: eight controversies resolved. Geologica Acta, vol. 4, no. 1-2, p. 303-341

Pindell, J.L., and Draper, G., 1991, Stratigraphy and geological history of the Puerto Plata area, northern Dominican Republic: Special Paper - Geological Society of America, v. 262, p. 97-114.

Pindell, J.L., Cande, S.C., Pitman, W.C., III, Rowley, D.B., Dewey, J.F., LaBrecque, J.L., and Haxby, W.F., 1988, A plate-kinematic framework for models of Caribbean evolution, in Scotese, C.R., and Sager, W.W., eds., Tectonophysics, Volume 155, p. 121-138.

Pinsent, R.H., and Hirst, D.M., 1977, The metamorphism of the Blue River ultramafic body, Cassiar, British Columbia, Canada: Journal of Petrology, v. 18, p. 567-594.

Ravizza, G. and Pyle, D., 1997. PGE and Os isotopic analyses of single sample aliquots with NiS fire assay preconcentration. Chemical Geology, v. 141, p. 251-268

Rinaudo, C., Gastaldi, D., and Belluso, E., 2003, Characterization of chrysotile, antigorite and lizardite by FT-Raman spectroscopy: The Canadian Mineralogist, v. 41, p. 883-890.

Rost F., 1961, Chlorit und Granat in ultrabasischen Gesteinen. Irtschr. Mineral. 39, 112-126.

Rublee, V.J., 1994. Chemical petrology, mineralogy and structure ofthe Tulameen Complex, Princeton area, British Colombia. Unpublished M.Sc. thesis. University of Ottawa, Canada. p. 179.

Rüpke, L.H., Phipps Morgan, J., Hort, M., and Connolly, J.A.D., 2004, Serpentine and the subduction zone water cycle: Earth and Planetary Science Letters, v. 223, p. 17-34.

Santti, J., Kontinen, A., Sorjonen-Ward, P., Johanson, B., and Pakkanen, L., 2006, Metamorphism and chromite in serpentinized and carbonate-silica-altered peridotites of the Paleoproterozoic Outokumpu-Jormua ophiolite belt, Eastern Finland: International Geology Review, v. 48, p. 494-546.

Sato, M., 1978, Oxygen fugacity of basaltic magmas and the role of gas forming elements. Geophysical Research Letters, vol. 5., p. 447-449.

Schertl, H., Krebs, M. and Maresch, W., 2006; The Eclogites From the Intraoceanic Rio San Juan Complex (Northern Dominican Republic): On the doorstep to UHP metamorphism, Eos, Transactions, AGU, 87 (52), Fall meeting supplement V44B-05

Schulte, M., Blake, D., Hoehler, T., and McCollom, T., 2006, Serpentinization and its implications for life on the early Earth and Mars, Astrobiology, vol. 6, no. 2, p. 364-376

Schwartz, S., P. Allemand, S. and Guillot, 2001, Numerical model of effect of serpentinites on the exhumation of eclogitic rocks: Insights from the Monviso ophiolitic massif (Western Alps). Tectonophysics, 342, 193-206.

Spangenberg K ., 1943, Die chromitlaagerstatte von tampedal in Zobten. 2. *Prukt. Geol.* 51, 13-35.

Tsujimori, T., Sisson, V.B., Liou, J.G., Harlow, G.E. and Sorensen, S.S., 2006. Very-low-temperature record of the subdcution processes: a review of worldwide lawsonite eclogites. Lithos, 92: 609-624.

Tsujimori, T., Kojima, S., Takeuchi, M., and Tsukada, K., 2004, Origin of serpentinites in the Omi serpentinite melange (Hida Mountains, Japan) deduced from zoned Cr-spinel: Chishitsugaku Zasshi = Journal of the Geological Society of Japan, v. 110, p. 591-597.

Ulmer, G.C., 1974, Alteration of Chromite During Serpentinization in the Pennsylvania-Maryland District: American Mineralogist, v. 59, p. 1236-1241.

Wang, J., 2007, Oxidation condition and behaviour of PGE during the subduction-related metasomatism in the southern South American subcontinental lithospheric mantle. unpublished Ph.D. thesis, University of Ottawa, Canada.

Weyl, R., 1941, Bau und Geschichte der Cordillera Central von Santo Domingo: Hamburg, Detsch-Dominikausche Tropenforshungsinstitut, Veroffentilichurgen, v. 2, 60 pp.

Wicks, F.J., and O'Hanley, D.S., 1988, Serpentine minerals; structures and petrology, in Hydrous Phyllosilicates (exclusive of micas), ed.: S.W. Bailey, Reviews in Mineralogy, v. 19, p. 91-167.

Williams, H.A., Cassidy, J., Locke, C.A., and Spoerli, K.B., 2006, Delineation of a large ultramafic massif embedded within a major SW Pacific suture using gravity methods: Tectonophysics, v. 424, p. 119-133.

Wunder, B., and Schreyer, W., 1997, Antigorite; high-pressure stability in the system MgO-SiO 2 -H 2 O (MSH): Lithos, v. 41, p. 213-227.

Wylie, A.G., Candela, P.A., and Burke, T.M., 1987, Compositional zoning in unusual Zn-rich chromite from the Sykesville District of Maryland and its bearing on the origin of "ferritchromit": American Mineralogist, v. 72, p. 413-422.

Yamamoto, K., Masutani, Y., Nakamura, N., Ishii, T., Tanaka, T., and Togashi, S., 1992, REE characteristics of mafic rocks from a fore-arc seamount in the Izu-Ogasawara region, western Pacific: Geochemical Journal, v. 26, p. 411-423.

Zack, T., Rivers, T., Brumm, R., and Kronz, A., 2004, Cold subduction of oceanic crust: Implications from a lawsonite eclogite from the Dominican Republic: European Journal of Mineralogy, v. 16, p. 909-916.